R. Naporowski   4421477   13-2-2020

Long waves in the North Sea

Distribution, generation and measurement methods

Rijkswaterstaat

TUDelft

Long waves in the North Sea

Distribution, generation and measurement methods

by

R. Naporowski

to obtain the degree of Master of Science
at the Delft University of Technology,
Faculty of Civil Engineering and Geosciences,
to be defended publicly on Thursday February 20, 2020 at 13:30 PM.

Rijkswaterstaat
Ministry of Infrastructure and the Environment

TU Delft

PREFACE

This thesis presents the work I have done on the research on long waves in the Dutch part of the North Sea. It is the final product of my master in Hydraulic Engineering at the Delft University of Technology. The research has been performed in close collaboration with Rijkswaterstaat.

First, I would like to thank my graduation committee from TU Delft for the time and effort they have put into guiding me through the research. To all of you, both your enthusiasm and expertise in the field of hydraulic engineering is inspiring and gave me a lot of motivation to work on my thesis. Your doors were always open to me if I needed help, which I much appreciated. Special thanks to Ad, for being a great mentor to me. You provided me with support whenever I needed it, and played a crucial role on most of the important decisions. We had many pleasant and constructive meetings in your office, and you even allowed me to work there for some time. Matthieu, your reporting skills, in combination with reviewing my report many times, has significantly improved the structure of the report and it's readability. Marion and Gal, thanks for the constructive meetings we had and the sharp comments during these meetings, and on my report.

I would like to thank my graduation committee from Rijkswaterstaat, and the organization itself. They have provided me with all the facilities I needed to perform this research, and supported me all the way through the process. Your enthusiasm and knowledge were of great support to me. The constructive and pleasant meetings we had were a valuable asset to the outcome of the research. Herman, reading through the report numerous times has greatly improved the quality of the report, and saved me from making some embarrassing errors. Robert and Peter, thanks for bringing me in touch with the right people whenever I required additional information and contacts.

I owe a great deal of thanks to my close friends and family. Without them I would not have been where I am today. Their unconditional love and support, through good and hard times, is most dear to me. My mom (Jacqueline) and brother (Michel), you have always been there for me and provided me with financial and mental support all the way through. Opa (Gerard) and Nelke, my grandparents whom I have lost during working on the thesis; this will be the first ceremony in my life without you, I would have loved you to be part of it as well. Harry and mom, reading through my report countless times has helped me a lot in writing the report. It has given me an outsiders perspective on my own research, which was often really helpful. Zoé, for many years you were my best friend and loved one. You were a crucial factor in my decision to go to Delft, and motivated and supported me all the way through. I will never forget the time we have spent together. Emmy and Igor, during my time in Delft I could not have wished for better friends. I share my best memories in Delft with you, and have also enjoyed your support in hard times. Loes, though we are not together for a very long time you already are an important part of my life. Your enthusiasm and energy has often given me motivation to work on my thesis, and has given me a much more positive attitude in general. I am looking forward to our time together.

My office roommate Said, thanks for a lot of fun talks during research time, and often helping me out with my research.

Finally, I would like to thank all who supported me throughout my studies and have given me a student experience never to forget; My roommates from Huize Nette Broek, swimmings friends from ASZV SPONS and DSZ WAVE, fellow students from the faculty of Civil Engineering and Geosciences and the Hogeschool van Amsterdam, colleagues from Van der Valk and my family.

Remy Naporowski
Delft, February 2020

Rijkswaterstaat
Ministry of Infrastructure and the Environment

TUDelft

ABSTRACT

This report presents the results of a research concerning long waves in the North Sea. 'Long waves' in this research is a collective name for various types of waves that are longer than the well-known sea-swell waves, here referred to as 'short waves'. Wave types that are referred to as long waves are infragravity waves, meteo-tsunami's, seiches and tides. Besides their extensive length, they distinguish themselves from regular sea-swell waves by the mechanisms responsible for their generation and the scale of their impact. Whereas short waves are generated by wind, long waves are generated by short wave-group forcing, the breaking of short waves nearshore and large atmospheric pressure variations. Long waves play a crucial role in the processes of coastline erosion and the breaching of flood defenses, as well as in the formation of rip currents and seiches. These events can lead to severe damage to hydraulic structures and possibly even casualties. A better understanding of them is thus vital for coastal safety.

Rijkswaterstaat has been collecting data regarding the occurrence of long waves on the North Sea for over a decade. Their measurement campaign started in a time when digital broadcasting signals and digital storage space were not well developed yet, making sending and storing the water surface elevation time-series not feasible. The data is therefore filtered by a FIR filter, reducing the size of the data, but also reducing the information that is contained in the data. All frequencies of approximately $0,0125\ Hz$ and higher are removed by the FIR filter. As a consequence a significant part of the infragravity signal is missing and it is not possible to perform a bispectral analysis (used to determine the bound long wave contribution). Nowadays, digital broadcasting signals and digital storage space have plenty of capacity to send and store the data, making the filter unnecessary.

Analysis of the spatial- and temporal distribution of long waves in the North Sea, shows that the majority of long waves have a yearly averaged significant wave height of 2,4 - 3,3 cm and a yearly averaged mean wave period of 125 to 140 cm. Based on data from the full decade, a clear trend in the spatial distribution of long waves cannot be distinguished, offshore and nearshore locations show approximately the same long wave properties. The seasonal analysis shows that the mean significant long wave height averaged out over all locations per season varies from 2,8 cm during summer, 2,9 cm during spring, 3,3 cm during winter to 3,5 cm during fall. For the mean wave period, the mean value averaged out over all locations per season varies from 127,5 s during summer, 128,1 s during spring, 135,6 s during winter to 136,3 s during fall. Predictions of the extreme wave conditions show that the significant wave height with a return period of 10.000 years (Dutch design condition for coastal flood defenses) are around 40-60 cm, although there is quite some uncertainty in these predictions. This uncertainty is due to a relatively short measurement period, usually 30 years of data is used for extreme wave predictions, and remarkable observations in the data.

Time-series analysis of the hourly significant wave height of long waves and predicted bound long waves (Hasselmann, 1962) (Hasselmann, 1963) shows that during mild weather conditions significant wave heights of long waves are low, with minimal contributions by the bound long waves. At the onset of a storm, the significant wave height of both long waves and bound long waves rapidly increase. At the end of the storm, they decrease to the pre-storm values. This shows that the generation of long waves occurs mainly during heavy weather conditions. Hourly significant wave heights of long waves, and especially bound long waves, show a strong correlation with significant short wave heights. The relative contribution of bound long waves (E_{blw}/E_{lw}) during a storm increases up to values of 60%, which is considerably higher than contributions of bound long waves found in other studies (Herbers et al., 1994). The high ratio of the relative bound long wave contribution, in combination with very low bound long wave activity during mild conditions, shows that the generation mechanism involving wave-group forcing is a major generation mechanism of long waves in the North Sea.

Keywords: long waves; infragravity waves; north sea; wave-group forcing

Rijkswaterstaat
Ministry of Infrastructure and the Environment

$\tilde{T}$UDelft

alt.	Altitude	
lat.	Latitude	
lon.	Longitude	
MSL	Mean Sea Level	
NAP	Normaal Amsterdams Peil	
pdf	Probability function	
cdf	Cumulative distribution function	

d	Water depth	m
D	Duration of block for spectral analysis	s
	Difference-interaction coefficient	?
$E(f)$	Wave energy density function (as function of frequency)	m^2/Hz
f	Wave or measuring frequency	Hz
h	Water depth	m
g	Gravitational acceleration	m/s^2
H	Wave height	m
H_{m_0}	Significant wave height (from spectral analysis)	m
H_s	Significant wave height	m
L	Wave length	m
m_n	n^{th} order spectral moment	
p	Atmospheric pressure	Pa
	Number of subsamples for block with length D (spectral analysis)	—
R	Reflection coefficient	—
r	Pearson's correlation coefficient	—
r^2	Coefficient of determination	—
T	Wave period	s
T_m	Mean wave period	s

Rijkswaterstaat
Ministry of Infrastructure and the
Environment

TUDelft

u_{10}	Wind velocity at 10m above surface level	m/s
β	Bed slope	$-$
β_H	Normalized bed slope	$-$
$\eta(t)$	Water surface elevation time-series	m
$\theta(f)$	Wave direction as function of frequency	deg
μ_i	Mean value of i	-
σ_i	Standard deviation of i	-
σ_i^2	Variation of i	-
$\sigma_\theta(f)$	Wave directional spreading as function of frequency	deg

Rijkswaterstaat
Ministry of Infrastructure and the
Environment

TUDelft

TABLE OF CONTENT

Rijkswaterstaat
Ministry of Infrastructure and the Environment

T̃U Delft

Rijkswaterstaat
Ministry of Infrastructure and the Environment

TUDelft

1 INTRODUCTION

1.1 INTRODUCTION

'Long waves' in this research is a collective name for several types of waves that have a period of approximately 25 s and longer. They discriminate themselves from 'regular' sea-swell waves by their extensive length and mechanisms that are responsible for their generation. Long waves play an important role in several coastal processes. They are essential in the generation of seiches[1], as well as in the processes of dune erosion, dune- and dike failure. Hence, they potentially contribute to severe damage to coastal structures as well as casualties resulting from, for example, floods.

High wind velocities and strongly varying atmospheric pressures are essential conditions for the generation of several types of long waves in the North Sea. High wind velocities generate short waves, which in its turn generate long waves through wave-group forcing. This makes storms an important driving mechanism for long wave generation. Since the North Sea is located in the same region as Westerlies[2], a lot of storms occur here. The generation of long waves is therefore ubiquitous in this area. On top of that, studies show that the process of long wave generation is most efficient in shallow water. Being a relatively shallow sea (especially the area in between the Netherlands and the United Kingdom) greatly enhances the generation of long waves.

The Netherlands has a long and intense history of floods and eroding coastlines. With the relative sea level rise due to climate change and land subsidence, these problems will become only worse. The effects of a flood are drastically increased by the fact that the country is for a large part positioned below sea level. This results in the range of the flood reaching further inland and a higher water level with respect to the ground level. The combination of favorable long wave generation conditions in the North Sea and the essential role these waves play in floods, makes a better understanding of them of crucial importance for Dutch flood safety and coastline maintenance.

At several locations in the Dutch part of the North Sea Shelf, Rijkswaterstaat has been recording water level data on the occurrence of long waves. The water level data includes low frequency oscillations. In order to specifically preserve low frequency oscillations in the water surface elevation time-series, the data has been subjected to a filter. The consequences of this filter on the data and the associated research possibilities are discussed. In addition to the long wave data, data has been collected on wind (velocity and direction), atmospheric pressure, short waves (energy density and frequency direction) and water depth. This information provides a unique opportunity to investigate the presence and magnitude of long waves in the North Sea Shelf.

1.2 RESEARCH OBJECTIVES AND APPROACH

This research is the first to be using the long wave data from Rijkswaterstaat. In order to specifically store long wave data, Rijkswaterstaat has applied a certain processing method. Applying this method had consequences for the content and usability of the data. The first step in this research is examining the data. This includes finding what the data exactly contains, and what the consequences of the filter are.

After the data examination, several aspects of long waves are studied using the data provided by Rijkswaterstaat. Several mechanisms are known to generate long waves. Knowing which ones are relevant for long wave generation in the North Sea is very useful for predicting when and where they could possibly occur. The long wave data is analyzed in relation with parameters that are known to be relevant for long wave generation, in order to find out which generation mechanisms are most relevant for the generation of long waves in the North Sea.

---

[1] When one of the eigenfrequencies of a basin is triggered by an incoming wave with the same frequency, the water level starts oscillating in a resonant mode. This phenomenon is called a seiche.
[2] Region with prevailing winds from west to east, located in between $30° - 60°$ latitude. Particularly strong winds in the Winter.

Rijkswaterstaat
Ministry of Infrastructure and the Environment

TUDelft

To get an impression of the long waves presence in the North Sea, the spatial and temporal distribution of long waves in the North Sea is analyzed. Long waves are studied per location (spatial distribution) and season (temporal distribution). Based on the provided data, an extreme wave prediction is performed to obtain an indication of possible extreme long wave conditions in the North Sea.

1.3   THESIS OUTLINE

This report is divided into several chapters, Chapter 0 gives an introduction into the research, research objectives and an outline of the thesis. Chapter 2 contains the literature review on infragravity waves, which is the type of long wave that is studied in this research. In chapter 3 the research objectives and research questions are presented. Chapter 4 presents the description of the data that Rijkswaterstaat has provided for this research. This includes the analysis of the long wave data and all other data that is required for this study. Chapter 5 discusses the approach and methods required to obtain results for the research objectives. The results of the analysis of the relevant long wave generation mechanisms are presented in chapter 6. Chapter 7 presents the results of the spatial and temporal distribution of long waves in the North Sea, together with the extreme long wave predictions. The discussion and conclusions based on the results from chapter 6 and 7 follows in chapter 8. Recommendations based on the performed research are presented in chapter 0.

Rijkswaterstaat
Ministry of Infrastructure and the Environment

TU Delft

Waves are ubiquitous in all sorts of open water bodies. They are classified by means of their period/frequency, see Figure 1. The dataset provided by Rijkswaterstaat, containing wave periods from 80 seconds and longer, covers a minor part of the infragravity wave frequency band and reaches into the frequency band denoted by 'Long period waves' and 'Ordinary tide waves' frequency band. The ordinary tide waves are the well-known tidal motions, causing the twice a day rise and fall of the water level at the Dutch coast.
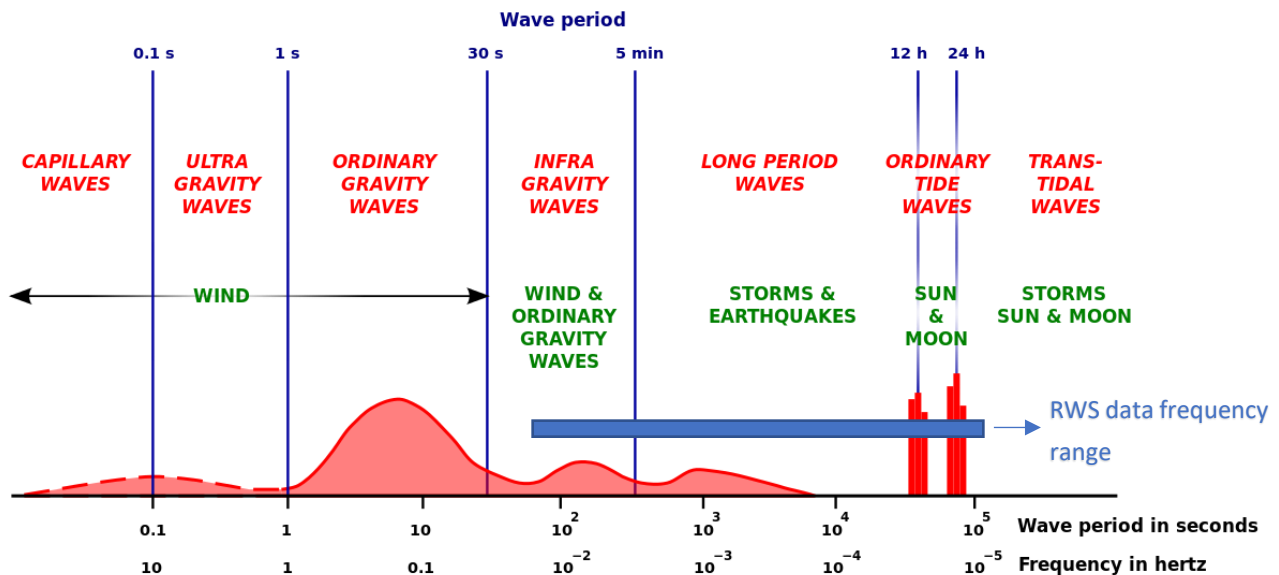
Figure 1: Classification of open water waves based on frequency/period (Munk, 1950). The red letters denote the name of the class of waves in that frequency band. All of these waves originate from a certain source. These sources are mentioned in green letters. Adaption to original figure; Frequencies concerning Rijkswaterstaat's long wave data are marked with a blue bar

2.1 INFRAGRAVITY WAVE THEORY

An infragravity wave is defined as a wave with typical periods varying from 25 to 250 seconds, meaning a $0.04 - 0.004\ Hz$ frequency bandwidth. This section discusses the main generation mechanisms of infragravity waves, followed by a description of several processes involved in their propagation. To illustrate the impact of infragravity waves, and thus the relevance of this research, this section concludes with describing several coastal processes infragravity waves have an impact on.

2.1.1 GENERATION MECHANISMS

Possible generation mechanisms for infragravity waves are (Bertin, et al., 2018):

- Bound wave interference
- Moving breakpoint
- Bore merging

When two monochromatic waves[3] with slightly varying celerities (with frequencies f_1 and f_2, where $f_2 > f_1$) travel in the same direction, they will interfere with each other. When this happens, their crest/trough levels add up to each other, usually resulting in either a higher or a lower water level. This superposition creates a wave height/amplitude

---

[3] Wave with a single frequency

Rijkswaterstaat
Ministry of Infrastructure and the Environment

variation of which the frequency is equal to the difference in frequency of the two monochromatic waves ($f_{new} = \Delta f = f_2 - f_1$). See an illustration of this phenomenon in Figure 2. In general, Δf is an order of magnitude smaller than $f_{1,2}$.
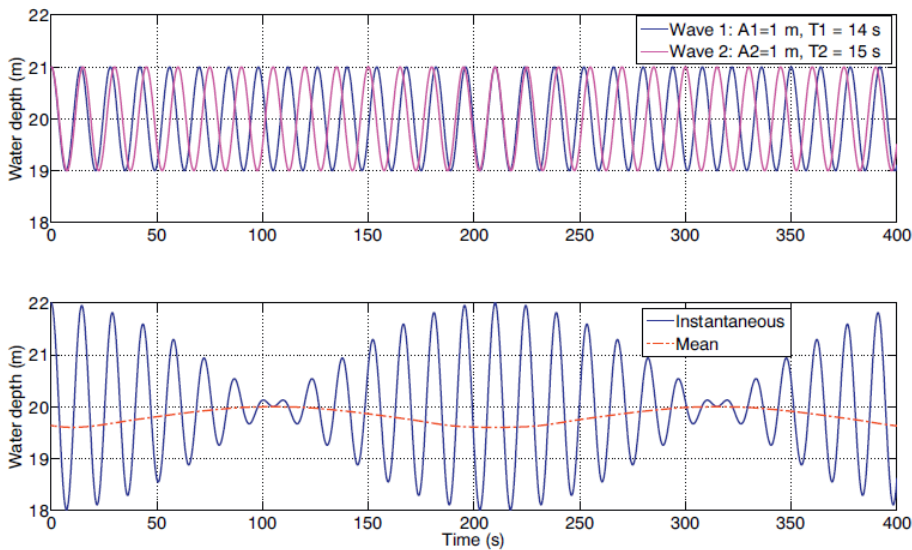
Figure 2: Time series of two monochromatic waves with a slightly varying celerity passing each other (top), and the resulting superposition (bottom). Radiation stress increases for higher waves, which is compensated by the set-down of the water level underneath the highest waves (red dashed line). (Bertin, et al., 2018)

Waves transport momentum while propagating, the depth-integrated short-wave-averaged momentum transported by waves is called radiation stress. Higher waves transport more momentum, which means a higher radiation stress. The spatial gradients in radiation stress in a wave group results in a set-down of the water level underneath the highest waves within a wave group, which in its turn results in a relative set-up of the water level below the smaller waves. This combination of set-up and set-down of the water level is in fact a long wave accompanying the short waves (red dashed line in Figure 2). This long wave is thus bound to the wave group structure and is therefore called a bound wave (Longuet-Higgins, et al., 1962). Being forced by other waves, this wave does not follow linear wave theory, but instead travels with the group velocity of the two monochromatic waves.

Having a longer period, the bound wave starts shoaling earlier in shallow water in comparison to the waves it is bound to, changing the phase difference between the two. This phase shift allows the transfer of energy from the short waves to the bound wave. The breaking of short waves at certain depth limits causes the wave group structure to vanish towards the shoreline. The wave group structure, which the long wave is bound to, then disappears at some point. This leads to the detachment of the bound wave from the short waves, transforming it into a free long wave.

Another mechanism generating infragravity waves is the varying location in time of the breakpoint of breaking short waves, therefore named the moving breaking generation mechanism (Symonds, et al., 1982). As mentioned earlier in this section, waves with larger heights cause a set-down of the water level underneath them due to large levels of radiation stress. When entering the shoaling zone, the wave heights increase due to shoaling, hence the radiation stress and thus set-down also increase. Propagating further towards the shoreline, the wave heights keep increasing until they reach the point of breaking. When they break, the waves disappear together with their radiation stress, removing the set-down. In order to achieve a force equilibrium, the water level set-down is compensated by a water level set-up near the shoreline. For a schematic of the water level set-down and set-up, see Figure 3. Wave groups entering the shoaling zone and subsequently breaking nearshore cause a varying breaking point location, varying radiation stress gradients and varying water level set-up/down in time. This corresponds to waves being created at infragravity frequencies.
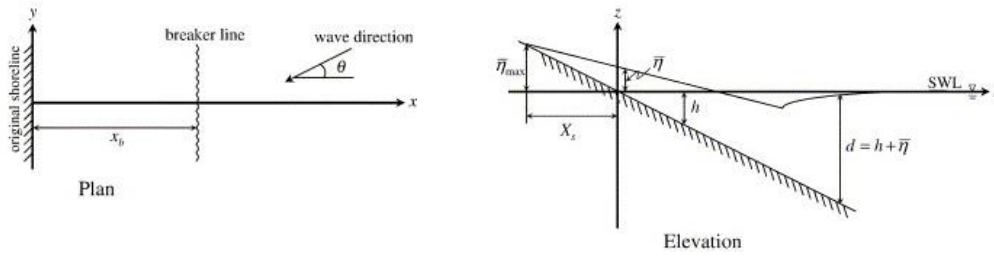
Figure 3: Schematic of wave induced set-up (breaking zone) and set-down (shoaling zone) (Coastal Dynamics 1, 2015)

The last generation mechanism to be discussed is the bore merging mechanism. After breaking, waves turn into bores in the inner surf zone. Depending on the waves' properties, these bores propagate with varying celerities and heights. Larger bores propagate faster than smaller ones. This results in the larger bores taking over and merging with the smaller ones. This nonlinear process leads to an increase of the wave period in the surf zone, and thus contributes to the earlier mentioned transfer of energy from short waves to infragravity waves (Senechal, et al., 2001), (Tissier, et al., 2015).

2.1.2 DETERMINING THE CONTRIBUTION OF BOUND AND FREE WAVES TO THE TOTAL INFRAGRAVITY WAVE ACTIVITY

Infragravity waves are either bound- or free waves, depending on whether they are bound to a wave group or not, see section 2.1.1. It is possible to predict the contribution of bound long waves to the total long wave activity with Hasselmann's second order non-linear theory (Hasselmann, 1963) (Hasselmann, 1962). The equation to predict the bound long wave contribution is shown below.

$$E_{forced}(\Delta f) = 2 \int_{\Delta f}^{\infty} df \int_{0}^{2\pi} d\theta_1 \int_{0}^{2\pi} d\theta_2 D^2(f + \Delta f, -f, \Delta\theta + \pi)E(f + \Delta f, \theta_1)E(f, \theta_2)$$

$$E_{forced} = Bound\ long\ wave\ energy\ [m^2/Hz]$$

$$f = Wave\ frequency\ [Hz]$$

$$\theta = Wave\ direction\ [deg]$$

$$D = Difference - interaction\ coefficient$$

$$E = (Short)\ wave\ energy\ density\ directional\ spectrum\ [m^2/Hz]$$

Based on short wave information (frequency-directional spectrum) and water depth, this theory is capable of predicting the amount of bound wave energy at a location accurately (Herbers et al., 1994)

The theory reproduces the non-linear interaction between short waves that result in long waves for a certain long wave frequency ($|f_1 - f_2| = \Delta f$). The parameter 'D' in this equation is the difference-interaction coefficient for the short waves with frequencies f and $f + \Delta f$ and directions $\Delta\theta = |\theta_1 - \theta_2|$.

Another method determines the bound long wave contribution to the total long wave activity. It does so by means of a bispectral analysis (Herbers et al., 1994). Since bound waves are phase locked to short wave groups it is possible to determine their contribution to the long wave spectrum by analyzing the amplitude/phase spectrum. This method requires the energy density spectrum and phase spectrum.

When the contribution of bound waves to the long wave spectrum is known, the free wave contribution is naturally equal to $E_{free} = E_{total} - E_{forced}$.

Rijkswaterstaat
Ministry of Infrastructure and the Environment

TU Delft

2.1.3 PROPAGATION

Now most of the major generation mechanisms of infragravity waves have been mentioned, it is important to look at how they propagate. Infragravity waves usually remain in the nearshore zone due to wave refraction based on local bathymetry. The part that is trapped in the nearshore zone are called 'Trapped waves'. On the other hand, waves that break out of the nearshore zone into the open ocean are called 'Leaky waves'. The nearshore zone is thus the zone where most of the infragravity waves are located, and is also the area where the most interesting propagation occurs. Processes like shoaling, shoreline reflection and refraction will be discussed in the following sub-sections.

While propagating, infragravity waves dissipate energy. The following mechanisms are believed to be the main dissipation mechanisms (de Bakker, et al., 2014), and will also be discussed in the next sub-sections:

- Wave breaking
- Non-linear energy transfer (from the infragravity frequency band back to the sea swell frequencies)
- Bottom friction

It is also possible that a (bound) infragravity wave gains energy during shoaling (Battjes, et al., 2004). This will be explained in this section.

When arriving in shallow water, a bound wave - longer than the short waves it is bound to - starts shoaling earlier than the short waves. Due to the shoaling of the bound wave, the phase lag between the bound wave and the short waves increases. This increase in phase lag allows the transfer of energy from the short waves to the bound wave, making the latter grow (Battjes, et al., 2004).

In terms of generation mechanisms, the relative importance of bound wave enhancement, compared to the moving breakpoint mechanism, is highly dependent on the normalized bed slope (Battjes, et al., 2004). A steep slope (i.e. 1:10) is dominated by the moving breakpoint mechanism, while for a mild slope (i.e. 1:70), this generation mechanism is negligible. As explained above, for a mild slope the transfer of energy from short to long waves dominates the infragravity wave generation.

During the shoaling process of bound waves, bound waves with a higher frequency experience a larger additional lag than waves with a lower frequency. A higher additional lag means that more energy is transferred from the short waves to the bound wave.

Upon reflection at the shoreline, the infragravity wave loses energy. This energy loss is the effect of the mentioned mechanisms at the start of 2.1.3. The energy loss due to wave breaking is believed to be the dominant one on mildly sloping sandy beaches (de Bakker, et al., 2014). The amount of energy lost by wave breaking during reflection varies greatly. Two important factors influencing the amount of energy lost by wave breaking during reflection are the frequency of the wave and the slope of the beach. Together, these two factors determine if shoreline reflection occurs in either a steep- or a mild-sloping regime. To indicate the type of sloping regime, the normalized bed slope is used. The definition of the normalized bed slope (β_H) is shown below:

$$\beta_H = \frac{\beta T}{2\pi} \sqrt{\frac{g}{H}}$$

$\beta_H = Normalized\ bed\ slope\ [-]$

$T = Wave\ period\ [s]$

$g = gravitational\ constant\ [m/s^2]$

$H = Wave\ height\ [m]$

$\beta = Bed\ slope\ [-]$

Results of a laboratory experiment conducted very close to a shoreline (van Dongeren, et al., 2007) indicate $\beta_H \geq 1,25$ as a steep-slope regime, while field experiments conducted a bit more seaward (de Bakker, et al., 2014) indicate a steep-slope regime for $\beta_H \geq 3$. A steep-slope regime corresponds to a high reflection coefficient 'R', meaning most of the energy is retained. For a mild-slope regime, it is the other way around. It has a low R and dissipates a large part of the energy.

For a steep-slope regime, an infragravity wave forms a standing wave, which means that there is barely any energy dissipation due to wave breaking. A mild-slope regime shows progressive waves. Progressive waves tend to dissipate far more energy than standing waves.

For obliquely incident waves (waves coming in under an angle different from the shore normal), refraction occurs. The concept of refraction can be explained by looking at obliquely incident long crested swell waves travelling towards an alongshore uniform coast with parallel depth contours. When they arrive in 'intermediate' water depths ($d < \frac{L}{2}$), the waves start 'feeling the bottom', resulting in a lower wave celerity. The part of the wave crest which is closer to shore travels at a lower celerity than the part further off-shore, forcing a bending of the wave crest towards the depth contours of the shore. An example of wave refraction is shown in Figure 4.

Whenever waves enter a coastal area with a bulge in the coast, waves will refract towards this bulge. A lot of wave energy is then focused on this bulge. This is called wave focusing. An example of wave focusing is shown in Figure 5. The relatively high concentration of wave energy on the bulge causes a local increase of wave attack and rapid currents flowing towards the sides of the bulge.

Figure 4: Refracting waves

The other way around, wave energy can also be spread out over a larger area when waves enter, for example, a bay. The depth contours of the bay cause the waves to spread out over a larger area due to refraction.

Rijkswaterstaat
Ministry of Infrastructure and the Environment

TU Delft
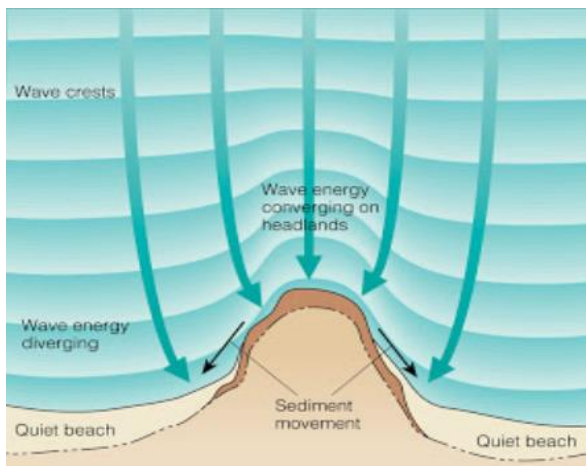
Figure 5: Wave focusing on bulge in coast

The concept of refraction does not only apply to short waves, but also, on a varying scale, to other types of waves. Infragravity waves are an important factor in coastal erosion processes and potential flooding. In combination with wave focusing, they could cause a strong growth of erosion and impose a greater risk of flooding.

2.1.4 IMPACT

Infragravity waves have a substantial effect on several important coastal areas, as they influence processes that govern them. The most important coastal areas impacted are listed below:

- Sandy dunes and beaches (shoreline erosion and increased run-up)
- Tidal inlets
- Harbors (seiches)
- Sea dykes.

A better understanding of infragravity waves means a better understanding of what exactly is going on in these areas. Since these areas are of great societal and economical interest in coastal regions, a better understanding is highly beneficial. Each of the areas will be discussed below. The coastal processes and their impacts will be mentioned, and the influence of infragravity waves on the processes will be explained.

Rip currents form one of the main coastal hazards for beach users and are also important in the transport and mixing of sediment, pollutants, nutrients, heat and biological species near the shore. Although infragravity waves are not required for rip current formation, they do influence the spatial and temporal distribution of certain types of rip currents (Symonds, et al., 2000) (Bowen, et al., 1969).

The dunes and beaches alongside the North Sea protect the hinterland from flooding during storms. Infragravity waves are expected to play a significant role in the several stages of a flooding event. Because of their long periods, infragravity waves persist quite far inshore, increasing the run-up distance on both dissipative and reflective beaches (Bertin, et al., 2018). On sandy dunes, this increases slumping of the wetted part of the dune face, which increases dune erosion and scarp formation (Roelvink, et al., 2009). Besides slumping, the increased run-up means an increased probability of overwash and higher overwash discharges, resulting in possible damage to infrastructure or even a flood (Bertin, et al., 2018). For a dissipative coast, overwash during storms consists mainly of longer period waves, since short waves are dissipated over the length of the beach (Baumann, et al., 2017).

In tidal inlets, infragravity waves start behaving in a notable manner, due to the complex bathymetry of the inlet and strong tidal currents.

Semi-enclosed basins (i.e. harbors or ports) have natural resonant periods. If these correspond with the incoming wave frequency, large water level fluctuations could occur in the basin, called seiches (Rabinovich, 2009). In the case of a

harbor or port, this could lead to damage to, for example, ships, facilities and sometimes even cause casualties. Infragravity wave frequencies often correspond to the natural resonant period of small-scale basins (Okihiro et al, 1993).

Just like dunes, sea dykes are used to protect the hinterland from a flood. Compared to dunes, sea dykes are far less sensitive to erosion. Usually the largest part of the sea dyke surface is covered by grass. The sea side of the dyke often has stronger protection, like a block mattress or asphalt, to protect against wave attack and currents. The wave run-up and overwash during (extreme) storm events are important design parameter for sea dykes. As mentioned before, infragravity waves strongly influence the wave run-up (and potentially overwash) due to their long periods and high nearshore wave heights.

Rijkswaterstaat
Ministry of Infrastructure and the Environment

TUDelft

2.2   METEO TSUNAMI THEORY

The other type of wave included in the frequencies lower than $0,04\ Hz$ is the meteo-tsunami. They are named like this because of their meteorological origin. The meteo-tsunami is a very rare wave as the generation circumstances do not occur very often.

2.2.1   GENERATION

Meteo tsunami's are generated by rapidly propagating storm fronts (squall lines) which cause (very) large fluctuations in atmospheric pressure. These large fluctuations in atmospheric pressure are caused by strong dynamic processes in the storm, i.e. rapidly rising warm air or rapidly falling cold air. When the storm front passes, an initial low pressure air wave is followed by a high pressure air wave. These atmospheric pressure fluctuations cause a depression and rise in the water level, hence a meteo-tsunami travelling with the same velocity as the storm front is created. In deep water the meteo-tsunami does not have a very large amplitude. Due to shoaling the wave height of the meteo-tsunami could increase to several meters nearshore.

2.2.2   IMPACT

There are several reasons why meteo-tsunami's are quite dangerous. Due to their large wave heights, meteo-tsunami's form a hazard for beach users. Several records of meteo-tsunami's show that they can have casualties as a result. Also, just like infragravity waves, they can cause seiches in semi-enclosed basins, i.e. harbors/ports. Since the period of meteo-tsunami's is usually larger, they affect larger basins as well.

T̃U Delft

3 RESEARCH OBJECTIVES

The main goal of this research is to study the magnitude and the spatial/temporal distribution of long waves in the North Sea. To this end, the following research objectives are defined:

- Determine the spatial and temporal distribution of long waves in the North Sea.
- Find a relation between long waves and the mechanisms relevant for the generation of long waves.

3.1 RELEVANT MECHANISMS FOR THE GENERATION OF LONG WAVES

The results from the previous research objective will show how the long waves are distributed spatially and temporally. Why they are distributed like that and how they are generated still remains unknown. This next objective is dedicated towards finding an explanation for their generation.

In order to do so, possible long wave source(s) are studied. Several mechanisms are known to generate long waves under certain conditions (see section 2.1.1). Based on the available long wave data and, for example, meteorological and hydrological data, it should be possible to relate the local presence of long waves to a generation mechanism.

As discussed earlier in section 2.1.1 bound long waves are generated by propagating wave groups. Wave grouping is usually the result of a storm, meaning there should be a relation between certain meteorological events and the presence of bound long waves.

When moving closer to the shoreline, the short waves start breaking earlier than the accompanying bound long wave, turning the bound long wave into a free long wave (see section 2.1.3). If this wave does not break at the shoreline, it is reflected away from shore. Together with the moving breakpoint generation mechanism explained in 2.1.1, these mechanisms are responsible for the majority of free long waves being generated nearshore.

Looking at the relevant generation mechanisms, the parameters wind velocity, significant short wave height, water depth and atmospheric pressure are expected to be the main parameters behind the generation of long waves.

The following research questions will be answered to find results for this objective.

- How does the total long wave signal correspond to the following time- and spatially varying processes:
  - Wind velocity, atmospheric pressure, water depth and short waves
- What is the contribution of free- and bound long waves to the total long wave signal during varying conditions?
- Is it possible to find a relation between bound/free long wave signals with certain time- and spatially varying processes?
  - Wind velocity, atmospheric pressure, water depth and short waves

Bound long waves are the result of wave-group forcing, since wave groups are mainly or completely the result of storms, this gives rise to the expectation that long waves are (mainly) generated during heavy weather conditions.

Shorelines that are exposed to open oceans (usually) experience incoming free long waves from, for example, far away storms and shorelines (Rawat, et al., 2014). The North Sea is a basin that is almost completely surrounded by land, which gives rise to the expectation that a large part of the long wave action will be the result of local generation. Since the North sea (and especially the Dutch part of it) are relatively shallow, the wind-water interaction is quite strong. Therefore, a strong relation between meteorological events and (bound) long wave presence is expected. Previous studies (Herbers et al., 1994) show that bound long waves contribute to the total long wave spectrum with a percentage ranging from 0.07% (mild long wave energy levels) up to 30% (high long wave energy levels).

TUDelft

3.2 SPATIAL AND TEMPORAL DISTRIBUTION OF LONG WAVES IN THE NORTH SEA

Since long waves could have a large impact on coastal areas, it is important to be able to know when and where they occur. This chapter focusses on finding a relation between long wave presence and their spatial and temporal distribution. Long wave presence in the last years is therefore studied. The following questions will be answered to achieve this objective:

- How is the presence of long waves distributed in time?
  - o Is there a seasonal variation in their presence, and if so, how is it distributed?
- How is the presence of long waves distributed in space?
  - o Is there a trend in the spatial distribution of the long waves?
- Based on the (relatively short) duration of the available data, what are the possibilities of predicting extreme wave conditions?

Meteorological conditions vary considerably per season. Since meteorological conditions are major driving mechanisms for short waves, they are expected to be an important driver in long wave generation in the North Sea (see section 2.1.1). A strong variation in long wave activity is therefore most likely. Storms occur the most during seasons like fall, and in particular winter, causing the more energetic wave environments in these seasons. In general meteorological conditions, besides storms, are heavier during these two seasons. The significant wave heights and mean wave periods are expected to be higher/longer in these periods. Spring and summer are usually the more quiet seasons, with summer being the most quiet one. Less storms occur during spring and summer, and meteorological conditions are in most cases mild.

The path over which a long wave has propagated before arriving at a location, together with the spatial properties of the area in which a long wave is propagating, is of major influence on certain properties of the wave. Mainly the wave height is expected to be sensitive for spatial variation, due to processes like shoaling and refraction, see 2.1.3. Because of the effect of shoaling, the wave heights are expected to be higher nearshore. Since spatially varying properties do not influence the wave period, the mean wave period is expected to vary less.

Long waves have been measured for a certain period of time. During this period varying long wave conditions have been observed. The probability that each of these conditions has occurred, can be determined with the number of times that a specific condition has occurred within the duration of the measurement period. Based on this information it is possible to make a prediction on wave conditions with a long return period, i.e. extreme wave conditions. The reliability of such a prediction increases with an increasing duration of the measurement period. Making predictions based on the given dataset is possible, but the reliability of these predictions are strongly dependent on the total duration of the measurement period.

Rijkswaterstaat
Ministry of Infrastructure and the Environment

TU Delft

The data on which this thesis is based, is discussed in this chapter. To answer the research questions, data is required that describe the following physical phenomena:

- Long waves
- Short waves (frequency direction spectrum and energy density spectrum)
- Water level
- Meteorology (wind velocity, wind direction, atmospheric pressure)

To gather all of the required data several sources have been used. The majority of the data is provided by Rijkswaterstaat. Being an institution that plays a major role in, amongst others, water management and flood safety in the Netherlands, it has a widespread network for gathering all sorts of data on water and related topics. This network covers all of the country and its regional waters. Rijkswaterstaat has provided data on long waves, short waves and meteorology.

All data provided by Rijkswaterstaat has been collected on multiple fixed locations spread out over the North Sea. Together they cover the Dutch territorial waters, which is an area of approximately 57.000 km^2 (CBS, PBL, RIVM, WUR, 2017), see Figure 6 (left and right). The locations vary from very close to shore (practically inland) to off-shore, see Figure 6 (left).

For the data that has been measured at these stations, several properties and methods to process the data will be described in this chapter. This includes the location coordinates, measurement periods, type of measurement and processing methods (i.e. FIR filter, see 4.1.2).

The data most relevant for this research is the surface elevation data that shows long wave motions and will be discussed in paragraph 4.1. After that short wave data is discussed in paragraph 4.2, followed up by water levels in paragraph 4.3 and wind data in the paragraphs 4.4 and 4.5. The end of each paragraph concludes with describing the relevance of the data to answer the research question it is obtained for. How samples are analyzed is shown in appendix A, following the same order of parameters. Appendix B contains tables with the information on the (exact) measurement location and period per station.

1: Euro Platform

2: Lichteiland Goeree

3: Platform A12

4: Platform D15

5: Platform F16 A

6: Platform Hoorn Q1A

7: Platform J06

8: Stroommeetpaal IJmuiden
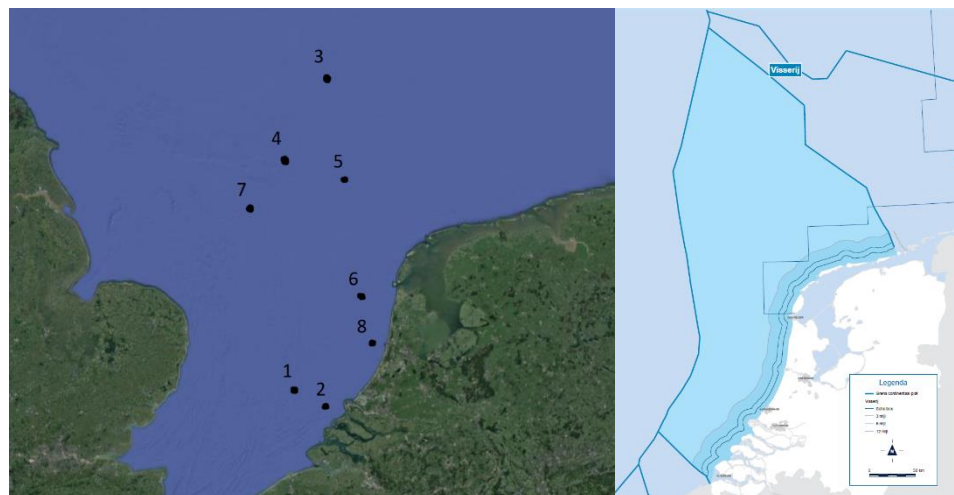
Figure 6: Left: Long wave data measurement locations (left) (Source: Google Maps). Right: Dutch territorial waters (Source: https://www.noordzeeloket.nl/functies-gebruik/visserij/)

4.1 LONG WAVE DATA

An example of the provided long wave data is shown in Figure 7. It contains data on the water level fluctuation with respect to MSL, given with a sample frequency of $0,08\ Hz$ (a data point every 12,5 seconds). In the graph of Figure 7 the tidal motion is clearly visible, it oscillates around zero with approximately two cycles every day, and has the typical skewed tidal profile. In this case the water level oscillates around 0, while for some other locations the water level oscillation is given with respect to another reference point, i.e. NAP or the frame the measurement device it is rigged to.
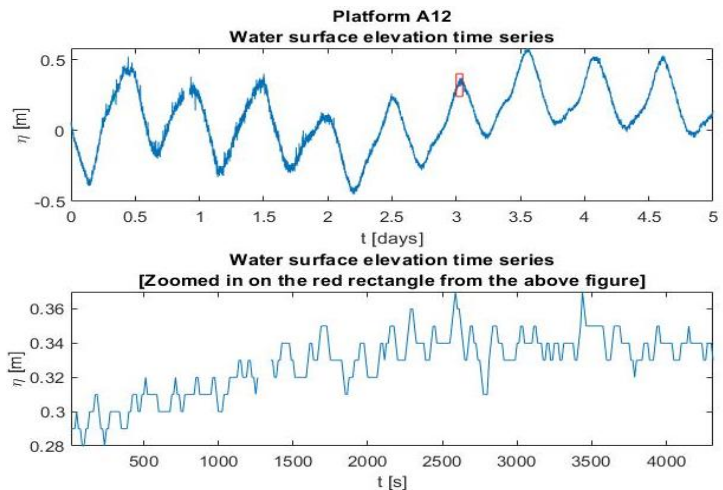
Figure 7: Water surface elevation time-series from measurement location Platform A12

Measuring the raw water surface elevation time-series is performed with a wave radar, see Figure 8. Mounted on an offshore structure the radar measures, processes and send the data to ground stations. The measurement error[4] of the wave radar is $\leq 1\ cm$.

Figure 8: Left: Wave radar used to measure the raw water surface elevation time-series (Source (official website): https://radac.nl/wave-height-tide/).

The long waves are not really visible in the above graph of Figure 7, since their height is small compared to the height of the tidal motion. To illustrate what a long wave looks like in the dataset, the lower graph is zoomed in on the time series. Wave heights up to 5 cm and wave periods of a few hundred seconds are visible in this sample. The graph does not have a smooth wave shape, which is presumably the result of the type of earlier mentioned measurement device.

4.1.1 MEASUREMENT PERIOD AND LOCATION

A list of the locations where long wave data has been recorded is given in Table 11 in appendix a, together with their measurement periods. Where they are located can be seen on the satellite image shown in Figure 6. The measurement locations are mainly off-shore locations.

---

[4] According to the manufacturer: https://radac.nl/docs/Radac_productsheet_WG5_Height&Tide.pdf

For some locations the measurements are not continuous from start to end. This could be the result of, for example, maintenance works, defective measurement equipment or for some other reason. The missing data is given below Table 11 in appendix a.

4.1.2 PROCESSING METHODS

Rijkswaterstaat has provided the long wave data. They have subjected the raw data to a FIR-filter (Kamminga, 2001), so that only long wave data remains.

Long wave data is often recorded at off-shore locations some distance away from land based data receiving stations. Sending raw data from an off-shore location to a ground station requires the broadcasting signal to have a certain capacity. In the period the recording of this data started, such a signal was not (always) available. Therefore a processing technique ((Kamminga, 2001)) was developed to filter out information and reduce the size of the data, so the capacity of the broadcasting signal would suffice. The main goal of the filter is to remove short wave information (here defined as 0,03 Hz – 1,28 Hz or 780 ms – 30 s) with a minimal error (<5%). The method will be summarized in this section.

The algorithm that reduces the data in size is based on the following assumptions:

- The data is gathered with either a radar or tide gauge
- The total frequency spectrum is characterized by low energy in the long wave frequency band (here defined as 0,083 – 8,33 mHz or 120 – 12000 s)
- Water level fluctuations are assumed to be Gaussian distributed

Subsequently, the algorithm consists of the following three steps

- Preparing data (spot outliers and filling up smaller gaps)
- Filter out short wave information (filter short waves, resample to 0,08 Hz, Fill in larger gaps)

Filtering out the short waves is done with a FIR (Finite Impulse Response) low pass filter. This filter removes high frequency motions and keeps low frequency motions in a certain frequency 'Passband'. All frequencies in this Passband are preserved with a minimal error (<5%). For increasing frequencies the error increases up to the 'Stopband', frequencies in the Stopband are removed. The Passband and Stopband frequencies are displayed in Table 1. Figure 9 shows the damping the filter causes to the relevant frequencies. In the Passband the error is very small (<5%) and grows exponentially towards the Stopband. Frequencies in the Stopband contain a very large damping. Applying the filter for small waves causes small errors ($\approx 2\ cm$ for a wave with an amplitude of 1m, which meets the <5% error criterium) to the long wave data.

Boundary	Period [s]	Frequency [Hz]
Stopband	>30	<0,0333
Passband	<120	>0,00833

Table 1 Stopband and Passband boundaries

Rijkswaterstaat
Ministry of Infrastructure and the Environment

TUDelft
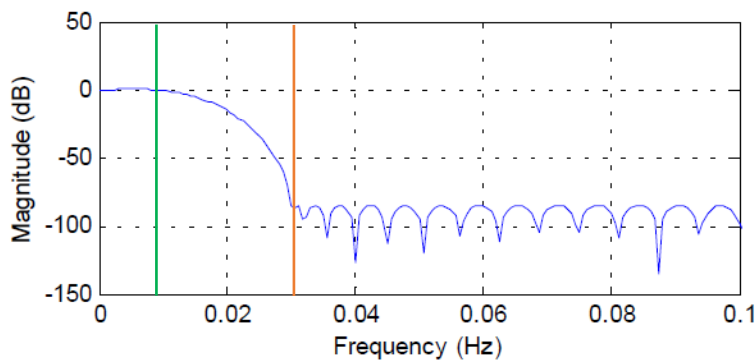
Figure 9 Graph showing the amplitude response of the applied filter to the relevant frequencies. The green line indicates the Passband, the red line indicates the Stopband (Kamminga, 2001).

4.1.3 ALTERNATIVE METHOD FOR PROCESSING MEASURED DATA

In the previous section the current method for processing long wave data has been described. In this section the consequences of applying the filter to the data are discussed, and an alternative method for processing the data is suggested.

Applying the described FIR filter to the water surface elevation time-series has the benefit that it greatly reduces the size of the data, and thereby decreases the size of the required broadcasting signal and storage capacity. The downside of applying the FIR filter is that a significant amount of information in the data is lost.

In the current situation waves with frequencies higher then $0,0125\ Hz$ are filtered out of the water surface elevation time-series, see Figure 9. A large fraction of the data on infragravity waves, which have a frequency range of $0,004 - 0,04\ Hz$, are contained in the filtered out frequencies. This means that approximately 75% of the infragravity wave frequencies are lost.

In addition to the loss of most infragravity wave frequencies, short wave information is lost as well. This means that when an energy density- and phase spectrum are composed from the water surface elevation time-series, only the long wave frequencies are taken into account. Since infragravity waves play an important role in several coastal processes, see section 2.1.4, losing a considerable fraction of infragravity wave data could mean losing some critical information. Furthermore, when the short wave frequencies are missing from the energy density- and phase spectrum, it is not possible to perform a bispectral analysis (see section 2.1.2).

When the raw data is directly stored and not subjected to the FIR filter, the frequencies higher then $0,0125\ Hz$ remain available for analysis. This has some important benefits. First of all, this opens up the opportunity of researching the majority of infragravity wave frequencies that were previously filtered out. Also, all ingredients for performing the bispectral analysis (see section 2.1.2) are then available. The bispectral analysis is capable of accurately determining the bound long wave contribution to the total long wave spectrum.

Rijkswaterstaat
Ministry of Infrastructure and the Environment

TUDelft

4.2 SHORT WAVE DATA

Data on short waves is available in various forms. For a limited amount of locations the energy density- (E(f)) and frequency direction spectra are provided. With these spectra a lot of characteristic wave properties can be determined. For most locations a time-series of the significant wave height (Hm$_0$) is provided. All short wave data is provided as an average value each 10 minutes. Short wave information is measured with either the same radar long waves have been measured with (water surface elevation), see Figure 8, or wave buoys (wave direction), see Figure 10.

Figure 10 Source (official website): www.datawell.nl/products/buoys.aspx

4.2.1 MEASUREMENT PERIOD AND LOCATION

Table 12 in appendix A shows the locations where short wave data is available. For those locations the start and end time of the measurements are given. For the locations where both short and long wave data are available, the availability of short wave data covers the whole period of long wave measurements.

4.2.2 PROCESSING METHODS

Rijkswaterstaat has processed and provided data on short waves. In this section the processing methods used by Rijkswaterstaat are analyzed. Short waves are defined by Rijkswaterstaat as waves with $0,03 < f < 0,5\ Hz$.

Short waves are being measured with a frequency of 2,56 Hz and are processed in blocks of 20 minutes. Processing starts every 10 minutes, which means each block has a 10 minute overlap with the previous and subsequent block. Processing the vertical wave motions will be discussed first, followed by processing the horizontal wave motions.

Processing the vertical motions is done to obtain the energy density spectrum and thus obtains characteristic wave parameters like the significant wave height and mean wave period. Processing starts with filtering out the tidal motion. With the tidal motion filtered out and the data subdivided in blocks, the spectral analysis follows. This calculation is summarized in the following step-by-step plan:

1. Each time series is equally distributed in 6 parts (200 s each)
2. 10% Cosine tapering is applied to each partial time series to prevent leakage in the frequency domain
3. A fast Fourier transform is applied to each tapered partial time series
4. The energy density spectrum is constructed by averaging the resulting wave height-frequency spectra
5. Filters are applied to compensate for earlier applied sensor- and tidal motion filters, varies per measurement device used
6. A 10 mHz resolution energy density spectrum (E(f)) is constructed.

In order to include wave direction in the spectrum, the process described above is performed in x, y and z direction. The obtained spectra are then used to calculate the auto-, co- and quad-spectra, which are required to calculate the Fourier coefficients. Wave directional properties are determined with these Fourier coefficients.

Several processing methods are mentioned in the metadata of the short waves. These depend on what kind of method has been used in the fifth step, as well as the type of device (often related). All methods used for the short wave data are mentioned below:

- F040;Tijdreeks en frequentie analyse, methode WAVEBA
- F041;Tijdreeks en frequentie analyse, methode GOLVEN

Rijkswaterstaat
Ministry of Infrastructure and the Environment

TU Delft

- F042;Tijdreeks en frequentie analyse, methode CIC/MAREG
- F043;Tijdreeks en frequentie analyse, methode CIC/GLFPAR
- F045;Frequentie analyse energie en richting, methode WAVDIR
- F046;Freq/tijd analyse energie en richtingen, methode CIC/GLFPAR

Rijkswaterstaat subtracted and provided the following parameters from the results of the performed spectral analysis:

- Significant wave height (H_{m0} [m])
- Energy density spectrum ($E(f)$)
- Frequency direction spectrum and directional spreading ($\theta(f), and\ \sigma_\theta(f)$)

Calculating the significant wave height is done with the below formulas.

$$m_n = \int_0^\infty f^n E(f) df$$

The lower and upper boundaries of the integral are equal to the short wave frequency band boundaries:

$$0,03\ Hz \leq f \leq 0,5\ Hz$$

Since we are taking the 0th order moment $n = 0$, resulting in:

$$m_0 = \int_{0,03}^{0,5} E(f) df$$

$$H_{m0} = 4\sqrt{m_0}$$

Following up on the vertical wave motions, the processing method of the horizontal wave motions will now be discussed. The horizontal motions are processed to obtain the frequency direction spectrum, and thus obtain the directional properties of short waves.

Processing the horizontal wave motions starts with composing 9 spectra ($C_{zz}, C_{xx}, C_{yy}, C_{zx}, C_{zy}, C_{xy}, Q_{zx}, Q_{zy}, Q_{xy}$) analogous to the energy density spectrum derived above; three auto-spectra, three co-spectra and three quad-spectra. These are used to determine four Fourier components;

$$A_1(f) = \frac{Q_{zx}(f)}{W(f)C_{zz}(f)}$$

$$A_2(f) = \frac{C_{xx}(f) - C_{yy}(f)}{C_{xx}(f) - C_{yy}(f)}$$

$$B_1(f) = \frac{Q_{zy}(f)}{W(f)C_{zz}(f)}$$

$$B_2(f) = \frac{2C_{xy}(f)}{C_{xx}(f) + C_{yy}(f)}$$

Based on these coefficient the direction and directional spreading are then determined;

$$\tan(\bar\theta_0) = \frac{-\overline{A_1}}{-\overline{B_1}}$$

$$\bar\sigma = \sqrt{2\left(1 - \sqrt{\frac{1}{\overline{A_1}^2 + \overline{B_1}^2}}\right)}$$

Rijkswaterstaat
Ministry of Infrastructure and the Environment

TUDelft

4.2.3 DATA EXAMPLES

The main application of short wave data will be to assess the contribution of bound long waves to the total long wave signal (see 2.1.2). For this analysis the short wave directional energy density spectrum is required. This spectrum is computed based on the energy density spectrum and wave directional information shown in Figure 12. Not only does the short wave directional energy density spectrum contain data which can be used to determine the bound long waves, it also contains data regarding infragravity waves. Starting from a frequency of 0 Hz and reaching up to approximately 1 Hz the spectrum covers a wide variety of waves. The short wave energy density spectrum therefore also contains some long wave information which could be used as a complement to the long wave data from paragraph 4.1. It regards the frequencies $0,0125\ Hz$ (where long wave data ends) up to $0,04\ Hz$, see Figure 11.
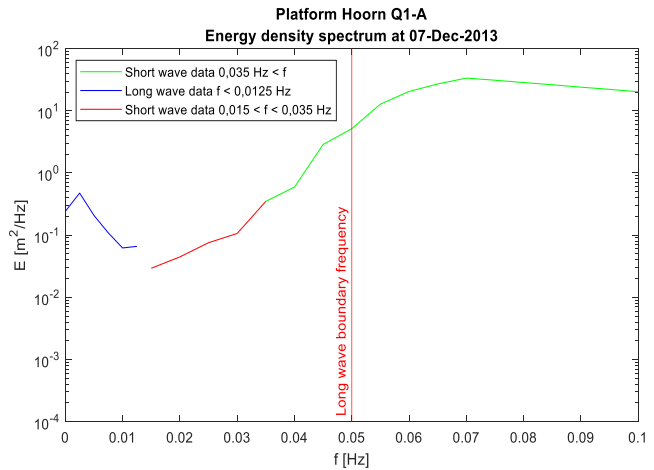
Figure 11 Energy density spectrum of the available long wave frequencies from both the long wave data and short wave data
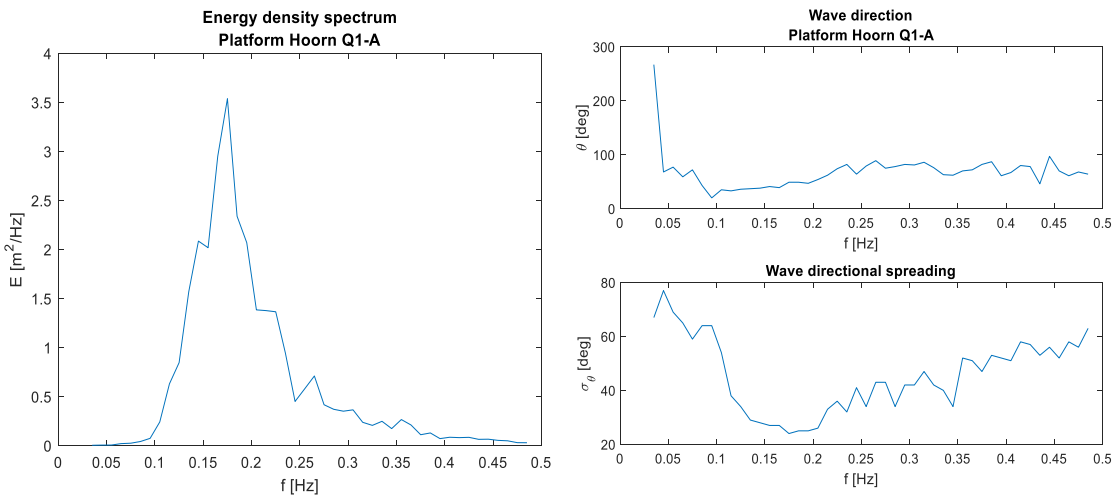
Figure 12 Left: Short wave energy density spectrum. Right: Short wave frequency direction, and frequency directional spreading spectrum

4.3 WATER LEVEL DATA

Data on the water level is given with respect to either MSL or NAP. Both are approximately equal to the average water depth. See Table 2 of average water depth per measurement station. The water level data shows the water level with respect to either of the two reference points in centimeters. Water level data is provided as the average value over 10 minutes.

No.	Naam	Coordinates [WGS84]	Depth [m]
1	Europlatform	3,25 ; 52,03	32,86
2	Lichteiland Goeree	3,76 ; 51,93	16,34
3	Platform A12	3,48 ; 55,23	27,95
4	Platform D15	2,56 ; 54,19	46,40
5	Platform F16 A	4,00 ; 52,93	47,08
6	Platform Hoorn Q 1A	4,15 ; 52,93	25,52
7	Platform J06	2,20 ; 53,80	33,30
8	Stroommeetpaal IJmond	4,52 ; 52,46	15,55

Table 2 Average water depths of measurement stations

4.3.1 MEASUREMENT PERIOD AND LOCATION

The locations and their respective measurement periods are given in Table 15 in appendix A. Missing data is given below that table.

Rijkswaterstaat
Ministry of Infrastructure and the Environment

TUDelft

4.4 WIND DATA

The data describing wind is divided in two parts. One file describes the wind velocity in meters per second, the other shows the mean wind direction given in degrees with respect to some reference point. Wind data is provided as the average value over 10 minutes.

4.4.1 MEASUREMENT PERIOD AND LOCATION

Table 16 in appendix A shows the availability of both the wind velocity- and direction..

4.4.2 PROCESSING METHOD

The wind velocity and direction are measured with Anemometer and a wind direction sensor respectively. The data processing requires less computational effort compared to the short- and long waves. For both parameters the scalar average over the past 10 minutes is taken.

Figure 13 Left: Wind direction sensor. Right: Anemometer. Source (official website): https://www.knmi.nl/kennis-en-datacentrum/achtergrond/recent-developments-in-knmi-s-surface-observing-methods

4.4.3 DATA EXAMPLES

Wind data is mainly used to evaluate the relation between storms and bound long wave generation. An example of how the wind velocity and wind direction is given in Figure 14.
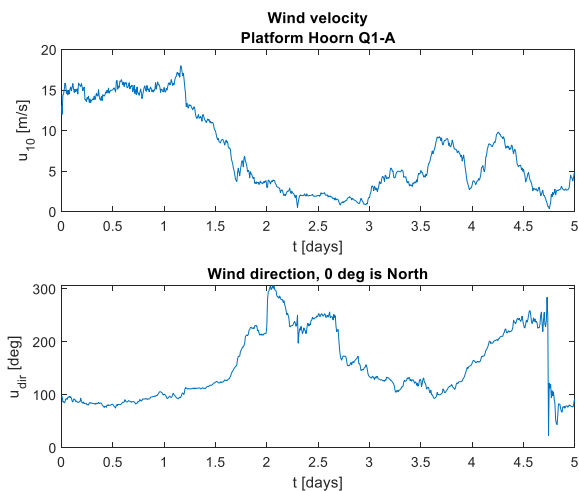
Figure 14 Upper: Wind velocity. Lower: Wind direction.

Rijkswaterstaat
Ministry of Infrastructure and the Environment

TUDelft

4.5   ATMOSPHERIC PRESSURE DATA

The pressure exerted on a surface by an atmospheric column of air is called the atmospheric pressure. Atmospheric pressure is strongly related with wind and shows large variations during storms. Data obtained on this phenomenon is measured and processed by a collaboration between Rijkswaterstaat and KNMI, and provided by the KNMI. Atmospheric pressure data is provided as the average value over 10 minutes.

4.5.1   MEASUREMENT PERIOD AND LOCATION

Table 17 in appendix A shows the availability of atmospheric pressure data.

4.5.2   DATA EXAMPLES

The atmospheric pressure data is used to study a possible relation with bound long waves. An example of the time-series is shown in Figure 15.
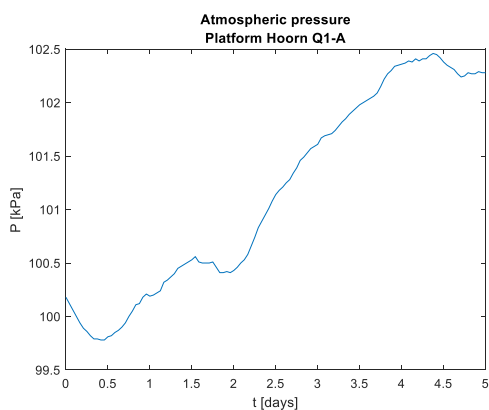
Figure 15 Atmospheric pressure time-series

An overview of which type of data is provided per location is shown in Table 3. All types of data cover at least the period of the years 2009 to 2019.

Location	Short waves (H_{m_0})	Short waves $(E(f))$	Short waves $(\theta(f))$	Water level $(h(m))$	Wind $(u_{10}(m/s)$, $u_{10}(\theta))$	Atmospheric pressure $(p(Pa))$
Europlatform	√			√	√	√
Lichteiland Goeree	√			√	√	√
Platform A12	√	√	√	√	√	√
Platform D15	√			√	√	√
Platform F16 A	√			√	√	√
Platform Hoorn Q 1A	√	√	√	√	√	√
Platform J06	√			√	√	√
Stroommeetpaal IJmuiden	√			√		

Table 3 Overview of available data per location

Rijkswaterstaat
Ministry of Infrastructure and the Environment

TUDelft

In this chapter the approach and methods used to find results for these research objectives are described.

5.1 POSTPROCESSING

For all research questions, the raw long wave data needs to processed to data suitable for analysis. This process is called postprocessing and is described in this chapter.

5.1.1 DATA FILTERING

The data (depicted in the left graph in Figure 16) shows the surface elevation time-series. The vertical lines in the graph are errors, which are denoted by the value 99.999. The first operation to be performed with the data is to remove these errors with a filter. This filter reads the data in blocks of half an hour and replaces error values by NaN values, for small gaps in the data the NaN values are replaced by linear interpolation between nearby points. In this case, small gaps are defined as a maximum of 3 consecutive errors, which is equal to 50 s of missing data. Applying linear interpolation for longer periods would create unjustifiable data. Whenever more than 3 errors occur subsequently, or whenever 10% or more of a certain data block is an error, that specific block is entirely deleted. An example of the conversion from raw to filtered data is shown in Figure 16 (the left graph is made from the initial data, the right graph from filtered data).
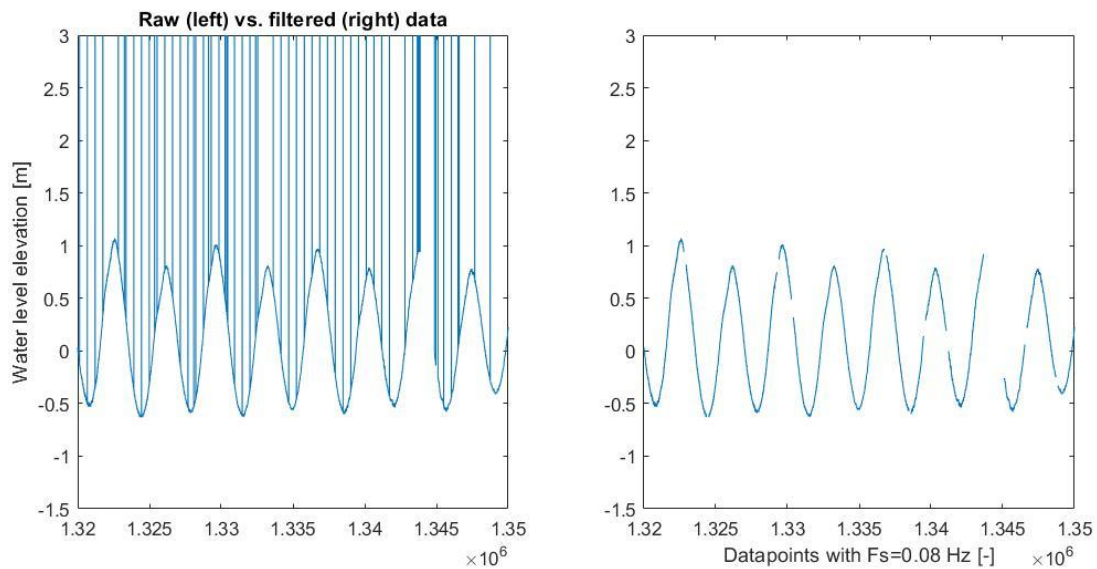
Figure 16 Initial- (left) vs. filtered (right) data

The errors in the data that are denoted by 99.999, are errors that have been noticed by the algorithm from Rijkswaterstaat that processed the initial data. Unfortunately these are not all errors present. Other types of errors are present as well, for an impression, see Figure 17. What makes these errors tricky is that they look like regular waves (when zooming in they show a sine-like shape). The difference with the actual long waves is that they have an extremely high wave height, and are only present on top of MSL (only peaks, no trough) or below MSL (only trough, no peak). These wave-like errors would cause incorrect results when

Figure 17 Impression of errors still present in data after applying the filter

incorporated in the computations, therefore they are filtered from the data.

Because these waves only shows peaks or troughs with respect to MSL, spotting and removing them is relatively easy. After the removal of the errors with the value of 99.999, the surface elevation per block is detrended. The detrended time-series is then used to calculate the absolute value of the minimum and maximum value of the data in the block. Whenever the absolute value of the maximum or minimum is a factor 5 larger than the other, the data in the whole block is replaced by NaN values.

5.1.2 SUBDIVIDING DATA

For the time-series/spectral analysis time-series per location will be divided into wave records over which the calculation will be performed. These wave records should be short enough so they can be considered stationary, but also as long as possible to increase reliability (Holthuijsen, 2007). In section 4.1.2 the frequency range of the long wave data has been determined at $\approx 0 - 0,0125\,Hz$. The aim of this section is to obtain a reliable frequency resolution of approximately $0,005\,Hz$ to accurately represent the data. How this is done is described below.

Starting off with the stationarity criterium. Data in a certain time interval is considered stationary when the statistical properties (i.e. mean and variance) more or less stay the same. To determine how long such an interval needs to be, the filtered data is used. This data is detrended, which means the mean has been removed. In order to be stationary, the variance should thus be more or less the same during a certain time interval.

Energetic wave events are the most varying, and also most interesting ones. A (heavy) storm will therefore be analyzed to determine the desired block length, see Figure 18, Figure 19 and Figure 21. Figure 18 shows a 10 day sample of the data, containing regular conditions (day $0 - 4$ and $6 - 10$) and a storm (day $4 - 6$). During regular conditions the standard deviation is more or less constant, confirming that these are the less interesting events. During a storm on the other hand, the standard deviation increases rapidly. A zoomed in picture of the storm showing the variance is displayed in Figure 19.
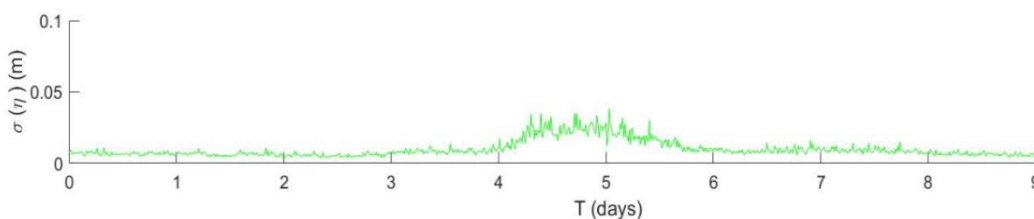
Figure 18 Wave surface elevation variance of a 9 day sample from the long wave data, containing a (heavy) storm. Blocks of 1 hour are used
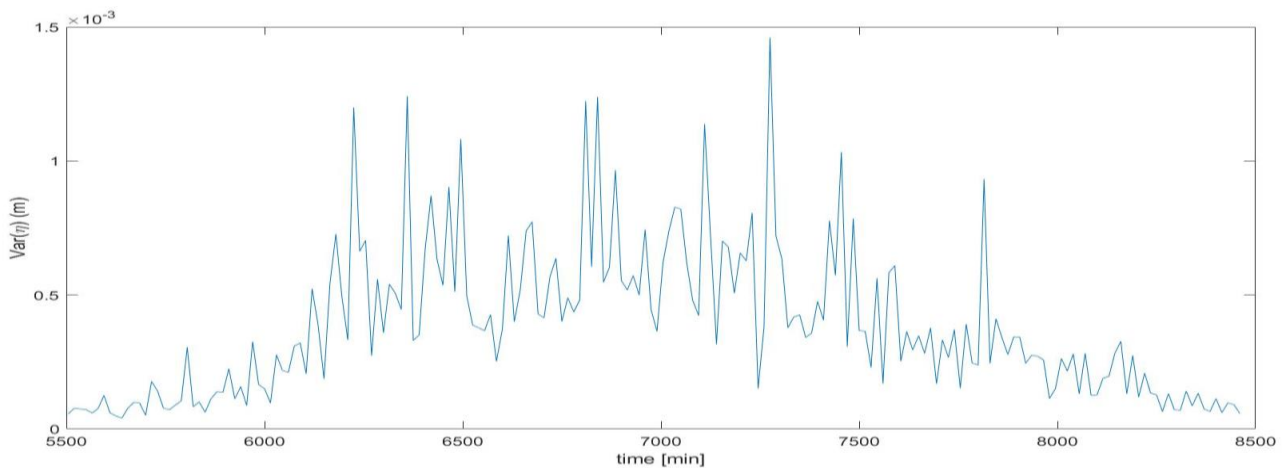
Figure 19 The storm shown in Figure 18, zoomed in on the storm from day 4 to 6. $Variance = \sigma^2$

In order to find out which time interval is more or less stationary during a storm, several time intervals have been visually inspected. The results of which are shown in Figure 21. The two hour intervals still have quite some variance in between each interval, making it an unsuitable interval duration for the analysis. Decreasing the block length by taking half of it already makes quite a difference. A lot of intervals show relatively constant variance levels, while others show strong variations. Overall the one hour interval should be fairly stationary. By again taking half of the duration, the interval duration has decreased to half an hour. Again the amount of intervals with relatively constant levels has increased, but still some intervals with significant variance are present.

Because of the strong variance during a storm, decreasing the interval duration until a point has been reached where all time intervals have more or less constant variance levels, would require a drastic decrease of the wave record duration. Since the wave record duration is related to the reliability of the calculation, a further decrease of the wave record duration is not desirable. In the following section the reliability criterium is tested.

Increasing the wave record duration means increasing the amount of measurements being taken into account for the analysis, and thus increasing the reliability. The mathematical relation between the wave record duration and obtained frequency resolution is given below:

$$\Delta f = \frac{1}{D}$$

Composing a spectral analysis based on one wave record, results in a very 'grassy' spectrum (Holthuijsen, 2007). A wave record is therefore subdivided into a certain amount (p) of blocks over which the spectral analysis is performed. The frequency resolution relation changes into:

$$\delta f = p\Delta f = \frac{p}{D}$$

41

The wave record is then composed based on the average of these blocks, increasing the records reliability. How the increase of reliability is quantified is shown in Figure 20. The two curves represent the upper- (CI_{upper}) and lower (CI_{lower}) confidence intervals, which grow towards the value 1 (=exact) with an increasing amount of blocks. An 'economic optimum' is found at 48 degrees of freedom ($p = 9$).

Looking back at the desired frequency resolution of $\delta f \approx 0,005\ Hz$, this results in a block length of 1 hour ($\delta f = \frac{9}{3600} = 0,0025\ Hz$).
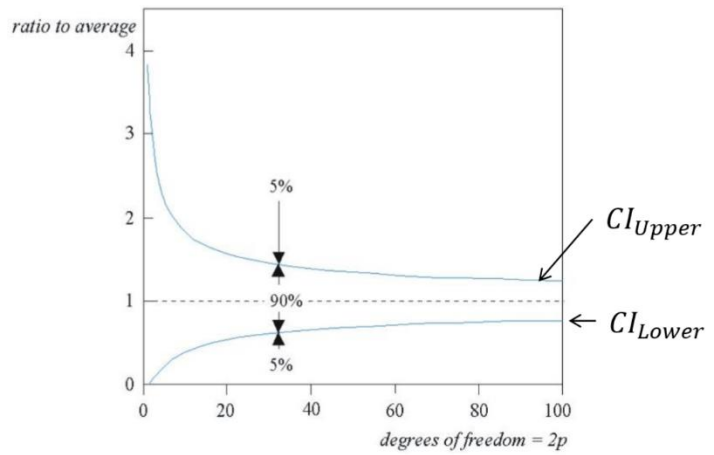
Figure 20 Size of 90% confidence interval for varying degrees of freedom (Holthuijsen, 2007)

Type of data	Measuring frequency (f [Hz])	Wave record duration (D [s])	Number of blocks (p [$-$])	Overlap between blocks [%]	Frequency resolution (δf [Hz])
Long waves	0,08	3600	9	50	0,0025

Table 4 Computational settings used for long wave data analysis

TUDelft
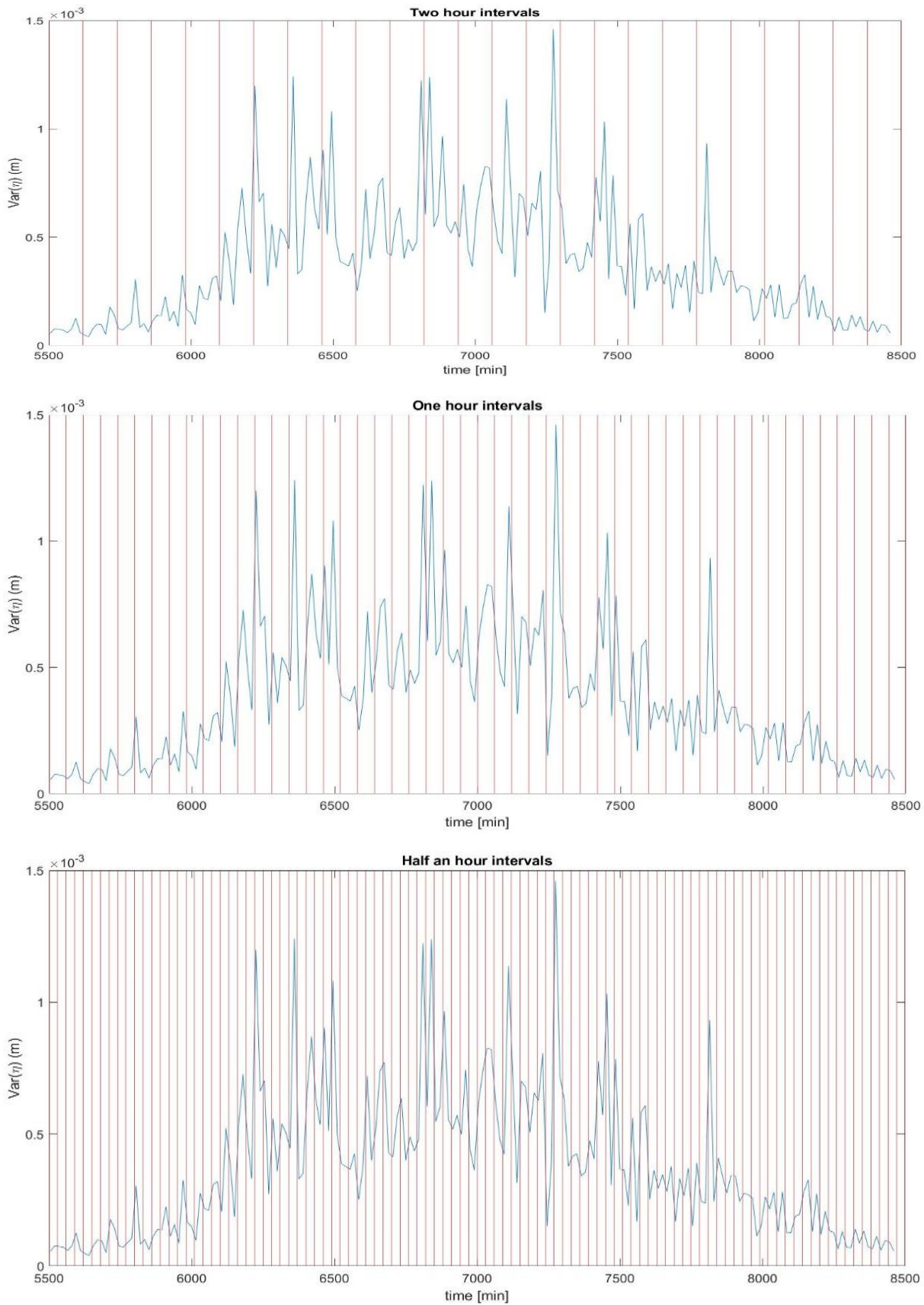
Figure 21 The storm shown in Figure 19, with intervals annotated by vertical red stripes. The figure contains 30 minute intervals (lower graph), 1 hour intervals (middle graph), 2 hour intervals (upper graph) for visual inspection of the stationarity during a storm.

5.2   GENERATION MECHANISMS

Long waves are mainly generated during storms, see 2.1.1. Observations of long waves at the measurement locations can be used to relate long wave activity to possible sources, by comparing the long wave activity to, for example, meteorological conditions. If observations of high long wave activity correspond to a nearby storm, the relation between the magnitude of the storm and the magnitude of the wave activity can be studied. This regards the study of, for example, the intensity of the storm and its influence on the resulting wave heights and periods. Performing the above analysis for varying situations gives more insight into the relation of a storm to the long wave signal. Not only the relation with meteorological conditions will be studied, the relation with hydrological conditions, like storm surge or short waves, will be studied as well.

5.2.1   CORRELATION COEFFICIENT

The correlation between the (bound) significant long wave height and other parameters is determined by means of the coefficient of determination, which is equal to the Pearson correlation coefficient squared. The equation is found below:

$$r^2(A,B) = \left(\frac{1}{N-1} \sum_{i=1}^{N} \left(\frac{A_i - \mu_A}{\sigma_A} \right) \left(\frac{B_i - \mu_B}{\sigma_B} \right) \right)^2$$

5.2.2   LONG WAVES

Long wave activity is known for being most energetic during storms and heavy meteorological conditions, see 2.1.1, which is the reason why the focus of this analysis will be on mainly those periods. The parameters that are involved in both long wave generation (see 2.1.1) and storms, will be compared to long wave activity. These parameters are:

- Wind velocity u_{10} $[m/s]$
- Wind direction [deg]
- Atmospheric pressure p $[Pa]$
- Short waves H_s $[m]$
- Storm surge h_S [m]

The last parameters, storm surge, is determined with the water surface elevation time-series and the Godin filter. This is a low-pass filter that retrieves the tide from the water surface elevation time-series (Godin, 1972).

As described earlier in sections 4.1.2 and 4.2.3 long wave data is contained in both the long wave data and the low frequency part of the short wave data. Together they span the frequencies $0 < f < 0.05\ Hz$. Three frequency classes are distinguished:

- Class 1: $0 \leq f \leq 15\ mHz$
- Class 2: $15 \leq f \leq 35\ mHz$
- Class 3: $35 \leq f \leq 50\ mHz$

The analysis will be performed for the long wave data (frequency class 1), and the long wave data complemented by frequency class 2. Frequency class 3 will not be used since this frequency class often contains short wave information (most likely long period swell), see Figure 22.

In Figure 22 the energy density spectra during and before a storm are shown. In the graph before the storm (the left graph, mild/regular conditions) short waves above the long wave frequency boundary reach up to approximately $0.3\ m^2/Hz$, and have their peak at $f = 0.15\ Hz$. During the storm (heavy conditions) short wave energy reaches up to $50\ m^2/Hz$, which is a factor 167 higher. Also, the peak has shifted towards the long wave frequency boundary, most likely due to the net effect of wind input, white capping and quadruplet wave-wave interactions (Holthuijsen, 2007). Which means the waves in the long wave frequency band are actually short waves shifted towards lower frequencies

Rijkswaterstaat
Ministry of Infrastructure and the Environment

TU Delft

due to the heavy storm conditions. The waves of interest, infragravity waves, are generated by the mechanisms explained in section 2.1.1. This means that frequency class 3 is not of interest during these storm conditions, since the waves in that frequency band are generated by another mechanism. The analysis is therefore performed only with frequency class 1 and 2.
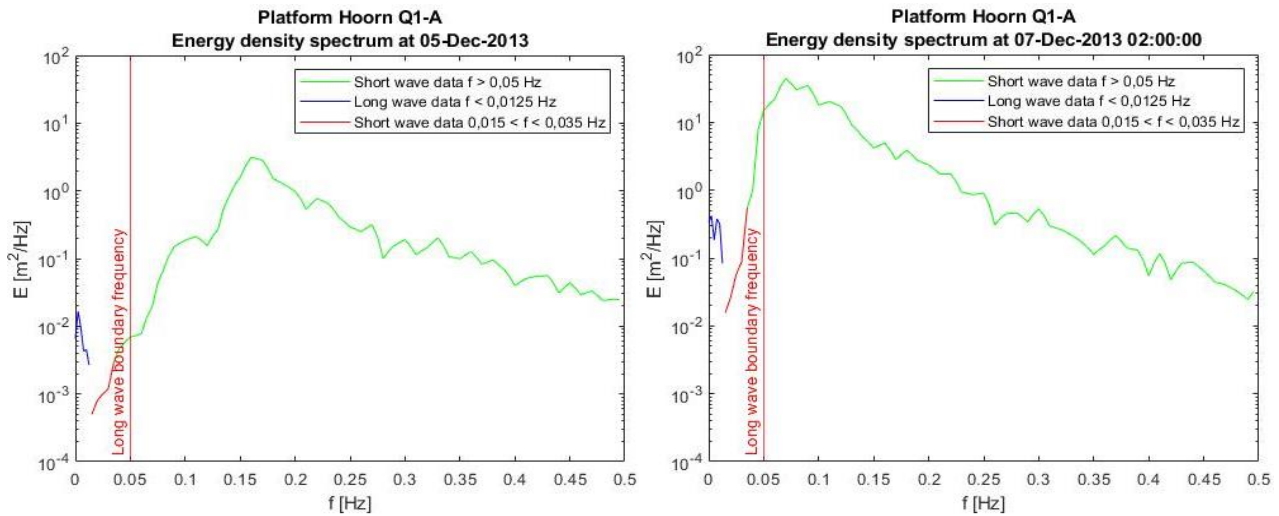
Figure 22 Energy density spectra of the (complemented) long wave data. Before (left, mild conditions) and during (right, storm conditions) the storm.

Comparing the time-series of the long wave signal with the time-series of the abovementioned parameters gives an impression of how they are related, but not a quantifiable relation. In order to arrive at a quantification of the relation between the long wave signal and the compared parameters, a scatter plot in combination with correlation coefficients is used. A scatter plot displays the values of two variables plotted against each other and gives an visual representation of how the variables are correlated. The correlation coefficient then quantifies this relation.

5.2.3   BOUND LONG WAVE PREDICTIONS

Whether a long wave is bound to shorter waves can be determined by examining several properties. The method used to predict bound long waves is Hasselmann's second order non-linear theory (see section 2.1.2). With the results of the bound long wave predictions, it is possible to study the behavior of bound waves under certain conditions. Since bound waves are bound to wave groups, which in its turn are created by heavy weather conditions/storm, their behavior will be studied under various conditions of wind (velocity), atmospheric pressure, storm surge and short wave activity. With Hasselmann's theory bound long waves can be determined for frequencies from 0,005 Hz to 0,05 Hz. This means the frequency intervals 0,005 − 0,0125 Hz and 0,015 − 0,035 Hz contain both the observed long waves and bound long waves, see 4.2.3.

After the study of the relation between the bound long waves and parameters relevant for their generation, a study of the relative contribution of bound long waves to the total long wave activity will be studied. In order to do so the bound long wave frequency interval $0,005 - 0,0125 \, Hz$ will be subjected to the same FIR filter as the long wave data has been subjected to, see section 4.1.2. The 'relative' contribution of bound long waves to the total long wave activity is defined as:

$$\%_{blw} = \frac{E_{blw}}{E_{lw}} * 100$$

The computation is performed over the full length of the available data, which means it runs from 2-2-2009 until 26-4-2019, which is approximately 10 years.

Rijkswaterstaat
Ministry of Infrastructure and the Environment

TUDelft

5.3 LONG WAVE PRESENCE IN THE NORTH SEA

In this chapter the approach of the long wave data spatial- and temporal analysis will be presented.

The period over which the data has been recorded covers approximately 10 years. Running all locations over their full length would require a lot of computational time, data from each location is therefore first processed for one year to get a general impression of the wave climate in the North Sea. To include seasonal variation of the wave climate, this year is divided into seasons. After performing the one year run, a probability- and cumulative distribution function are determined. These functions are then compared to certain probabilistic distribution types to find a good fit. These functions can then be extrapolated to determine extreme wave conditions with a certain confidence interval.

This chapter will include:

- A short (one year) run for all measurement locations
- An analysis of those locations and selecting some of the most relevant measurement locations
- An in-depth analysis of long runs

5.3.1 SPATIAL AND TEMPORAL DISTRIBUTION OF LONG WAVES

For the analysis of the spatial and temporal distribution, the results of the spectral analysis are used, this regards the obtained significant wave heights and mean wave periods. For the spatial and temporal distribution data from the year 2013 is taken.

For the analysis of the spatial distribution a probability function is composed for both the significant wave height and mean wave period per location over the full year 2013. The probability functions of all location are then compared to study the spatial variation.

In the analysis of the temporal distribution the data is sorted per season, meaning it is divided into 4 blocks per year. Each block represents one season, where the seasons contain the following months:

- Winter: December, January and February
- Spring: March, April and May
- Summer: June, July and August
- Fall: September, October and November

The probability functions for the significant wave height and mean wave period are then determined per location and per season. The probability functions of all locations are then studied per season to study the temporal variation.

5.3.2 EXTREME LONG WAVE CONDITIONS

Spectral analysis of all available data per location results in a significant wave height per wave record, which in this case is each hour, see section 5.1.2. When a probability- or cumulative distribution function of all of these significant wave heights is composed, the probability of occurrence of all significant wave heights during that time span can be determined. The composed probability- and cumulative distribution functions of the significant wave heights have a certain shape, that shape can be mimicked by setting the parameters of matching probabilistic distribution types to the right values. When the set of parameters of a probabilistic distribution is found that mimics the original data with the smallest error, the 'best fit' of that probabilistic distribution type has been found. The process of finding this best fit is called curve fitting. Several probabilistic distribution types that are well known for being a good representative of significant wave heights will be used for this process:

- Weibull distribution
- Exponential distribution
- Gumbel distribution.

Rijkswaterstaat
Ministry of Infrastructure and the Environment

TU Delft

The advantage of finding a best fit to the data is that the best fit approximation can be extrapolated to approximate the probabilities of extreme significant wave heights, whereas extrapolation is not possible for the original data of significant wave heights.

The equations for the cumulative distribution functions of the probabilistic distribution types, and their parameters, are given below.

Weibull distribution

$$P = 1 - \exp\left(-\left(\frac{H_{ss} - \gamma}{\beta}\right)^{\alpha}\right)$$

$$\beta = \frac{\sigma_{Hss}}{\sqrt{\Gamma\left(1 + \frac{2}{\alpha}\right) - \left[\Gamma(1 + \frac{2}{\alpha})\right]^2}}$$

$$\gamma = \overline{H_{ss}} - \beta * \Gamma\left(1 + \frac{2}{\alpha}\right)$$

Exponential distribution

$$P = 1 - \exp\left(-\left(\frac{H_{ss} - \gamma}{\beta}\right)\right)$$

$$\beta = \sigma_{Hss}$$

$$\gamma = \overline{H_{ss}} - \beta$$

Gumbel distribution

$$P = \exp\left(-exp\left(-\left(\frac{H_{ss} - \gamma}{\beta}\right)\right)\right)$$

$$\beta = \sigma_{Hss} \frac{\sqrt{6}}{\pi}$$

$$\gamma = \overline{H_{ss}} - \epsilon * \beta$$

$$H_{ss} = Significant\ wave\ heights\ that\ exceed\ a\ certain\ threshold\ (= top\ 1\%\ of\ H_s)\ [m]$$

$$\alpha, \beta, \gamma = Probabilistic\ distribution\ parameters\ [-]$$

$$\epsilon = Euler - Mascheroni\ constant = 0,5772\ ...$$

In order to find 'the best fit', the cumulative distribution function is compared to the three abovementioned probabilistic distribution functions. The best fit parameters of the probabilistic distribution types are determined in either a iterative process (α parameters), or calculated with the above given formulas (α and β parameters). For each probabilistic distribution type the MSE is calculated with the cumulative distribution function. The best fit is determined as the probabilistic distribution type with the smallest MSE.

The cumulative distribution function 'P' can be seen as the non-exceedance function. By transforming this to the exceedance function 'Q' , the return period function 'R' can be determined. The R is then extrapolated to predict the extreme long wave conditions.

$$Q = 1 - P \qquad R = \frac{1}{Q * N_s}$$

Rijkswaterstaat
Ministry of Infrastructure and the Environment

TUDelft

6 RELEVANT MECHANISMS FOR THE GENERATION OF LONG WAVES

Storms are expected to coincide with more energetic long waves (Bertin, et al., 2018), since the conditions during a storm are favorable for long wave generation. This chapter is dedicated to finding the mechanisms most relevant for long wave generation in the North Sea.

Studying the relation between the long waves and their expected forcing conditions starts with looking at the time-series of the parameters relevant for long wave generation and the significant long wave height during certain storms. Looking at how the time-series of these parameters evolve during a storm provides a qualitative description of their relation. After the time-series analysis, data from the full measurement period is used to quantify the relation between long wave activity and the relevant parameters.

The observed long wave signal may consist of both free and bound long waves. The relative contribution of both free and bound long waves to the signal could tell a lot about the relevant generation mechanisms at that location. Bound waves are generated by the mechanisms explained in section 2.1.1, whereas free waves are generated by the mechanism explained in section 2.1.1 and 2.1.3, or perhaps even other mechanisms that cause water level fluctuations in the long wave frequency band.

Rijkswaterstaat
Ministry of Infrastructure and the Environment

T U Delft

6.1 LONG WAVES

The first event to be analyzed is the period of 5-8 December 2013, also referred to as the Sinterklaas storm. This storm is the heaviest storm recorded at the stations during the period of 2009-2019 in terms of wind velocities, significant short wave heights and storm surge levels. The time-series of all parameters are displayed in Figure 23. Unfortunately some of the long wave data during the storm is missing, which makes the analysis less comprehensive, but still valuable.

At both locations the significant long wave height ($0 < f < 0,015\ Hz$) rises up to approximately 30cm. The complemented significant long wave height ($0 < f < 0,035\ Hz$) rises up to approximately 50 cm at Platform A12 and up to approximately 40 cm at Platform Hoorn Q1A, meaning there is quite some energy contained in the frequency band $0,035 < f < 0,05\ Hz$.

The graphs show a trend in which the significant long wave height increases with increasing significant short wave height, wind velocity and water depth. When looking at the milder conditions before or after the storm, mild long wave conditions seem to correspond to lower values for the significant short wave height, wind velocity and water depth. Seeing these 4 variables increase and decrease during the same periods indicates a relation between them. The atmospheric pressure is more or less constant during the whole period, which implies it is independent of the other variables.

It appears that the wind velocity is the first parameter that increases during a storm, together with a decrease of the atmospheric pressure. This makes sense, since a storm is defined by meteorological conditions. Shortly after the variation of these two meteorological conditions, the significant short wave height starts increasing. This corresponds to the fetch and duration that is required in order to generate short waves. Long wave generation involves, amongst others, short waves (see section 2.1.1). Accordingly, the increase of the significant long wave height starts almost together with the increase of the significant short wave height.

At the start of the storm wind is blowing from the West direction, but then rapidly turns to blowing from the Northwest direction. The peak in wind velocity occurs at the start of the storm when wind is blowing from the West, but does not coincide with the peak in short and long wave significant long wave heights. When the wind direction changes from blowing from West to Northwest direction, the peak in short- and significant long wave height is reached. This is the result of a considerable increase in fetch when the wind turns from West to Northwest direction.

Storm surge levels at both locations experience a similar development. The increase in storm surge level starts at approximately the same time, and the graphs have approximately the same shape. A significant difference between the two is that the maximum storm surge level at Platform Hoorn Q1A is approximately twice the size of the storm surge level at Platform A12. Platform Hoorn Q1A's location is located much closer to the downwind coastline. Storm surge starts at the downwind coastline and gradually decreases in upwind direction, causing the large difference in storm surge levels at Platform A12 and Platform Hoorn Q1A. The value for the significant long wave height during the peak of the storm surge is higher at Platform A12 (=50 cm), with a difference of 15 cm with respect to Platform Hoorn Q1A.

Data from this storm suggests that the forcing mechanism where long waves are generated by short waves, see 2.1.1, is an important driving mechanism for long waves during a storm. Since short waves are generated by wind, and the magnitude of the short wave height depends on the fetch, wind in combination with wind direction are important indicators for long wave activity.

Rijkswaterstaat
Ministry of Infrastructure and the
Environment

TUDelft
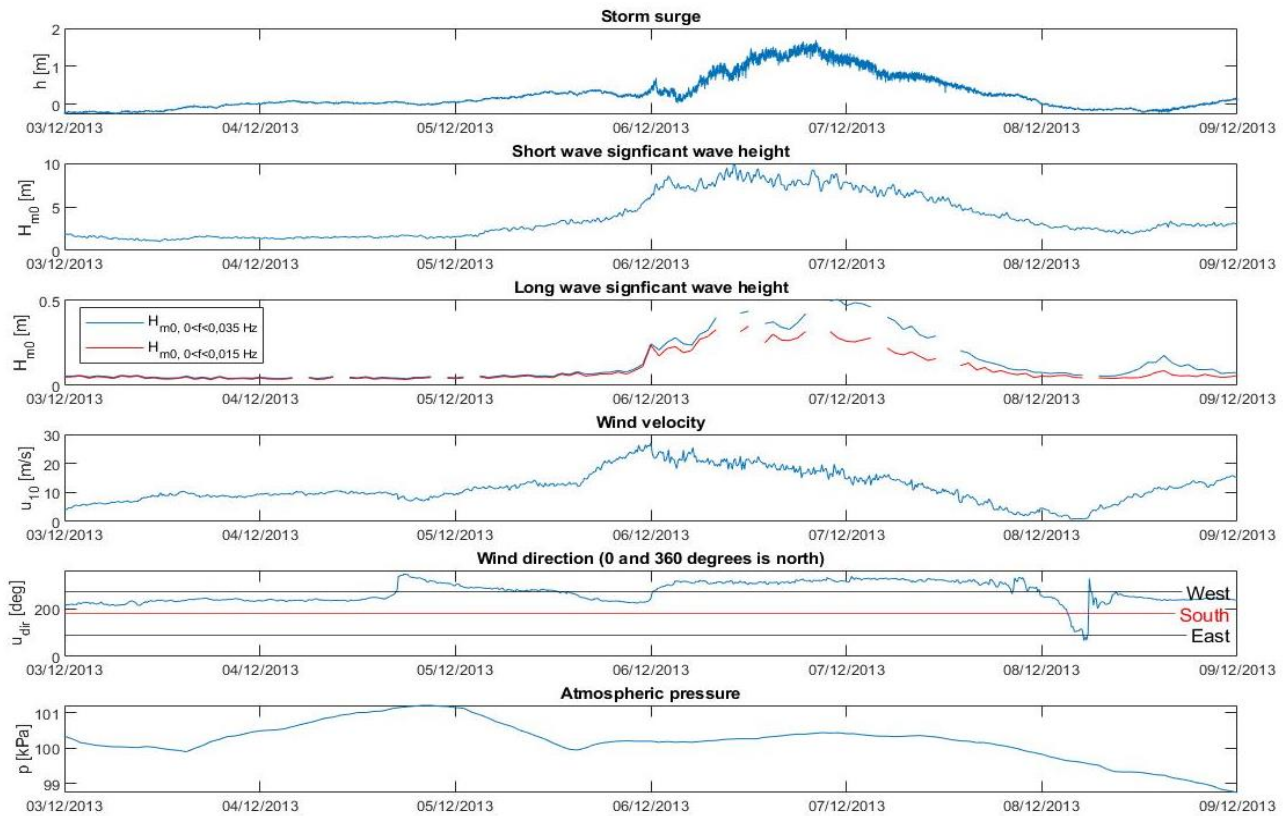
Figure 23 Graphs of the long wave significant wave height and other variables during the Sinterklaas storm of 2013 at the locations Platform Hoorn Q1A and Platform A12. They show the time-series of the storm surge level, short wave significant wave height, long wave significant wave height, wind velocity and atmospheric pressure. In the third graph the long wave significant wave height and the complemented long wave significant wave height (frequency class 1 and 2, see section 4.2.3) are displayed separately

TUDelft

The strongest correlation between the significant long wave height and the parameters, is with the significant short wave height, see Figure 24. With the coefficient of determination varying from 0,75 to 0,9, the correlation is strong. The storm surge level shows a slightly weaker but still strong correlation with the significant long wave height, with the coefficient of determination varying from 0,57 to 0,8. A medium to weak correlation is found between the significant long wave height and the wind velocity, with the coefficient of determination varying from 0,21 to 0,47. There appears to be no correlation at all with the atmospheric pressure, the coefficient of determination is 0.

The lower long wave frequency class shows the highest correlation with the parameters in all scatter plots of Figure 24.
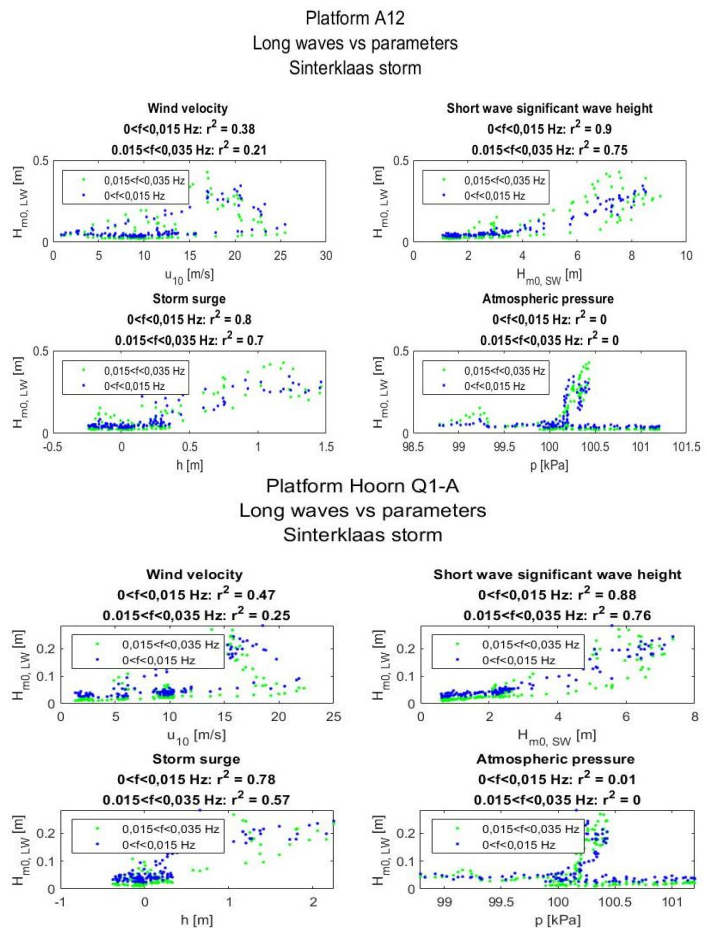
Figure 24 Scatter plots showing the relation between the long waves and the other parameters for the Sinterklaas storm for both long wave frequency classes.

Another storm that is analyzed is the summer storm which occurred in July 2015, see Figure 25. The graphs are organized in the same manner as in Figure 23. Again some of the data during the storm is missing.

Analysis of the July 2015 storm shows similar results as the analysis of the Sinterklaas storm. The wind velocity is the first parameter that increases during a storm, but the atmospheric pressure now stays approximately the same. Shortly after the variation of these two meteorological conditions, the significant short wave height starts increasing. An increase of the significant long wave height starts after the increase of the significant short wave height.

Overall the significant long wave height seems to be related closest to the wind velocity and significant short wave height. Storm surge seems to be relevant for Platform A12, but less for Platform Hoorn Q1A. A relation between the significant long wave height and the atmospheric pressure was not observed by analyzing the time-series analysis, since the atmospheric pressure does not seem to vary a lot during the storms.

TUDelft
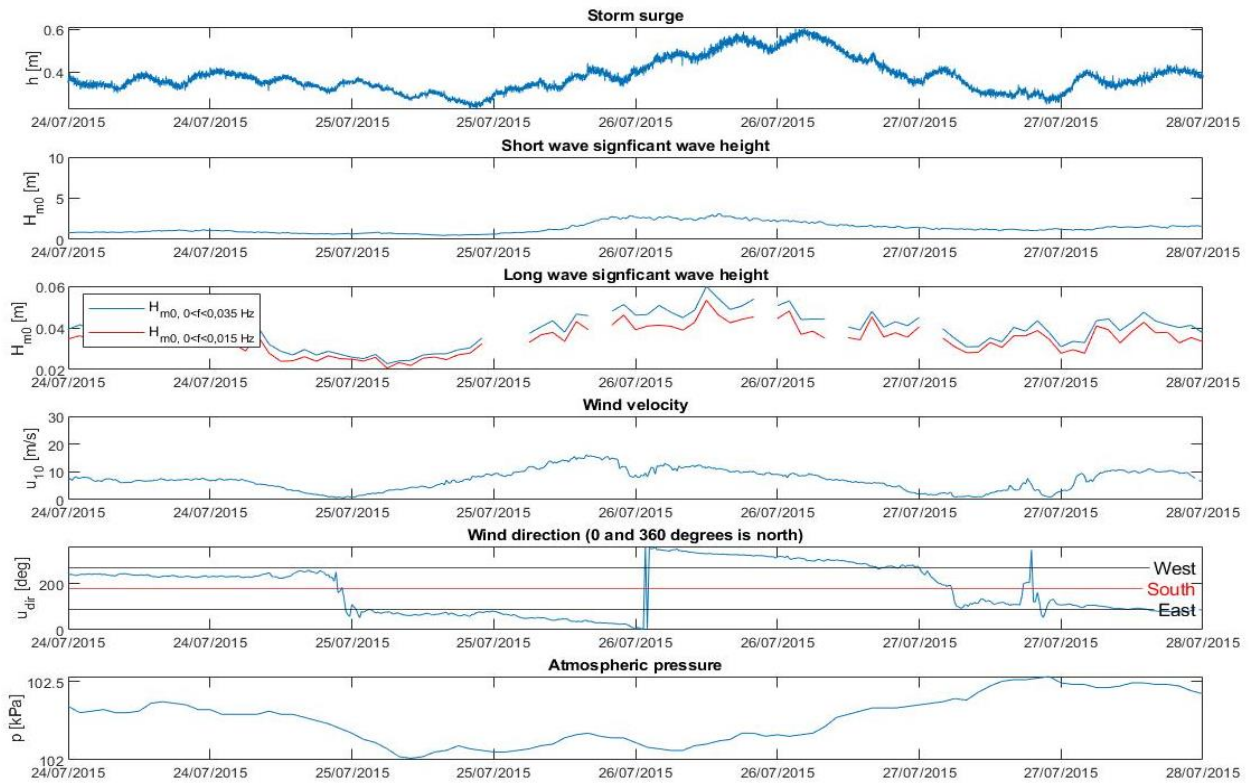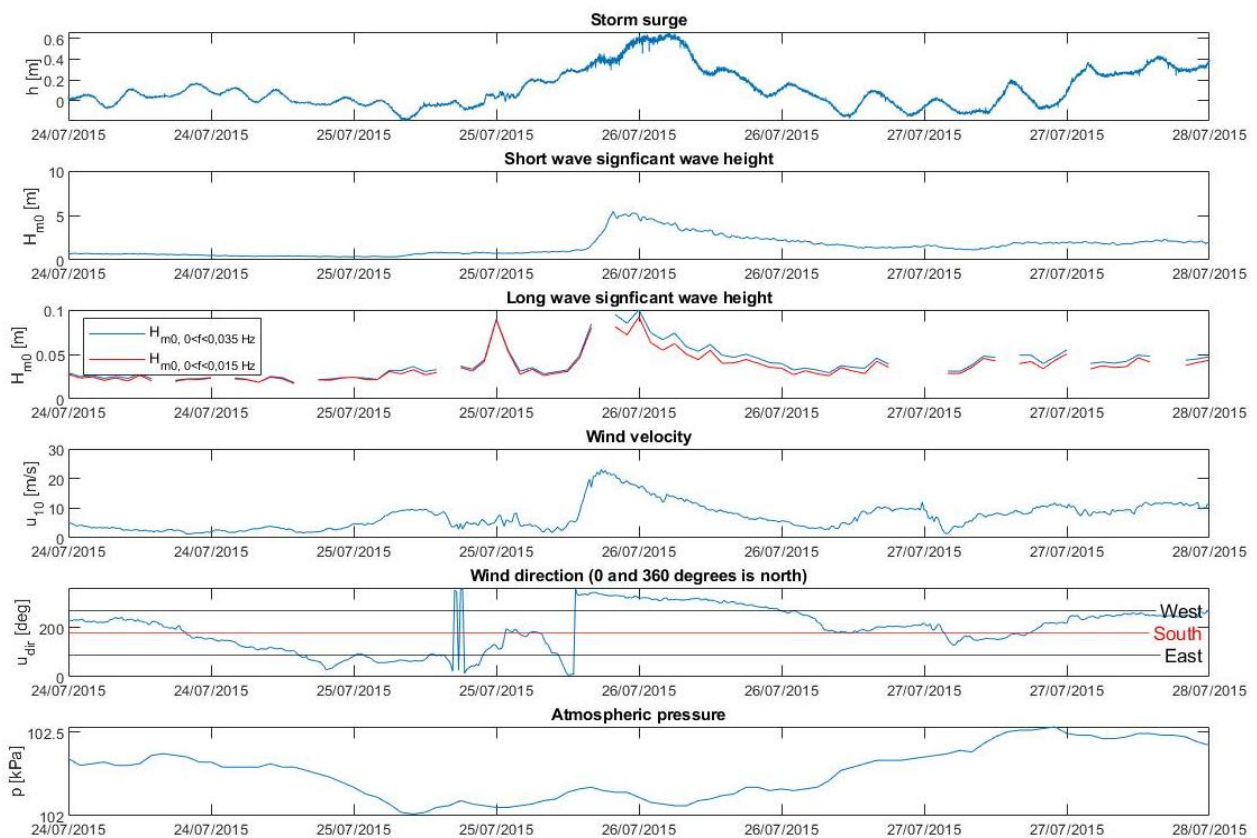
Figure 25 Graphs of the long wave significant wave height and other variables during the ummer storm of 2015 at the locations Platform Hoorn Q1A and Platform A12. They show the time-series of the storm surge level, short wave significant wave height, long wave significant wave height, wind velocity and atmospheric pressure. In the third graph the long wave significant wave height and the complemented long wave significant wave height (frequency class 1 and 2, see section 4.2.3) are displayed separately

The correlation between the significant long wave height and the parameters is in general weaker during the summer storm compared to the correlations during the Sinterklaas storm, see Figure 25 and Figure 26. Similar to the results of the Sinterklaas storm, the scatter plots of the summer storm shows the strongest correlation between the significant long wave height and the significant short wave height. With the coefficient of determination varying from 0,65 to 0,93 this is a medium/strong correlation. The storm surge level and wind velocity have approximately the same level of correlation and have a medium correlation with the significant long wave height. Again, the atmospheric pressure has no correlation with the significant long wave height.

In contrary to the Sinterklaas storm, the higher long wave frequency class shows the highest correlations with all correlations in Figure 26.

Analysis of the time-series provided a qualitative relation between the long waves and the parameters relevant for long wave generation. Following up on the time-series

Figure 26 Scatter plots showing the relation between the long waves and the other parameters for the summer storm for both long wave frequency classes.

analysis is the analysis where the significant long wave height is plotted against each individual parameter, see Figure 27.

The strongest correlation is between the significant long wave height and significant short wave height. The correlation between these two parameters is a linear correlation. When looking at the more extreme values, a curve seems to appear, indicating an exponential relation between the short and long significant wave heights.

After the significant short wave height, the strongest correlation with the significant long wave height is with the wind velocity. This correlation is linear. While wind velocity is indirectly responsible for long wave generation, the correlation between the significant long wave height and wind velocity is not very strong. Earlier it was stated that the wind direction, which influences the fetch, has a major influence on the resulting significant wave heights of both short and long waves.

In contrary to the results from Figure 26, where the long waves and storm surge showed a strong correlation during a storm, the correlation between the long waves and the storm surge over the full measurement period is weak. Apparently the strong correlation between the storm surge level and significant long wave height was particularly strong during the Sinterklaas storm. Both the wind velocity and storm surge level show a linear correlation with the significant long wave height.

Weakest of all correlations, is the correlation between the significant long wave height and the atmospheric pressure. A clear trend between in- or decreasing significant long wave heights cannot be distinguished. A remarkable observation though, is that the highest values for the significant long wave height are centered around certain values for the atmospheric pressure. The clustering of high wave heights occurs at 100 kPa at Platform A12, and 100- and 130 kPa at Platform Hoorn Q1A.
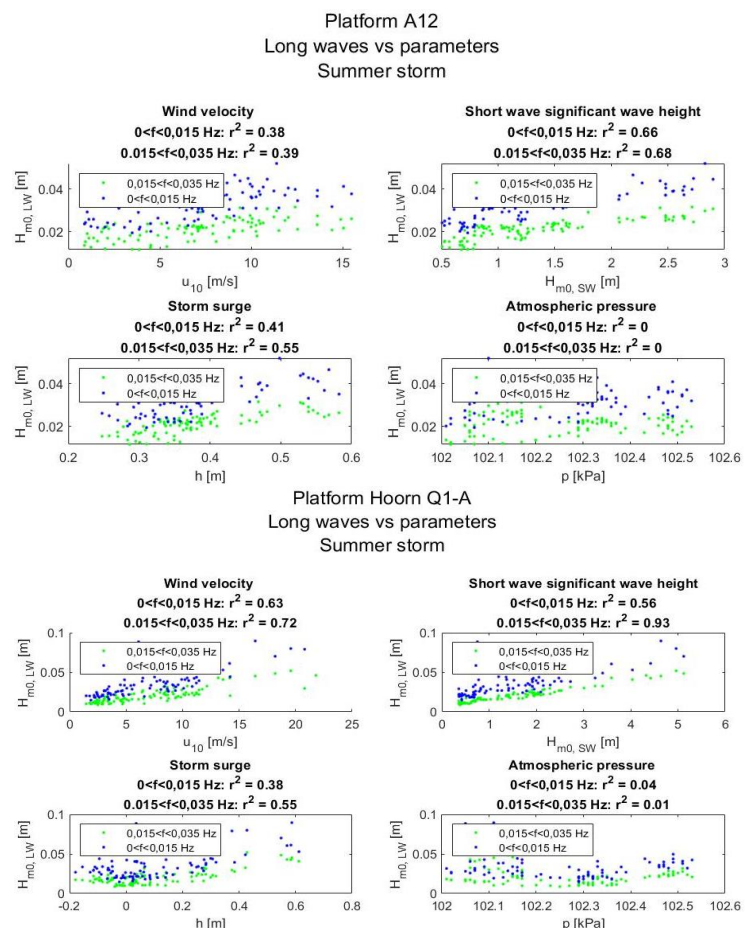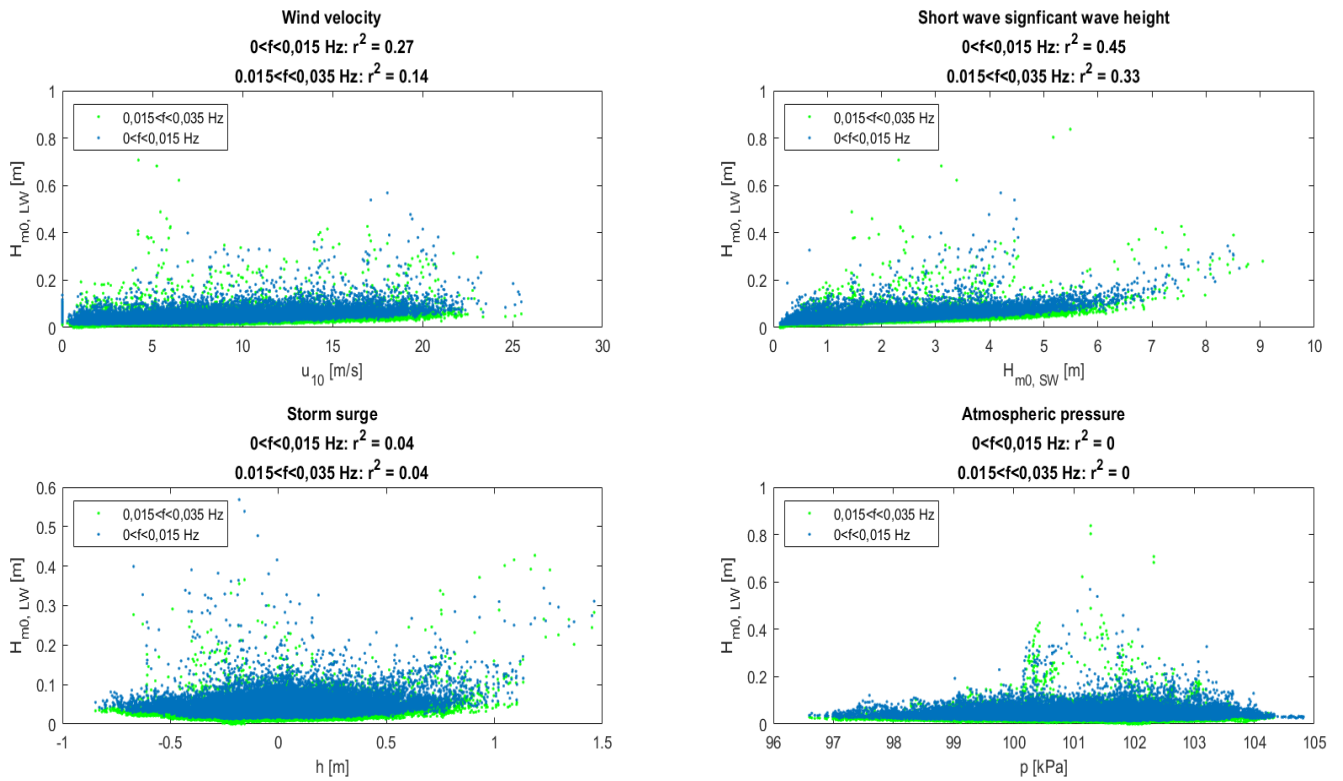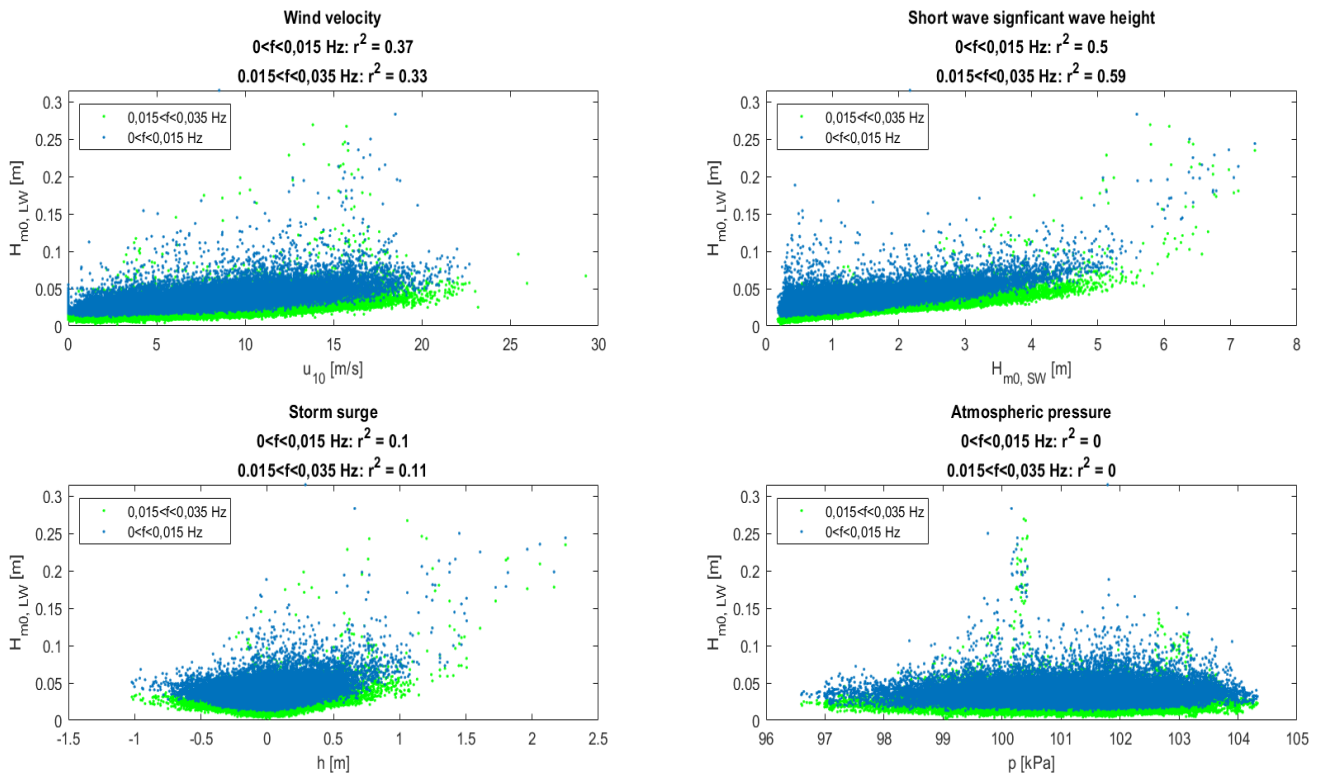
Figure 27 The (complemented) long wave significant wave height plotted against each parameter individually, for both locations.

6.2   BOUND LONG WAVES

Long waves consist of both bound- and free long waves. Presumably, a significant part of the free long waves originate from bound long waves, as explained in section 2.1.1. Bound long wave activity is usually strongest during storms, during mild conditions bound long wave activity is usually small or even absent. As explained in section 5.2.3, Hasselmann's theory is used to predict the bound long wave contribution to the total long wave signal. The analysis of the results will follow in this paragraph.

The set-up of the bound long wave analysis is the same as the analysis used to analyze long waves in the previous paragraph. First the bound long wave time-series is compared to the relevant parameters for a qualitative analysis, followed by a quantitative analysis by means of a scatter plot. After the bound long wave analysis a relative bound long wave analysis will follow, in which the relative contribution of the bound long waves to the total long wave activity is analyzed.

Looking at the graphs of Figure 28 and Figure 29, the significant bound long wave height shows the strongest correlation with the significant short wave height. The variation of the graphs of both parameters seem to be practically simultaneous, even small peaks and troughs in the graphs occur at approximately the same time. Which is not a surprise since bound long wave generation is driven by short waves as explained in section 2.1.1, and calculated with short wave data, as explained in section 5.2.3. This means that the bound long wave activity is indirectly also related to the wind velocity, since short waves generation is driven by wind. Wind velocity and bound long waves therefore also show a strong relation.

A strong relation is also visible between the significant bound long wave heights and storm surge, see the top- and middle graph of Figure 28. Both parameters show a strong increase and decrease around the same time, the highest values of both parameters are also at their peak during the same time span.

The relation with other parameters is weaker compared to the relation with the significant short wave height and wind velocity. A relation with the atmospheric pressure cannot be visually deduced from the graphs.

According to the graphs the highest bound long waves originate from the second frequency class ($0,015 < f < 0,035\ Hz$). The first frequency class $0,005 < f < 0,015\ Hz$ appears to be the class with the lowest wave heights during the heavier conditions. The third frequency class ($0,035 < f < 0,05\ Hz$) shows significant bound long wave heights in between the other two, during the analyzed events. For mild conditions the bound long wave activity is practically zero, which indicates that the hypothesis stating that (bound) long waves are generated during storms/heavy meteorological conditions is true.

TUDelft
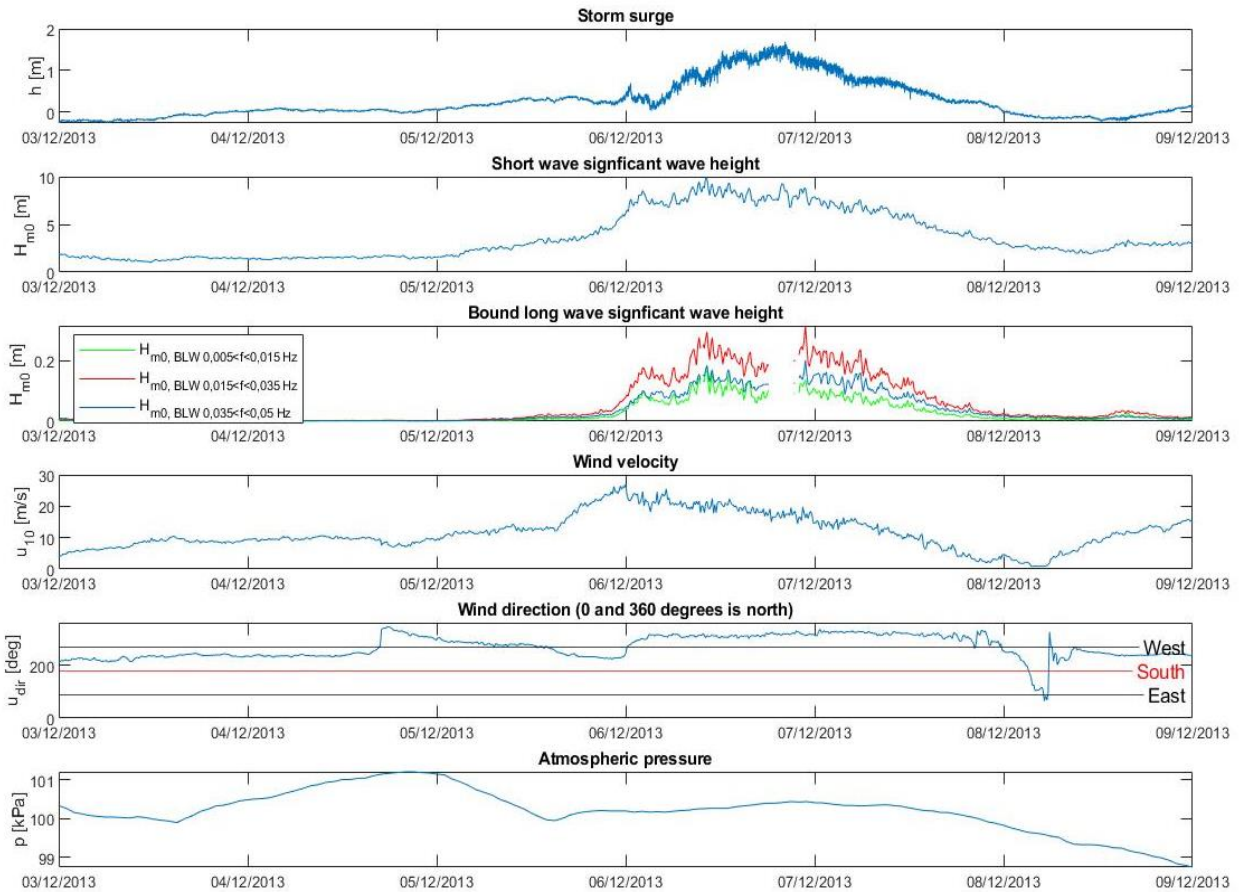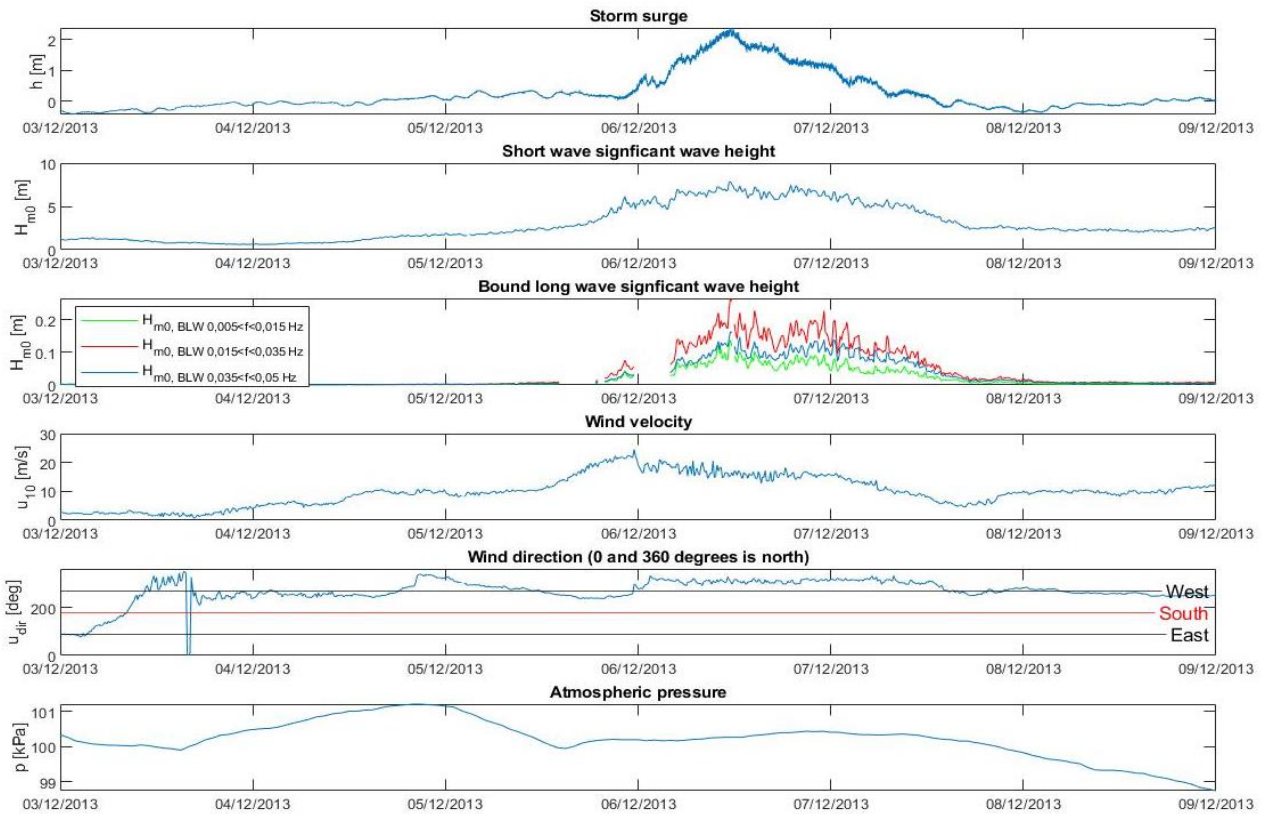
Figure 28 Graphs of the significant bound long wave height and other parameters during the Sinterklaas storm of 2013 at the locations Platform Hoorn Q1A and Platform A12
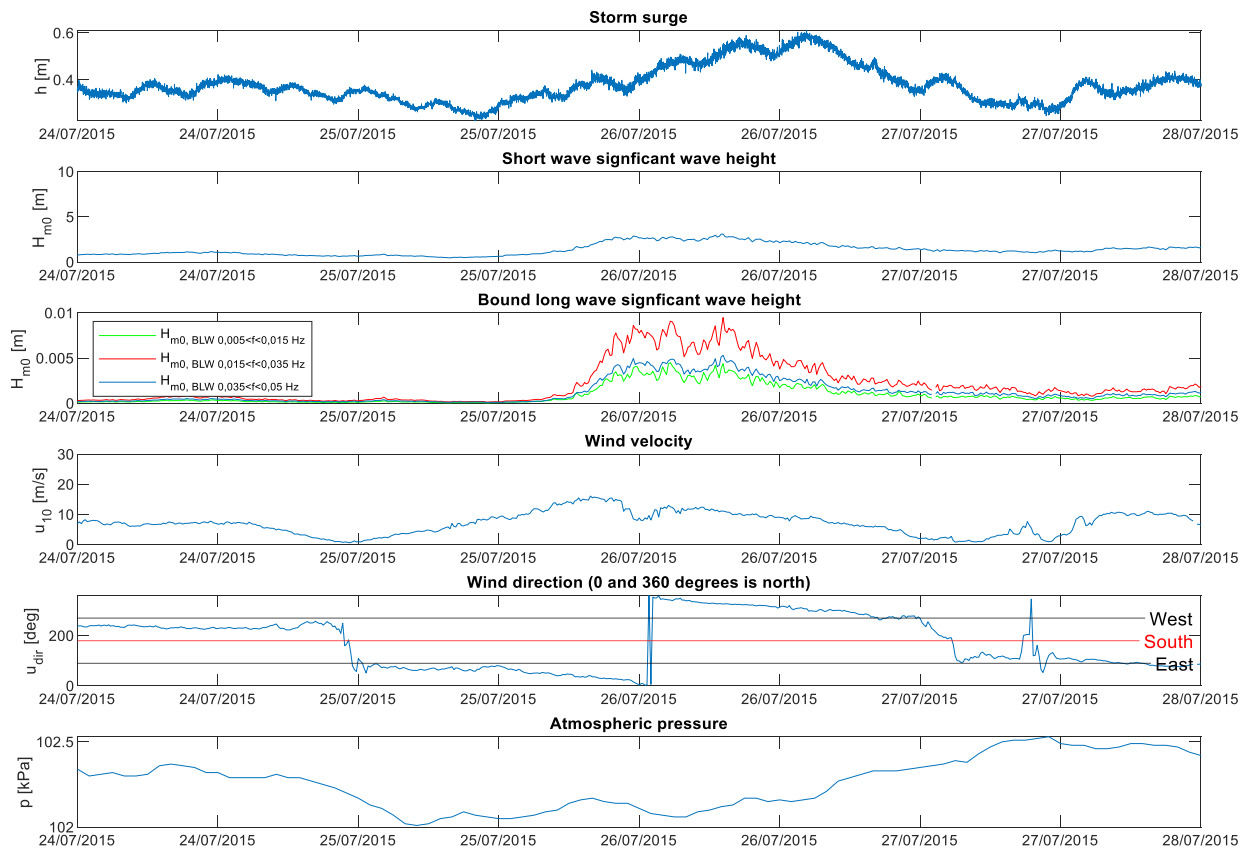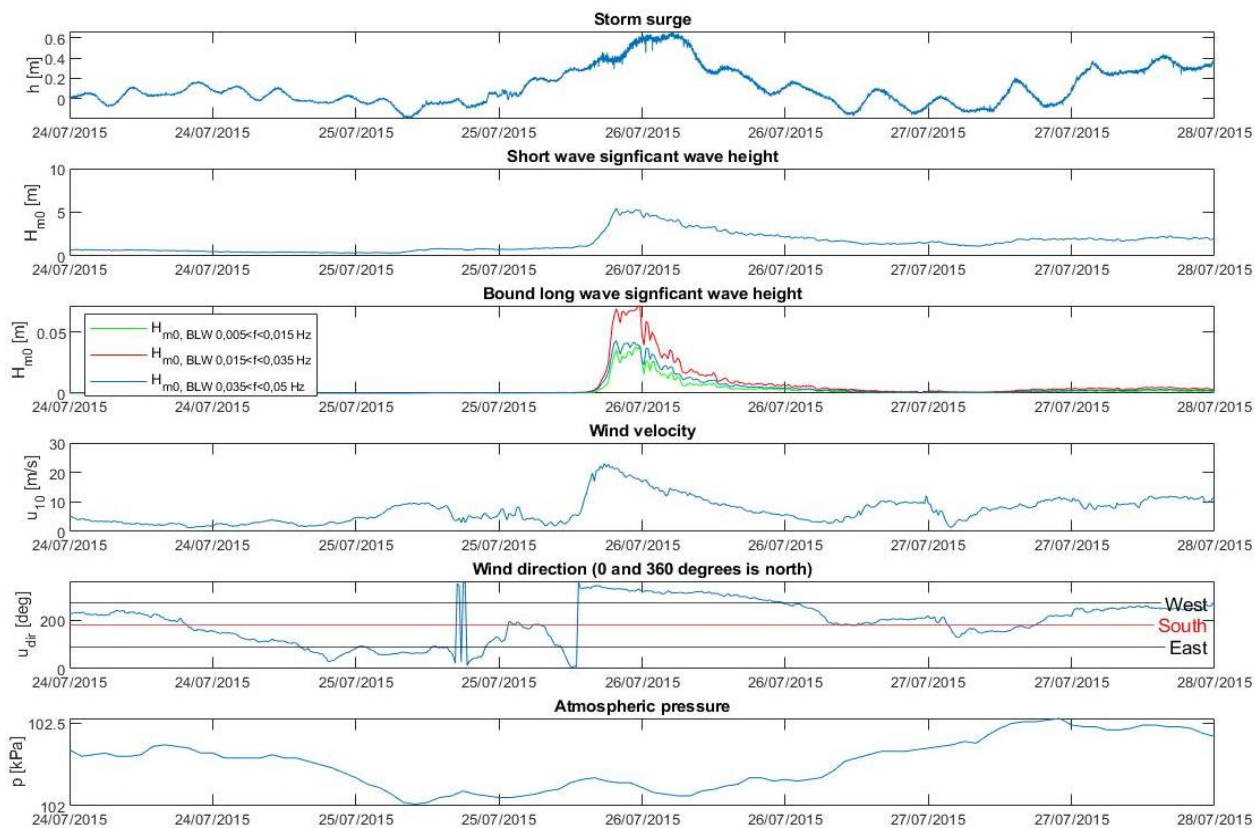
Figure 29 Graphs of the significant bound long wave height and other variables during the summer storm of 2015 at the locations Platform Hoorn Q1A and Platform A12

The parameter that has the strongest correlation with the bound long waves at both locations is the significant short wave height, showing a very strong third order correlation.

Wind velocity and bound long waves show a relatively weak correlation, but high values for wind velocity correspond to the highest values for the significant bound long wave height. Even though wind velocity shows a weak correlation, it is an important indicator for high bound long wave activity.

Storm surge shows little (Platform Hoorn Q1A) to no correlation (Platform A12) with the significant bound long wave height. Just like the wind velocity, the highest bound long wave activity occurs at the highest values for storm surge, meaning storm surge is an indicator for bound long wave activity.

Atmospheric pressure shows no correlation with bound long wave activity. At certain points in the scatter plots (100 and 103 kPa at Platform A12 and 100 kPa at Platform Hoorn Q1A) a cluster of high significant bound long wave heights is spotted.

The high bound long wave activity during heavy conditions (see Figure 32), in combination with little to no bound long wave activity during mild conditions (see Figure 28 and Figure 29), indicates that the local generation of long waves during storms is responsible for the majority of bound long waves in the North Sea.

TUDelft
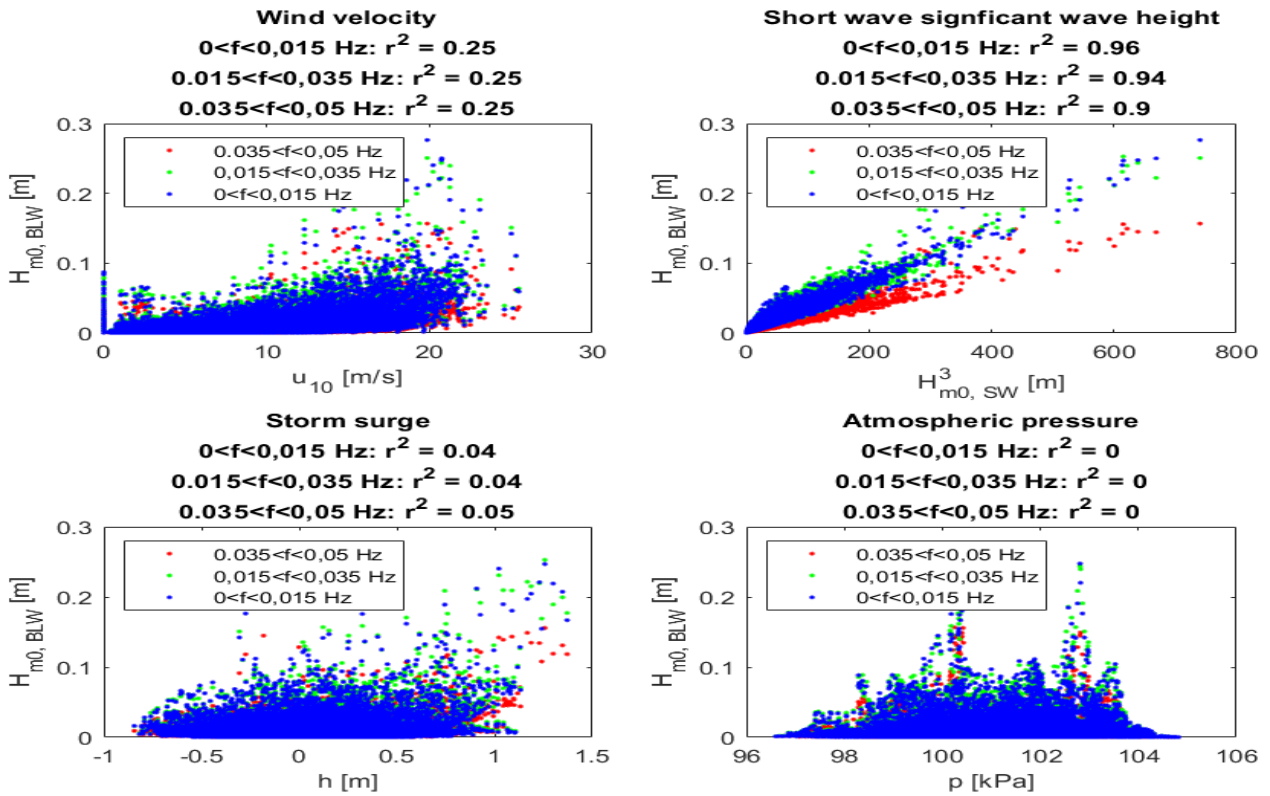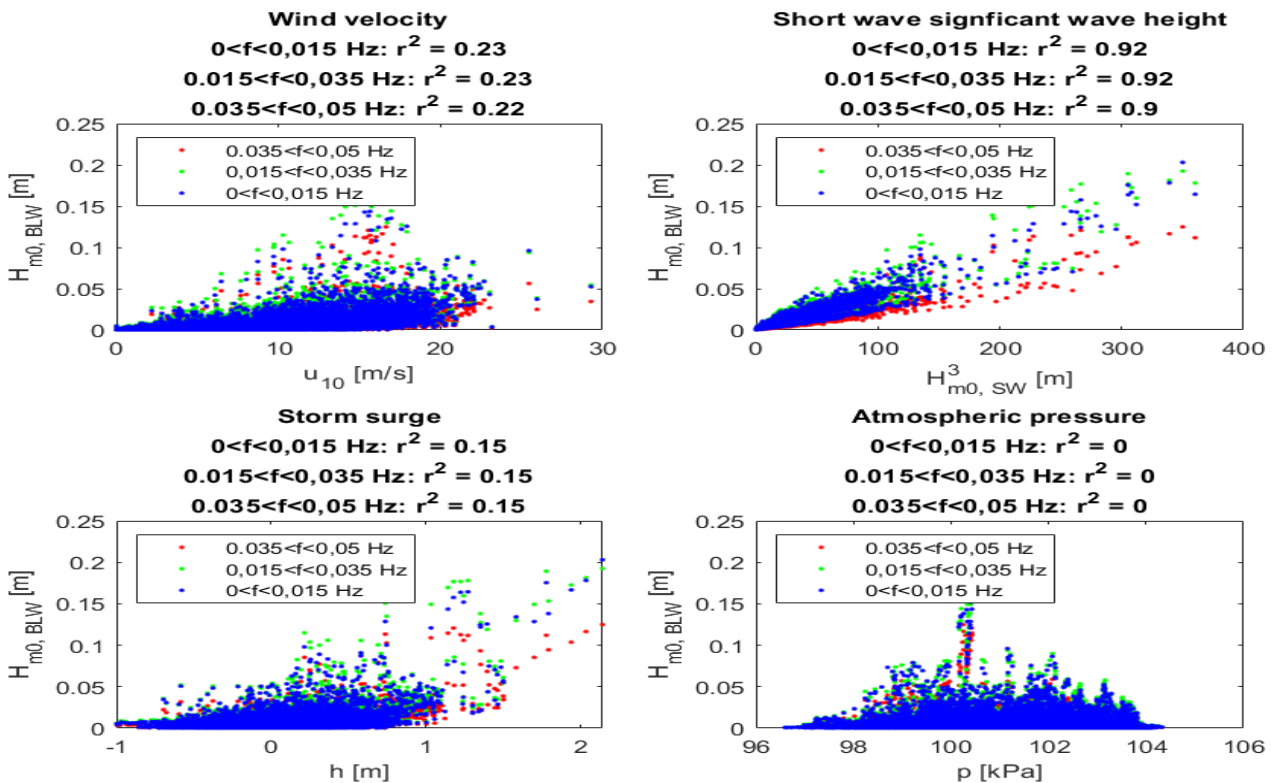
Figure 30 Scatter plots from both platforms showing the correlation between the bound long wave significant wave height from all three frequency classes with the parameters

6.2.1 RELATIVE CONTRIBUTION BOUND LONG WAVES

In the previous paragraph the results indicated that the hypothesis stating that (bound) long waves are mainly generated during storms is true. The results showed that significant bound long wave heights increase rapidly during a storm, and are practically zero in mild conditions, showing that the majority of bound long wave generation occurs during storms.

Looking at the relative contribution of bound long waves to the total long wave activity could tell more about the local generation of long waves in the North Sea. First the time-series of the long- and bound long waves from the 1st and 2nd frequency class ($0{,}005 < f_1 < 0{,}015\ Hz\ and\ 0{,}015 < f_2 < 0{,}035\ H$) are analyzed side by side, followed up by scatter plots indicating the correlation between the relative contribution ($\frac{E_{blw}}{E_{lw}}$) of the (bound) long waves and the parameters.

In mild conditions the bound significant long wave height is low to absent, but rapidly starts increasing at the start of the storm. For increasing total long wave activity, bound long waves show an even stronger increase. This indicates that whenever long wave activity starts increasing, the relative contribution of bound long waves to the total long wave activity starts increasing as well.

The wave heights of the lower frequency long waves ($0{,}005 < f < 0{,}015\ Hz$) are lower than the higher frequency long waves ($0{,}015 < f < 0{,}035\ Hz$), see Figure 31. At its maximum, the higher frequency waves are 2 to 3 times higher.

In the first frequency class the significant bound long wave height often reaches values of up to approximately 50% of the total long wave activity.

The significant bound long wave heights in the second frequency class exceeds the significant total long wave height at some points. Since Hasselmann's theory is a prediction of the bound long waves, and not an exact determination, small variations in the results with respect to the actual values are possible. Nonetheless, for this frequency range the bound long wave contribution is telling.

Rijkswaterstaat
Ministry of Infrastructure and the Environment

TUDelft
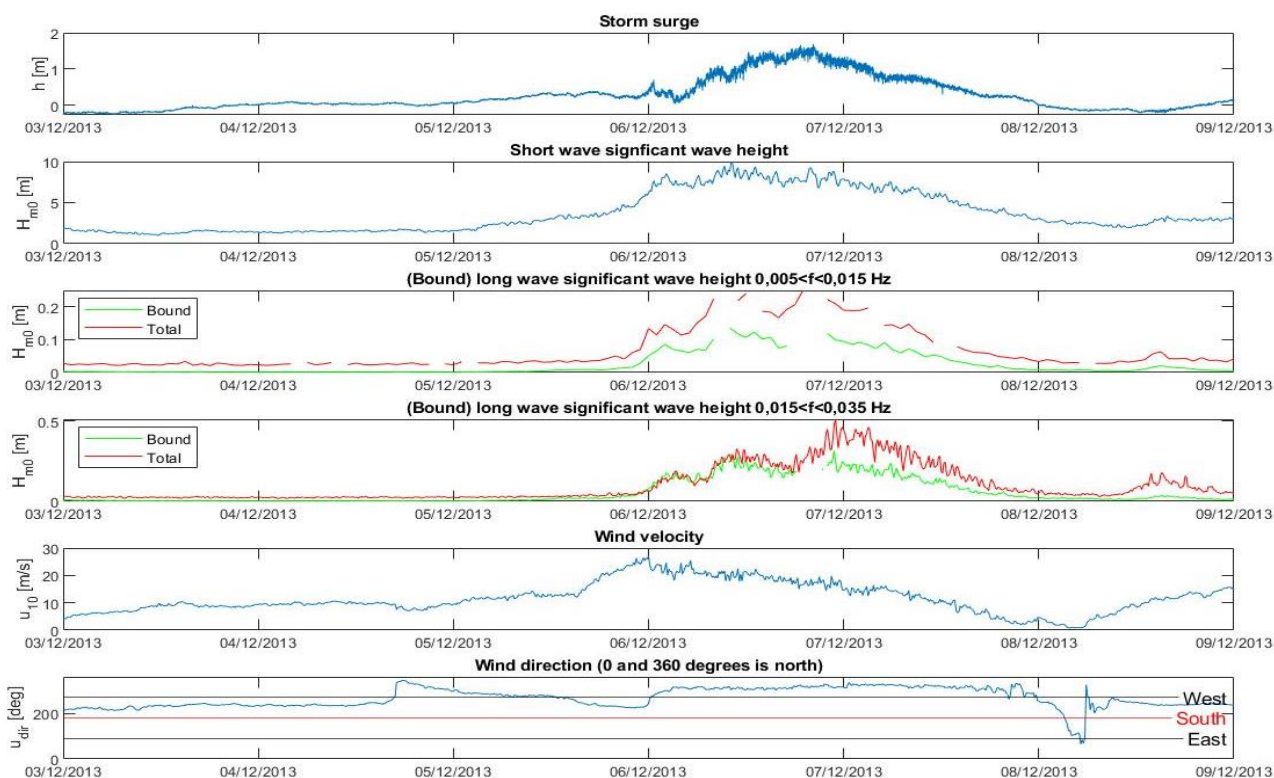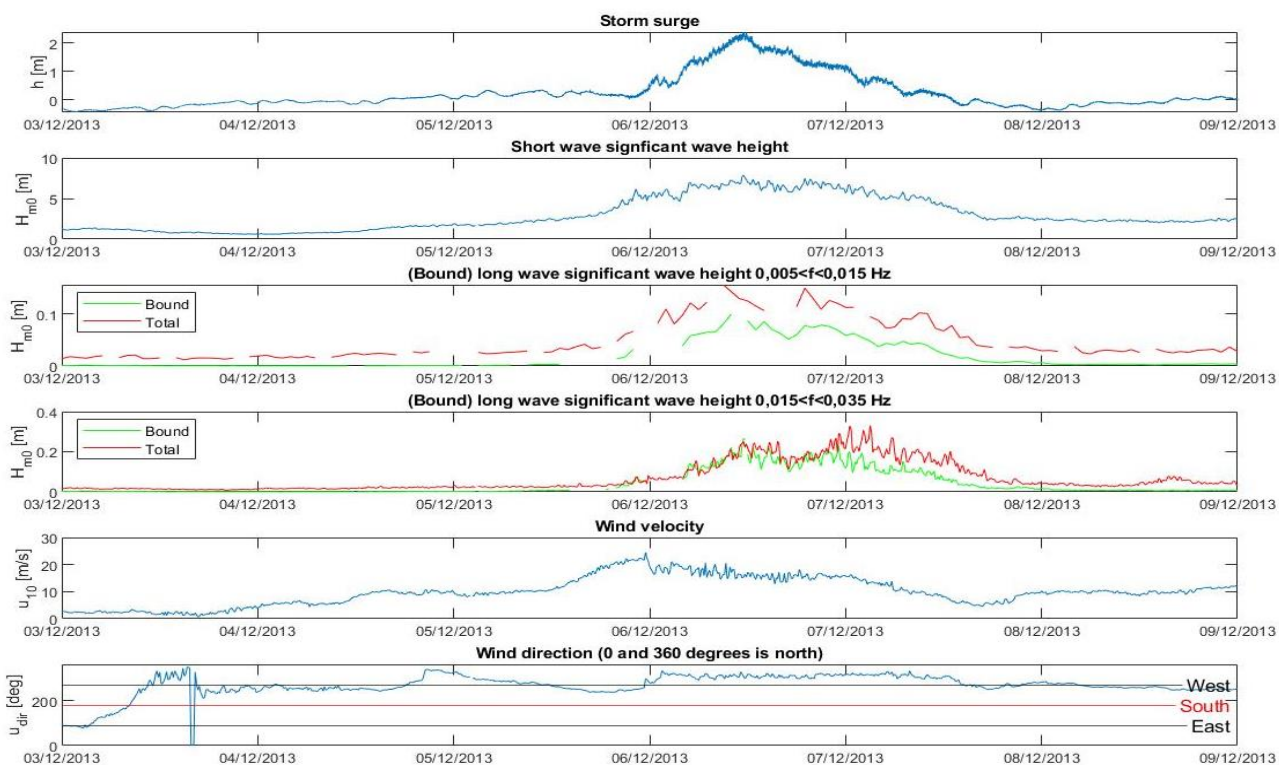
Figure 31 Graphs of the (bound) long wave significant wave height and other variables during the Sinterklaas storm of 2013 at the locations Platform Hoorn Q1A and Platform A12. They show the time-series of the storm surge level, short wave significant wave height, long wave significant wave height and wind velocity. In the third and fourth graph the long wave significant wave height and bound long wave significant wave height (frequency class 1 and 2) are displayed separately

No correlation exists between the relative contribution of bound long waves with storm surge and atmospheric pressure, see Figure 32.

The correlation between the relative bound long wave contribution with wind velocity is weak, but clearly present, see Figure 32. Wind velocity shows that it is an important indicator for a high relative contribution of bound long waves, the highest wind velocities correspond to the highest relative contributions.

Significant short wave height and the relative contribution of bound long waves show the strongest correlation, see Figure 32. This correlation is especially strong at Platform A12, where the strongest long wave activity is present, see Figure 31. At Platform A12 the relative contribution reaches up to 50% and slightly higher. On average the relative contribution is lower at Platform Hoorn Q1A, but incidentally reaches high values of up to 60%. The correlation appears linear at Platform A12 and exponential at Platform Hoorn Q1A.

The high relative contribution of bound long waves during heavy conditions compared to other research (Herbers et al., 1994) shows that the local generation of bound long waves is strong.

Rijkswaterstaat
Ministry of Infrastructure and the Environment

TUDelft
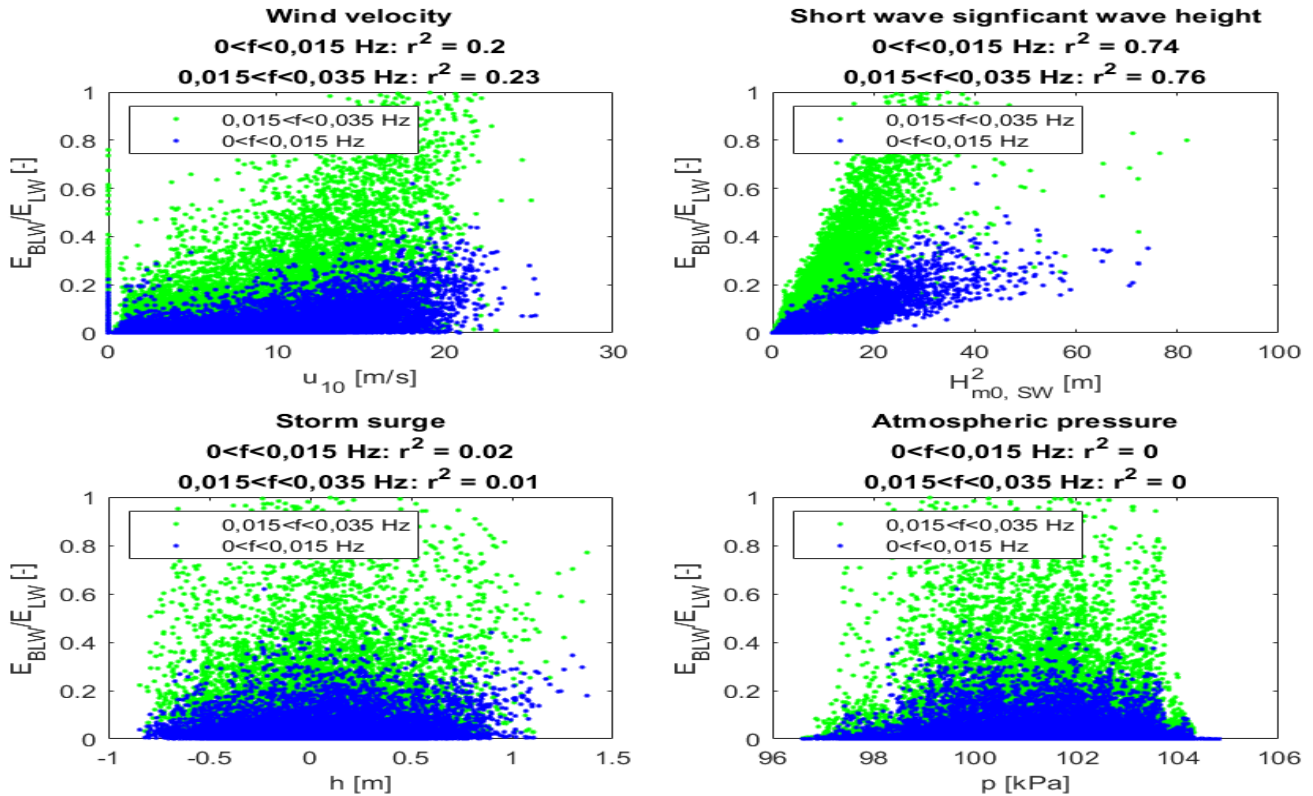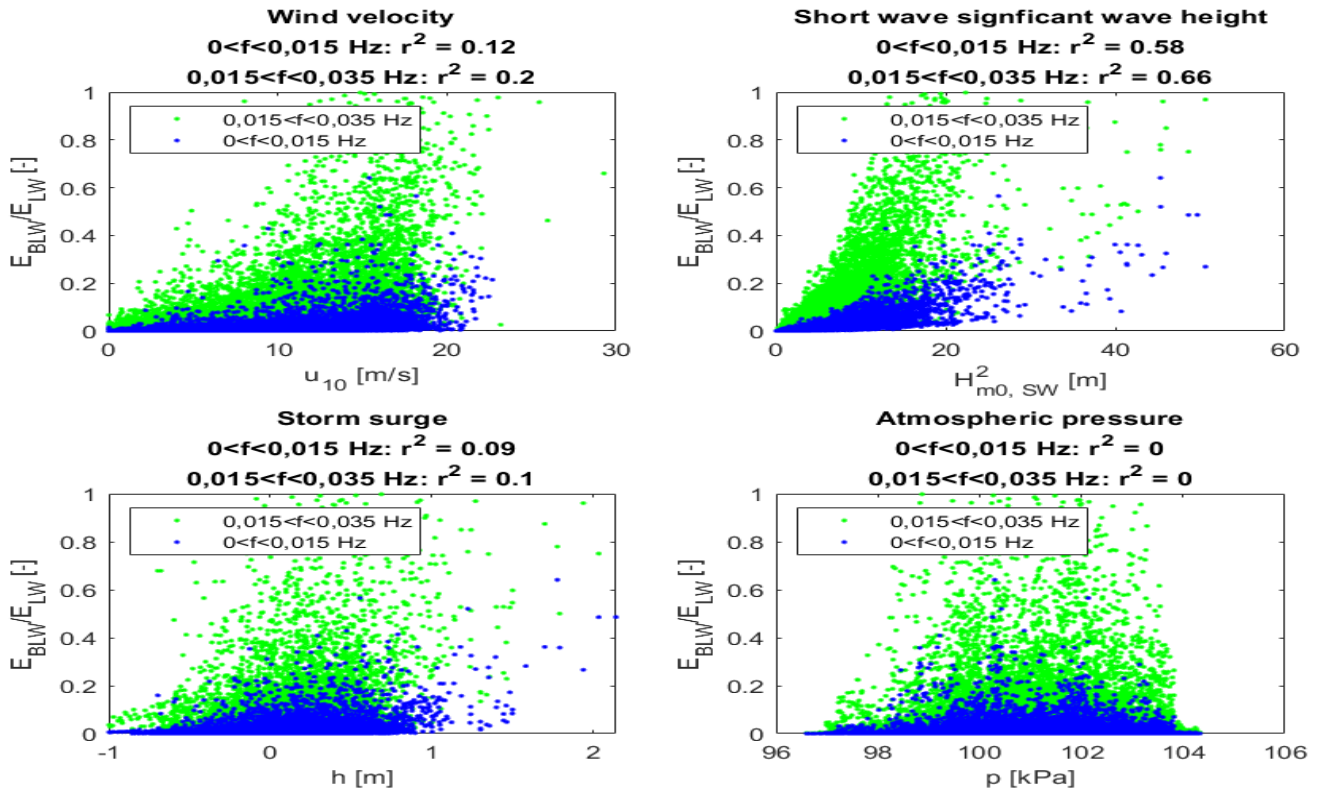
Figure 32 Relative contribution of the bound long wave significant wave height with respect to the total long wave significant wave height plotted against the relevant parameters for generation

7 LONG WAVE PRESENCE IN THE NORTH SEA

This chapter presents the results of the spectral analysis of the long wave data. Comparing the results of the spectral analysis at different locations, and for various seasons, provides a representation of the spatial and temporal distribution of the long waves. After the analysis of the spatial and temporal distribution of the long waves, a prediction of the extreme long wave conditions follows.

7.1 SPATIAL AND TEMPORAL DISTRIBUTION LONG WAVES

For an illustration of the present distribution of long waves, one year is selected for which data from all locations will be analyzed. Performing the short term run is done for the year 2013. In this year data from all locations is complete (no missing data, see appendix a). The outcome of the spectral analysis is used to calculate two characteristic wave parameters; the significant long wave height ($H_{m_0} = H_s$) and the mean long wave period ($T_{m_{01}} = T_m$).

7.1.1 SPATIAL DISTRIBUTION OF LONG WAVES

Figure 33 and Figure 34 show the probability function of the significant wave height and the mean wave period, respectively. The most probable values of both parameters are summarized per location in Table 5 and visually displayed in Figure 35. Besides the results shown in this section, which give an overview of the results, more detailed graphs are displayed in appendix A. These show the results per location and include the seasonal variation.

The majority of the locations show a most probable value of significant wave heights around 2,4 – 3 cm and mean wave periods of 125 – 135 s, see Figure 33 and Figure 34. Platform J06 distinguishes itself significantly with higher significant wave heights (highest concentration around 3,9 cm) and longer wave periods (highest probability of occurrence around 140 s).

Locations where the most likely value for the significant wave height is higher, take for example Platform J06 and Platform A12, seem to have a wider and lower probability function. Which means that at the locations where the probability for high waves is higher, also a wider variety of significant wave heights occur. Locations that have the peak of the probability function at the lower values of the significant wave height, take for example Europlatform, show a narrower and higher probability function.

Whereas the significant long wave height's most probable value and distribution seem to vary fairly per location, the mean long wave period's most probable value and distribution do not seem to vary a lot. The significant wave height therefore appears to be the more spatially dependent variable, see Figure 33 and Figure 34, which is verified by calculating the coefficient of variation for the most likely value of both parameters in the calculation below. The coefficient of variation is the ratio of the standard deviation over the mean and is therefore a relative value of the standard deviation.

$$c_{v,Hs} = \frac{\sigma_{Hs}}{\mu_{Tm}} = \frac{0,0047}{0,0296} = 0,159$$

$$c_{v,Tm} = \frac{\sigma_{Tm}}{\mu_{Tm}} = \frac{4,96}{130,63} = 0,038$$

Rijkswaterstaat
Ministry of Infrastructure and the Environment

TUDelft
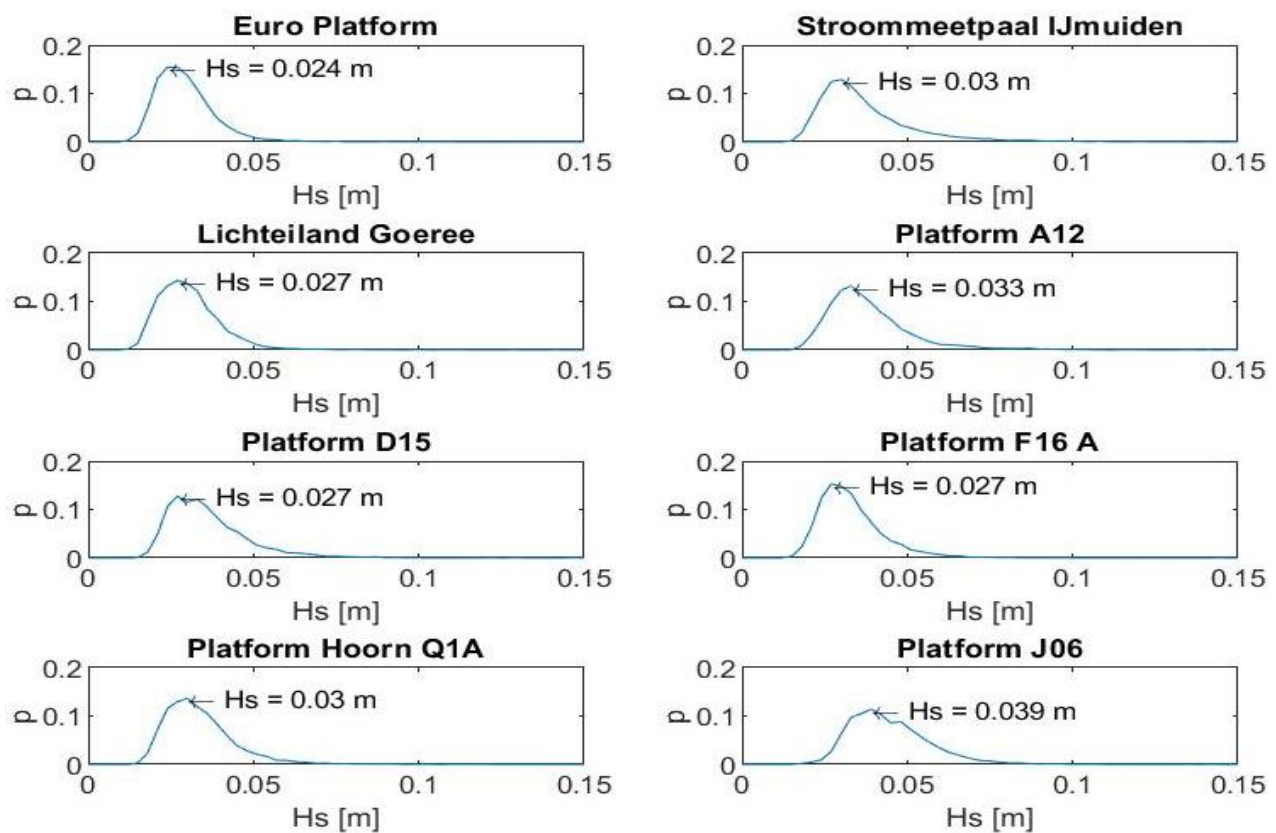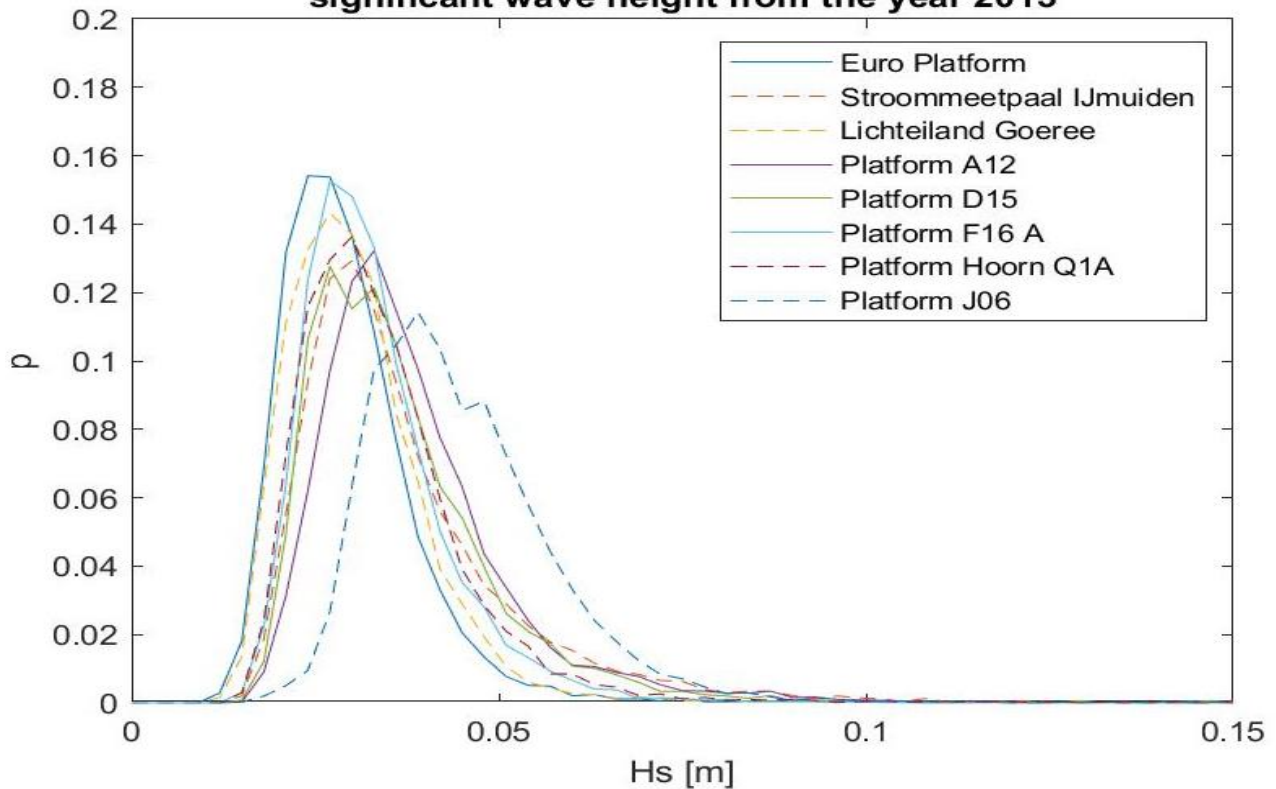
Figure 33 Upper graph: Probability function of the long wave significant wave height of all locations shown in one graph for comparison. Smaller lower graphs: The probability functions displayed in separate graphs per location, with the significant wave height that has the largest probability of occurrence annotated.
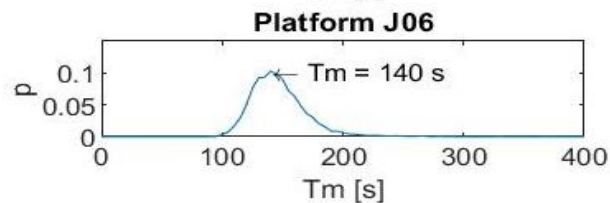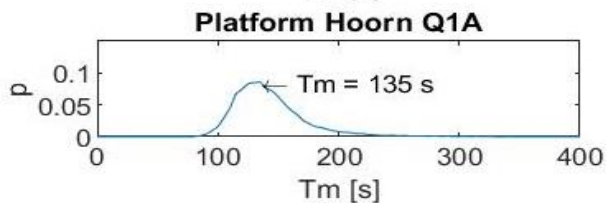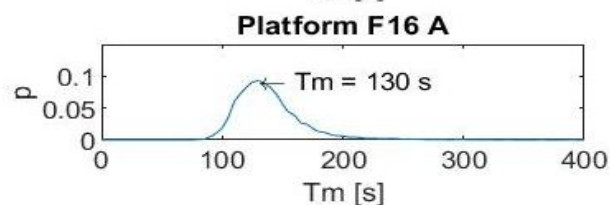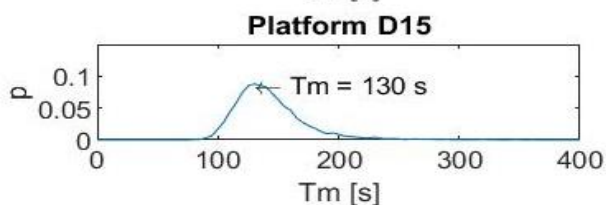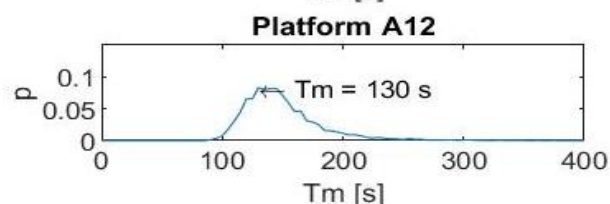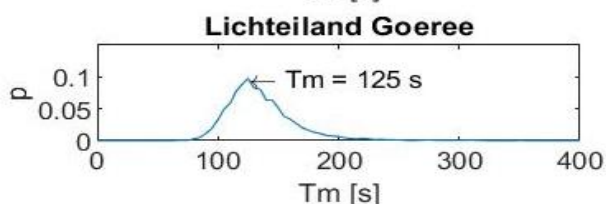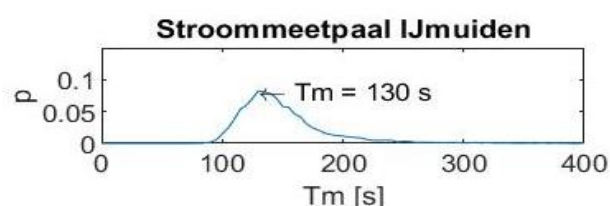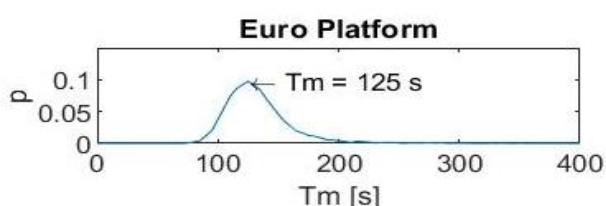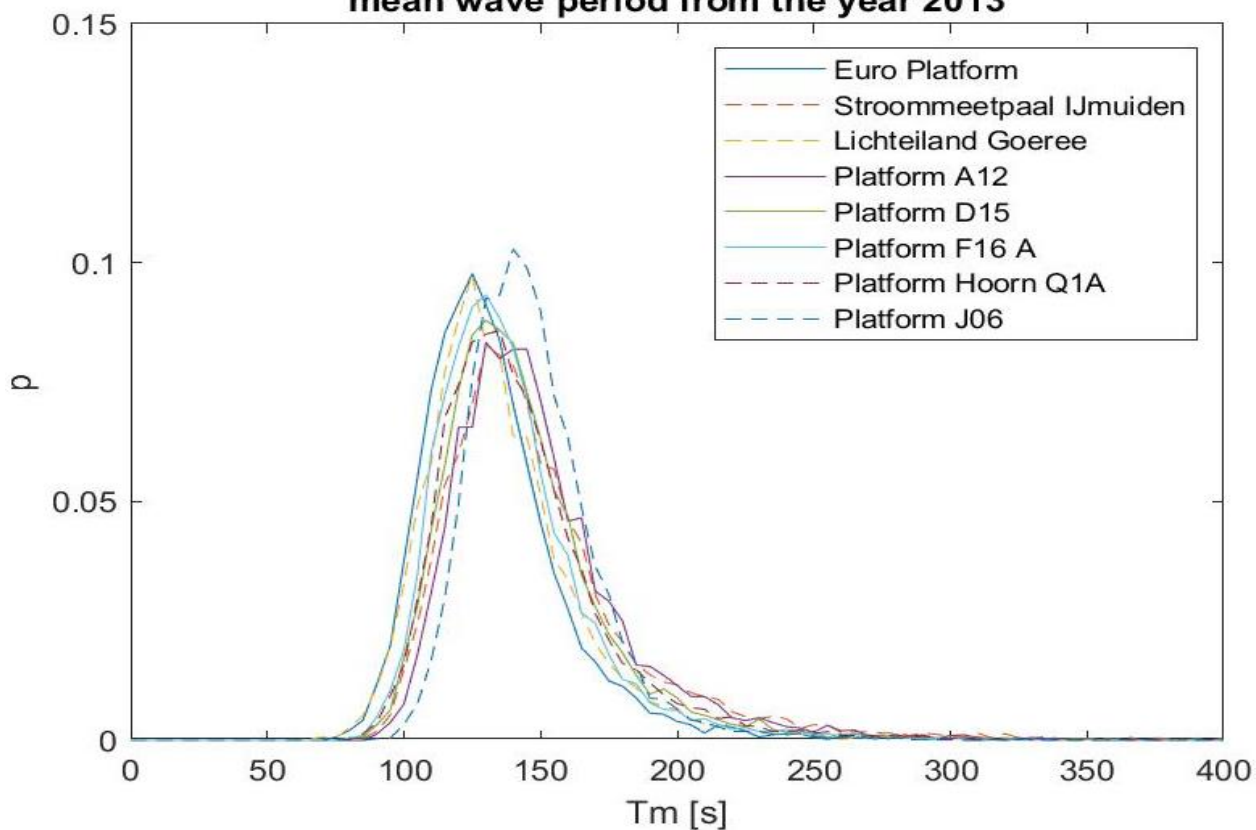
Figure 34 Upper graph: Probability function of the long wave mean wave period of all locations of the year 2013
Smaller lower graphs: The probability functions displayed in separate graphs per location of the year 2013, with
the mean wave period that has the largest probability of occurrence annotated.

Rijkswaterstaat
Ministry of Infrastructure and the
Environment

TUDelft

Figure 35 Wave atlas showing Hs and Tm for the year 2013 per location

No.	Naam	H_s [cm]	T_m [s]
1	Europlatform	2,4	125
2	Lichteiland Goeree	2,7	125
3	Platform A12	3,3	130 - 140
4	Platform D15	2,7	130
5	Platform F16 A	2,7	130
6	Platform Hoorn Q 1A	3,0	135
7	Platform J06	3,9	140
8	Stroommeetpaal Ijmuiden	3,0	130

Table 5 Most probable values for H_s and T_m for the year 2013

The coefficient of variation of the most probable value of the significant long wave heights is a factor 4 larger than the most probable value of the mean long wave period's coefficient of variation. Having a larger coefficient of variation shows that the significant long wave height is affected more by spatial variations.

Both coefficients of variation are quite small, which implies that neither of the two variables are affected much by spatial variation. However, both probability functions have been determined over the full year, including all periods with mild weather conditions. Storms only cover a minor part of the full year, but are the periods in which long waves are mainly present. Figure 36 shows that during the majority of the year, significant long wave heights are small. The majority of long wave activity is captured in only a couple of short periods.

In order to get a better impression of the distribution of long waves during storm conditions, the significant long wave heights during storms[5] are selected for analysis. Long wave data is selected at three stations, the three selected stations are based on the findings from Figure 33. These include the locations where the most probable value of the significant wave height is; the lowest (Euro Platform), the highest (Platform J6) and one somewhere in the middle (Platform A12). At Platform A12 and J6, storms cover 2,5% of the full year, storms cover 0,6% of the full year at Euro Platform. Even though the most probable value during storm conditions is the same for all three locations ($H_s = 5\ cm$), visual observations of the graph shows that variations in the distribution of significant long wave heights during storms (Figure 36) is considerably larger compared to the distribution over the full year (Figure 33). All three platforms show that the majority of their significant long wave heights is in between $0 - 10\ cm$. Looking at the distribution of the more extreme wave heights, Euro Platform shows a peak at $12{,}5\ cm$, Platform J6 at $20\ cm$ and platform A12 at $25 - 30\ cm$. Platform J6 showed the highest significant long wave height over the full year distribution, but shows lower significant long wave heights during storms conditions. Euro Platform showed the lowest significant long wave heights in the full year distribution and also shows the lowest significant long wave heights during storm conditions.
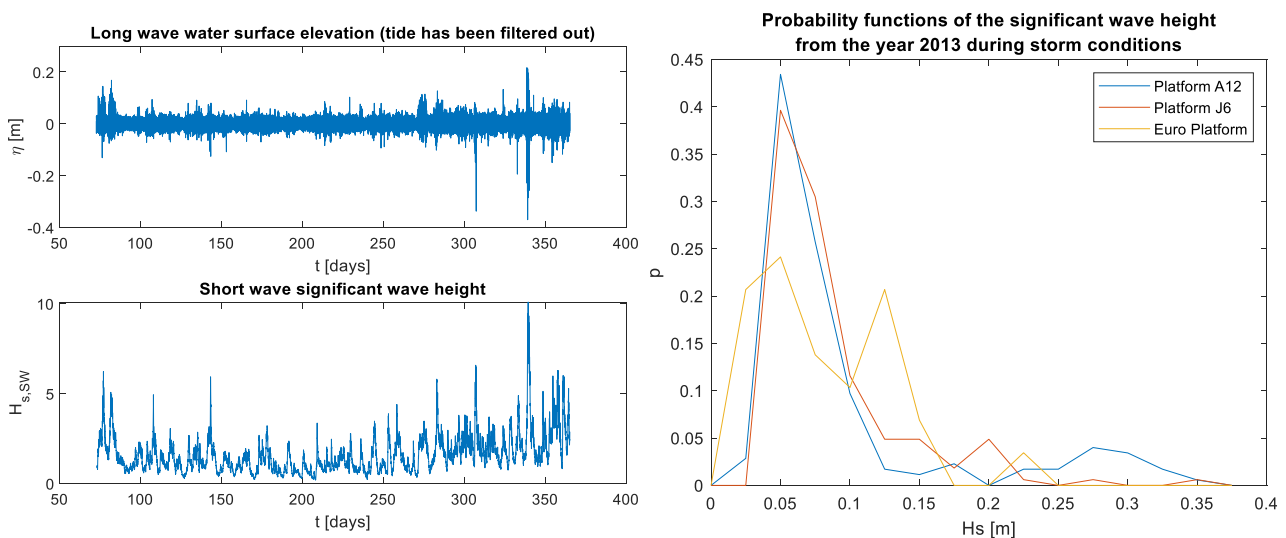
Figure 36 Left: Full year (2013) time-series of the significant wave height of the long waves (above) and short waves (below) at measurement station A12. Right: Distribution of the significant long wave height during storm conditions for various measurement stations.

---

[5] A storm is in this case defined as a period in time at a measurement station in which the short wave significant wave height is larger then 4m.

Since the nearshore measurement stations are located in shallower water compared to the offshore locations (see paragraph 4.3) it was expected that the nearshore measurement stations (Europlatform, Lichteiland Goeree, Platform Hoorn Q1A, Stroommeetpaal IJmuiden) would show higher values for the significant wave height compared to the offshore measurement stations (Platform A12, Platform D15, Platform F16A, Platform J6). Instead, there does not seem to be a clear trend in the location of the measurement stations and the significant wave height, see Figure 35. In order to get an impression of the depth dependency of long waves, the long wave amplitude-depth relation $\hat{\eta}_{lw} \sim h^{-\alpha}$ (Battjes, et al., 2004) is used. The value for α varies depending on the bed slope and long wave properties. It has been assumed to be 1/4 for free long waves (Green's law) and 5/2 for bound long waves (Battjes, et al., 2004). For the relevant water depths (mean water levels at the measurement stations from Table 2), the long wave amplitude-depth dependence relation shows that the amplitude dependence for the relevant depths does not vary a lot, see Figure 37.
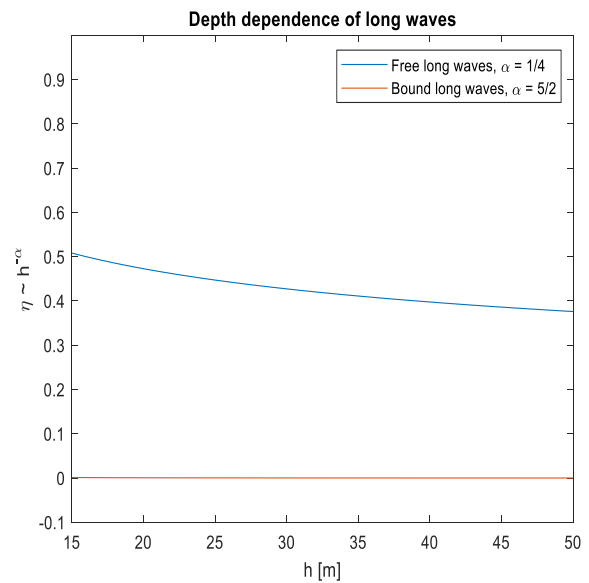
Figure 37 Long wave amplitude-depth dependency relation for both bound- and free long waves

Spatially varying wave heights could be the result of locally varying spatial conditions, locally varying forcing conditions or other surrounding factors. Locally varying spatial conditions could cause processes like shoaling, refraction and/or diffraction to influence the wave height. Spatial conditions that play a role in the processes of shoaling, refraction and diffraction are water depth, bathymetry and currents. Another possible explanation could be due to varying forcing conditions. When the forcing conditions are stronger, generated waves are more likely to become higher. Forcing conditions that could influence the generation, and there with the wave height, are short waves and meteorological conditions like wind velocity and atmospheric pressure. Other factors that could influence the wave height could be, for example, the bathymetry of the surrounding area, which could cause nearby long waves to refract towards the measurement location.

7.1.2 TEMPORAL DISTRIBUTION OF LONG WAVES

The temporal distribution is analyzed by plotting the graphs of the significant long wave heights and mean long wave periods of all locations from a certain season in one figure, thus showing how both parameters are distributed per season. The average of all the most probable values per season are taken and plotted as a vertical stripe in the figures.

When looking at the temporal dependence of both the significant wave height and mean wave period, see Figure 38 and Figure 39, the significant wave height appears to be the stronger varying variable, while the mean wave period is more or less constant through the year. This statement is quantified calculating the coefficient of variation, see the calculation below.

$$c_{v,Hs} = \frac{\sigma_{Hs}}{\mu_{Hs}} = \frac{0,0033}{0,0313} = 0,11$$

$$c_{v,Tm} = \frac{\sigma_{Tm}}{\mu_{Tm}} = \frac{4,7}{131,9} = 0,04$$

Again, the coefficients of variation are not very large. This is due to the same reason the coefficient of variation in the previous section are small. The significant long wave heights and mean long wave periods were taken over the full year, including mild conditions. Averaging out the events during which long waves are mainly active, namely storms.

The temporal variation of the significant wave height is the result of time-varying processes and is therefore most likely to be due to varying forcing conditions.

The graphs of Figure 38 and Figure 39 show that both the significant long wave height and mean long wave period are not equally distributed per season. Winter and fall are the most energetic seasons for both the significant wave height and mean wave period, see Table 6.

Whereas winter is usually the most energetic season in terms of wind velocities, short- and long wave activity, for this specific year and at the locations where long wave data has been gathered, fall is the most energetic season for both the significant long wave height and mean long wave period. Summer and spring are the less energetic seasons, where summer is the least energetic one.

Minor variations in the distribution of the wind velocities with respect to the distribution of the long wave statistics could be explained by, for example, varying wind directions (i.e. varying fetch).

In general the distribution of both parameters correspond well.

Season	Significant wave height [m]	Mean wave period [s]
Winter	0,033	135,63
Spring	0,029	127,5
Summer	0,028	128,13
Fall	0,035	136,25

Table 6 Mean values of the significant wave height and mean wave period most likely to occur per season (averaged over all locations).

Rijkswaterstaat
Ministry of Infrastructure and the Environment

TUDelft
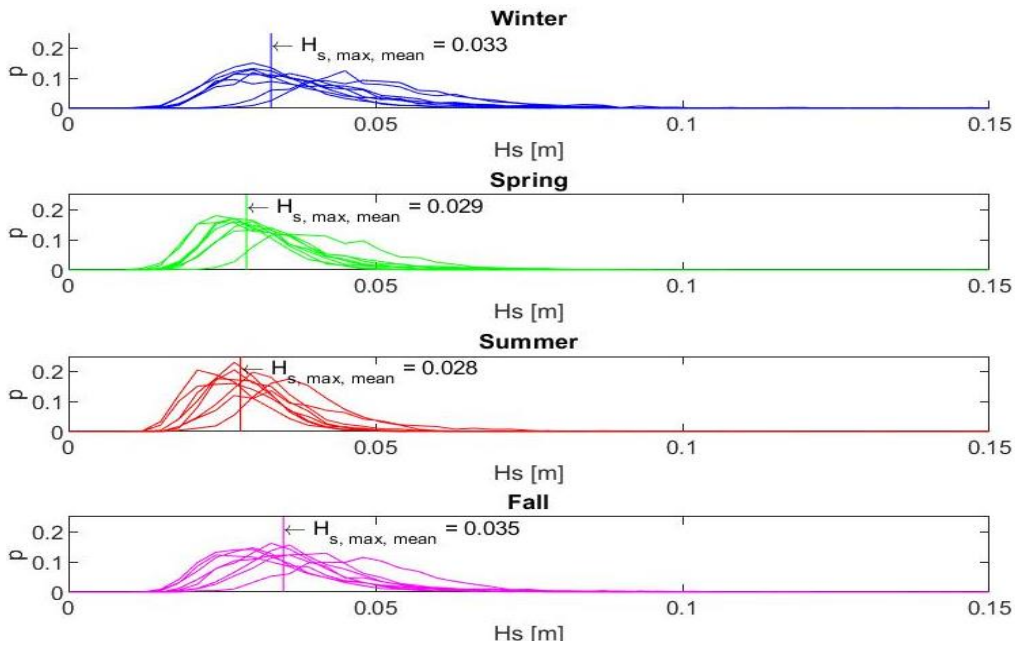
Figure 38 Each graph contains the probability functions of the significant wave height of all locations, from a certain season. The vertical line in each graph is the mean of the most probable values per location of that season.
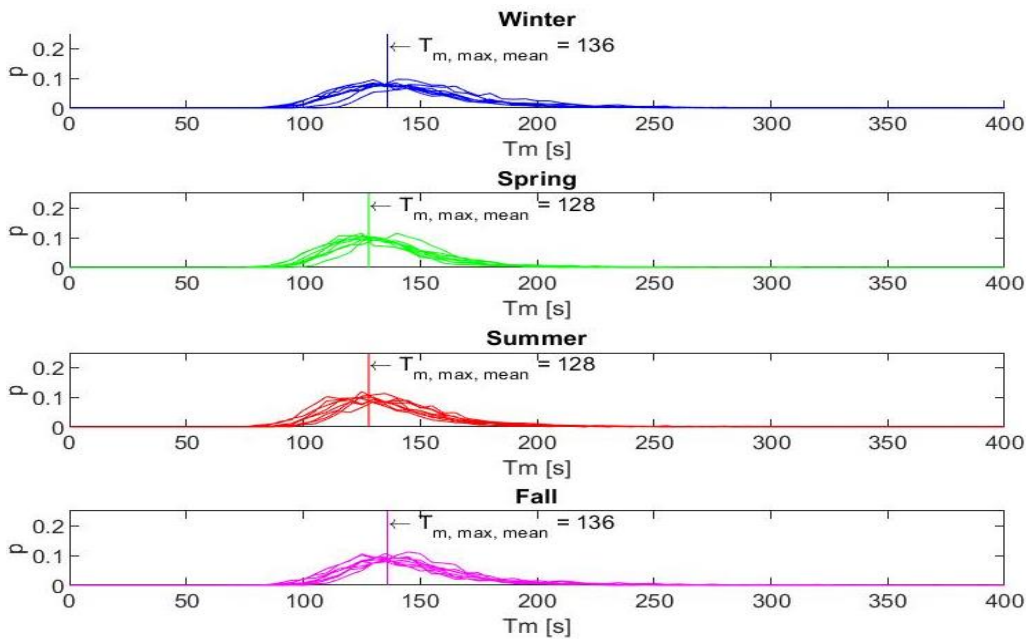
Figure 39 Each graph contains the probability functions of the mean wave period of all locations, from a certain season. The vertical line in each graph is the mean of the most probable values per location of that season.

7.1.3 PROBABILISTIC DISTRIBUTION TYPES

A full year probability function of the significant wave height (as shown in Figure 33) appears to be Rayleigh distributed, implying the significant long wave height per season is also Rayleigh distributed. But this is not necessarily correct. When looking at the significant wave height's probability function per season, see Figure 41, they appear to be Rayleigh- or Gaussian shaped. Typical shapes of the Gaussian- and Rayleigh distribution are shown in Figure 40.
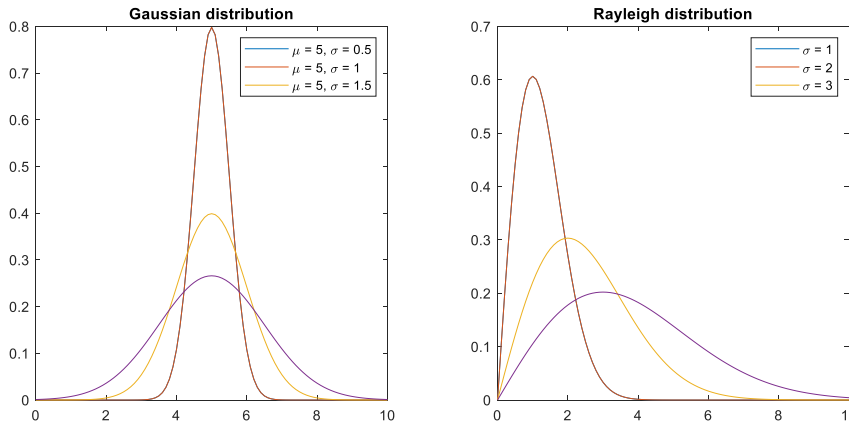
Figure 40 Typical shapes of the Gaussian distribution (left) and the Rayleigh distribution (right)
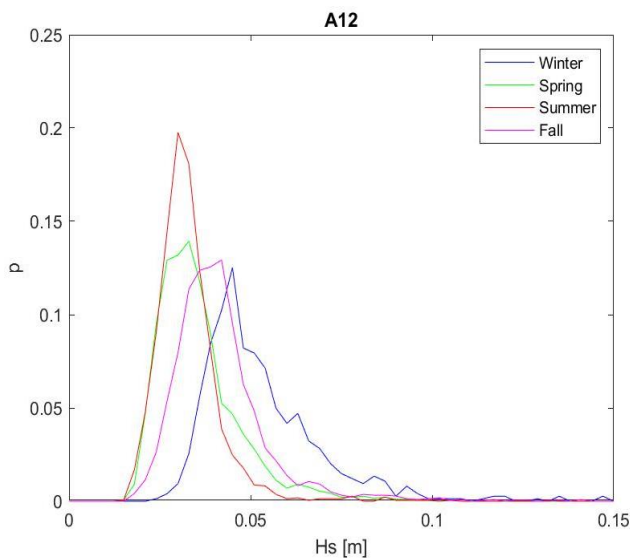
Figure 41 Probability function per season

To quantify this observation, all of the seasonal and full year graphs, for all locations, have been compared to the best fit of both distributions. Which one of the two distributions was the proper fit with the data has been determined with the least MSE technique.

The Gaussian distribution is by far the most similar distribution for the mean wave period's graphs, see Table 8. For the significant wave height the distribution type is approximately half Gaussian-, and the other half Rayleigh distributed, see Table 7.

Since the peak of a Rayleigh distribution is located further towards zero compared to the Gaussian distribution, the highest density of values of a variable with the Rayleigh distribution is located in the lower values. While the peak density is located at the lower values, the Rayleigh distribution has a considerable tail, meaning that the difference between the mean and maximum values is generally higher compared to the Gaussian distribution.

73

Hs	Euro plat.	IJm. Stroom.	Licht. Goer.	Plat. A12	Plat. D15	Plat. F16	Plat. Hoorn	Plat. J6
Winter	G	R	G	G	R	R	R	G
Spring	R	G	R	G	R	G	R	G
Summer	R	G	R	G	G	G	R	G
Fall	G	R	G	G	G	G	R	G
Year	R	R	R	G	R	G	R	G

Table 7 The significant wave height's probability distribution type for all seasons and locations. 'G' indicates that the Gaussian distribution is the best fit, 'R' indicates that the Rayleigh distribution is the best fit.

Tm	Euro plat.	IJm. Stroom.	Licht. Goer.	Plat. A12	Plat. D15	Plat. F16	Plat. Hoorn	Plat. J6
Winter	G	G	G	R	G	G	G	G
Spring	G	R	G	G	G	G	G	G
Summer	R	G	G	G	G	G	G	G
Fall	G	G	G	G	G	G	G	G
Year	G	G	G	R	G	G	G	G

Table 8 The mean wave period's probability distribution types for all seasons and locations. 'G' indicates that the Gaussian distribution is the best fit, 'R' indicates that the Rayleigh distribution is the best fit.

Rijkswaterstaat
Ministry of Infrastructure and the Environment

TUDelft

7.2   EXTREME LONG WAVE CONDITIONS

Flood defenses and several other types of hydraulic structures are designed for extreme wave conditions that usually have not occurred at the location yet. These extreme wave predictions are based on measured wave data and are a valuable asset for flood safety, since they provide insights into the probability of certain (extreme) wave conditions. Since the long wave data provided by Rijkswaterstaat has been measured over a fairly long duration, quite some events have been captured in the measurements. With the available data, the measurement duration and some probabilistic calculations, it is possible to make a prediction of the return period of certain extreme wave conditions. The reliability of this prediction is heavily dependent on the duration of the measurement period and the length of the chosen return period.

7.2.1   10 YEAR STATISTICS OF THE SIGNIFICANT LONG WAVE HEIGHT

First of all the results of the long term (decadal) analysis are compared to the results of the short term (yearly) analysis in order to get an impression of how the rest of the years in the measuring period from 2009 to 2019 relate to the year 2013.

Some variation in the results with respect to the short term analysis is expected, simply because not every year is the same. Variations in, for example, wind velocity/direction or temperature, influence the wave forcing conditions and could cause variations in the results. Since there have not been any significant changes to the North Sea or its environment, large variations in the results are not expected.

The most likely values for the significant long wave heights are annotated in the graphs of Figure 42. For comparison purposes the results from both the short term analysis from Table 5, and the just obtained results from the long term analysis from Figure 42, are shown in Table 9. Variations of the short term analysis with respect to the long term analysis vary from 0,1 – 0,9 cm, the mean variation being 0,46 cm. In percentages this variation varies from 3,1 – 25 %, with a mean of 13,5 %. A mean variation of 13,5 % is not considered to be a large variation. The only location undergoing a significantly larger increase in significant wave height is Platform D15. The most probable value for the significant wave height increases with 25%, and the whole probability function shows a shift to higher significant wave heights.

Rijkswaterstaat
Ministry of Infrastructure and the
Environment

TUDelft
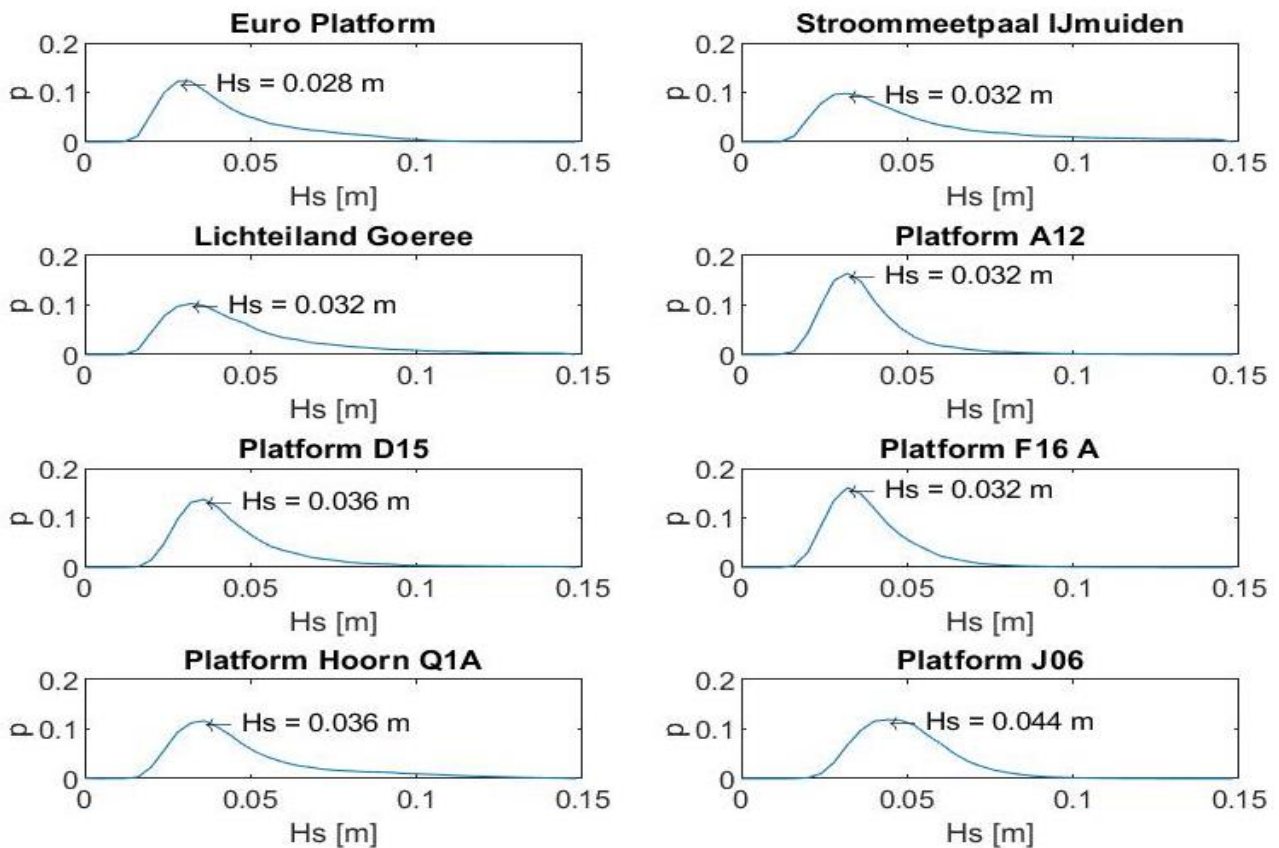
Figure 42 Probability functions of the significant wave height for each location separately, with the most probable significant wave height annotated. The results are composed of all available long wave data.

No.	Location	$\overline{H}_{s,short\ term}\ [cm]$	$\overline{H}_{s,long\ term}\ [cm]$	$\Delta\overline{H}_{s,ST\ vs.\ LT}\ [cm]$	$\Delta\overline{H}_{s,ST\ vs.\ LT}\ [\%]$
1	Europlatform	2,4	2,8	0,4	14,3
2	Lichteiland Goeree	2,7	3,2	0,5	15,6
3	Platform A12	3,3	3,2	0,1	3,1
4	Platform D15	2,7	3,6	0,9	25
5	Platform F16 A	2,7	3,2	0,5	15,6
6	Platform Hoorn Q 1A	3,0	3,6	0,6	16,7
7	Platform J06	3,9	4,4	0,5	11,4
8	Stroommeetpaal IJmuiden	3,0	3,2	0,2	6,3

Table 9 Comparison of the most probable values for H_s from the short term analysis and long term analysis. The columns with $\overline{H}_{s,i}$ contain the mean value of the significant wave height for the short- and long term analysis, $\Delta\overline{H}_{s,ST\ vs.\ LT}$ the variation of the mean value of the short term analysis with respect to the mean of the long term analysis

Overall, the results of the long term analysis show an increase in the significant wave height with respect to the results from the short term analysis. Which means that the year 2013 was probably a year with overall milder long wave conditions, compared to the other years from the full measurement period. Figure 43 visualizes this difference in significant wave height clearly in a graph. The graphs of the probability functions for the full measurement period clearly show a shift to larger wave heights with respect to the probability functions of the year 2013, which means an increase in the probability for higher significant wave heights. Not only do the graphs shift to larger wave heights, the tails of the graphs also seem to be rising. The rise of these tails implies an increase of the more extreme wave heights.
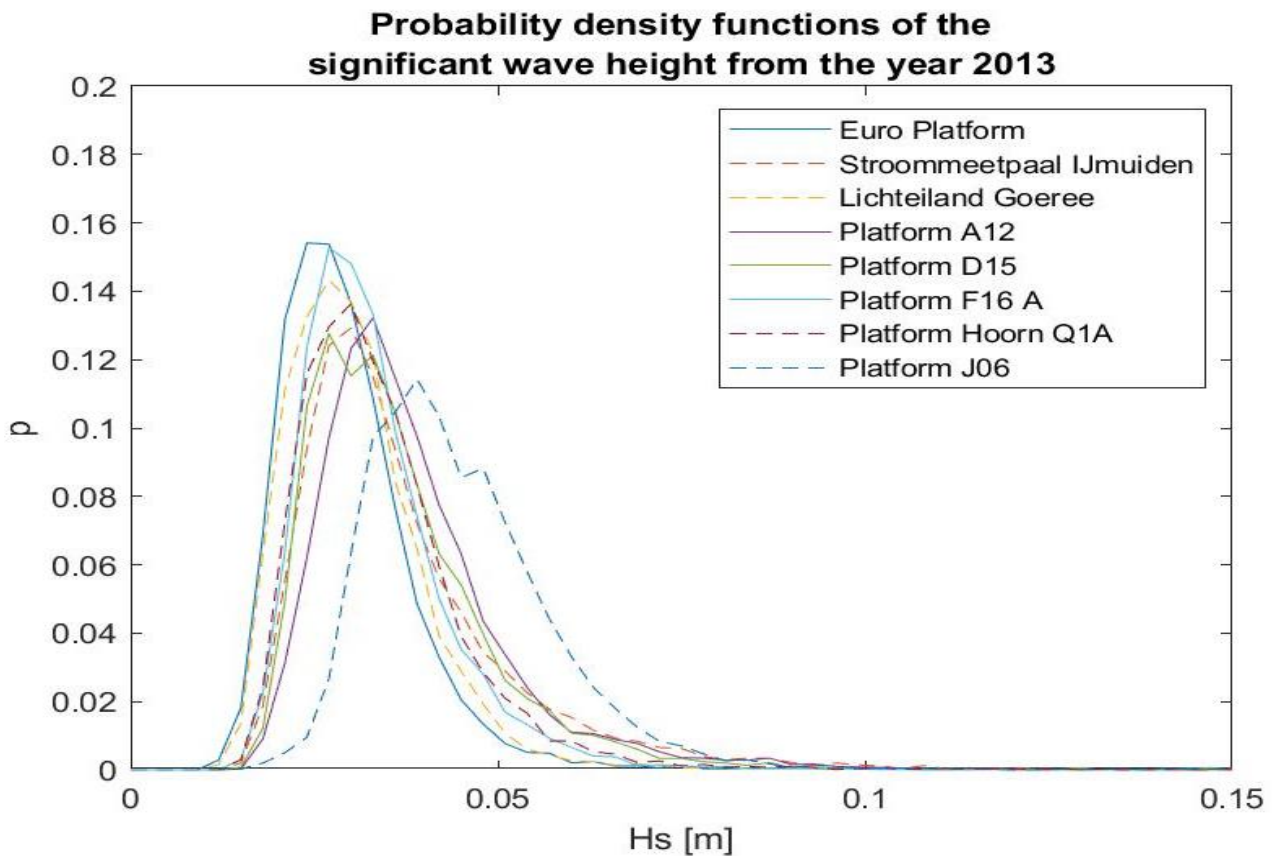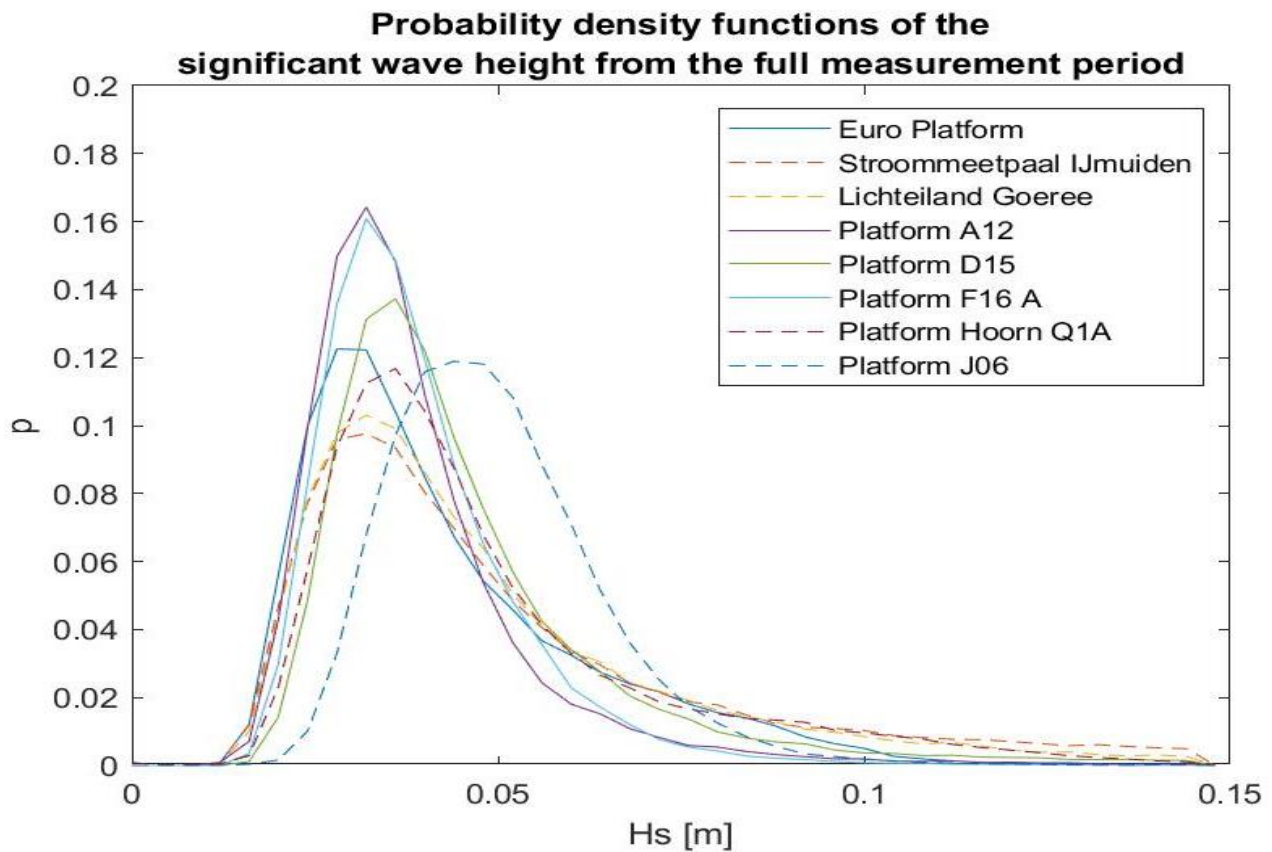
Figure 43 Comparing the probability functions of both the short term and long term analysis. Upper: Probability functions of the significant wave height from all locations over the full measurement period. Lower: Probability functions of the significant wave height from all locations for the year 2013.

The variation in the long wave distribution is possibly caused by varying wind velocities. Boxplots of the significant long wave height and wind velocity of the year 2013 and the full measurement period in Figure 44. These boxplots show that the distribution of the wind velocity at both locations, and for both periods, are approximately the same. The small variation of the distribution of the significant long wave height is most likely caused by varying wind directions (varying fetch lengths).
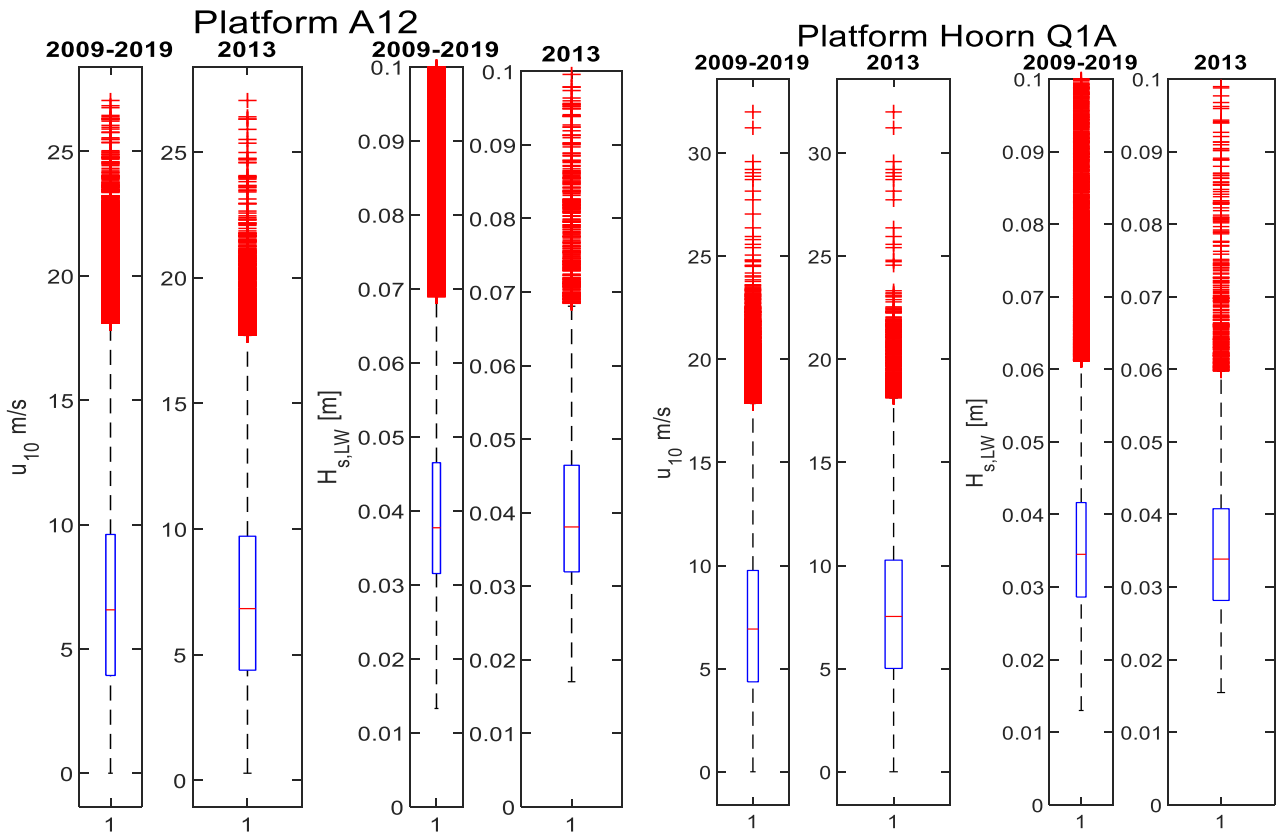
Figure 44 Boxplots comparing the distributions of the wind velocity and significant long wave heights for the year 2013 versus the full measurement period (2009-2019) for locations A12 (left) and Hoorn Q1A (right)

7.2.2 EXTRAPOLATED EXTREME VALUES

Now the results of the long term analysis have been compared with the results of the short term analysis, the long term results are used to determine extreme wave conditions and their return periods. The results of the curve fitting process for each probabilistic distribution type, together with the comparison of all those best fits with the results of the long term analysis, can be found in Appendix B. The best fit per location, together with the extrapolation of these best fits are shown in Figure 46 and Figure 47. A summary is given in Figure 45.

The first obvious observation from the results is the high values for the predicted extreme wave heights of Platform D15 and Stroommeetpaal IJmuiden with respect to the rest, see Figure 45. The values for the predicted extreme wave heights of the other platforms are more clustered together at lower values. Whereas Platform D15 and Stroommeetpaal IJmuiden did not stand out in the probability functions, see Figure 43, they now have the highest extreme wave conditions with a considerable variation with respect to the rest.

An explanation for the higher values of the predicted extreme wave heights of Platform D15 can be found by looking at the distribution of the significant wave heights from the data. Platform D15 shows a high concentration of values around $0,4 - 0,5m$ compared to the rest, see Figure 46 and Figure 47. It is these high values that strongly influence the curve of the predicted extreme wave conditions. Stroommeetpaal IJmuiden also shows a high concentration of significant wave heights around $0,4 - 0,5m$ and also contains some outliers which are even higher. An analysis of the time-series of the location Euro Platform, Platform D15 and Stroommeetpaal IJmuiden is performed in appendix B. The time-series of these three locations contain inexplicable observations, causing the uncertainty of the predictions of these three locations to strongly increase. They are therefor most likely not reliable.

Most of the values for the significant wave height with a return period of 100 years are centered around 30-40cm, Platform D15 and Stroommeetpaal IJmuiden stand out with wave heights of 70cm, see Table 10. For a return period of 1000 years this increases to 30-50cm for the majority of the platforms, and 80-90cm for the two standing out. The 10000 year return period coincides with the design conditions for the Dutch coastal defenses. Most of the platforms reach extreme long wave heights of up to 40-60cm, and the two platforms standing out reach values of up to 1m.

The graphs in Figure 45 and the results in Table 10 show a considerable variation of extreme wave heights between the locations, diverging from each other towards the longer return periods. Platform J6 is the location with the highest significant wave heights in the short term analysis, but is by far not the location with the highest extreme significant wave heights in the long term analysis. Platform D15 and Stroommeetpaal IJmuiden are the locations with the highest extreme significant wave heights. Not only do they have the highest extreme significant wave heights, the variation with respect to the other locations is significant.

Location	$H_{s,R=100\ years}\ [cm]$	$H_{s,R=1000\ years}\ [cm]$	$H_{s,R=10000\ years}\ [cm]$
Europlatform	41,24	50,09	59,34
Lichteiland Goeree	34,53	39,84	45,14
Platform A12	27,83	32,98	38,23
Platform D15	70,37	87,48	105,67
Platform F16 A	32,90	40,13	47,77
Platform Hoorn Q 1A	45,00	53,24	61,65
Platform J06	38,37	47,08	56,37
Stroommeetpaal IJmuiden	67,98	80,45	93,11

Table 10 The predicted values of the significant wave height for certain return periods.
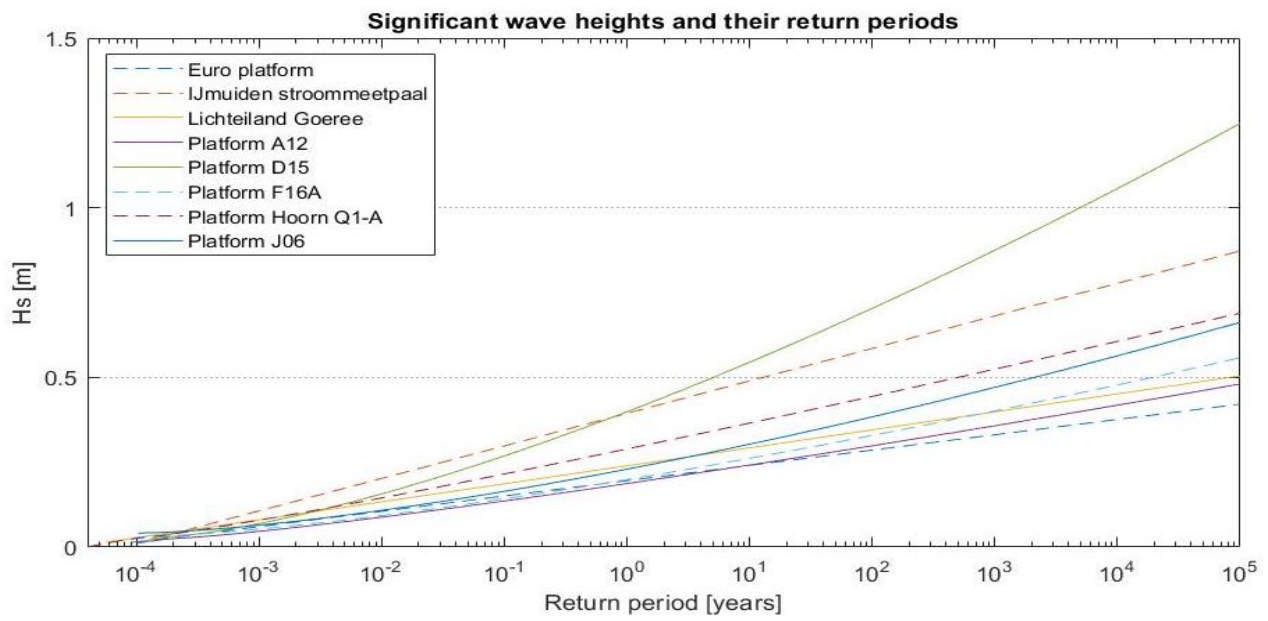
Figure 45 The extrapolated graphs of the best fit probabilistic distribution types per location
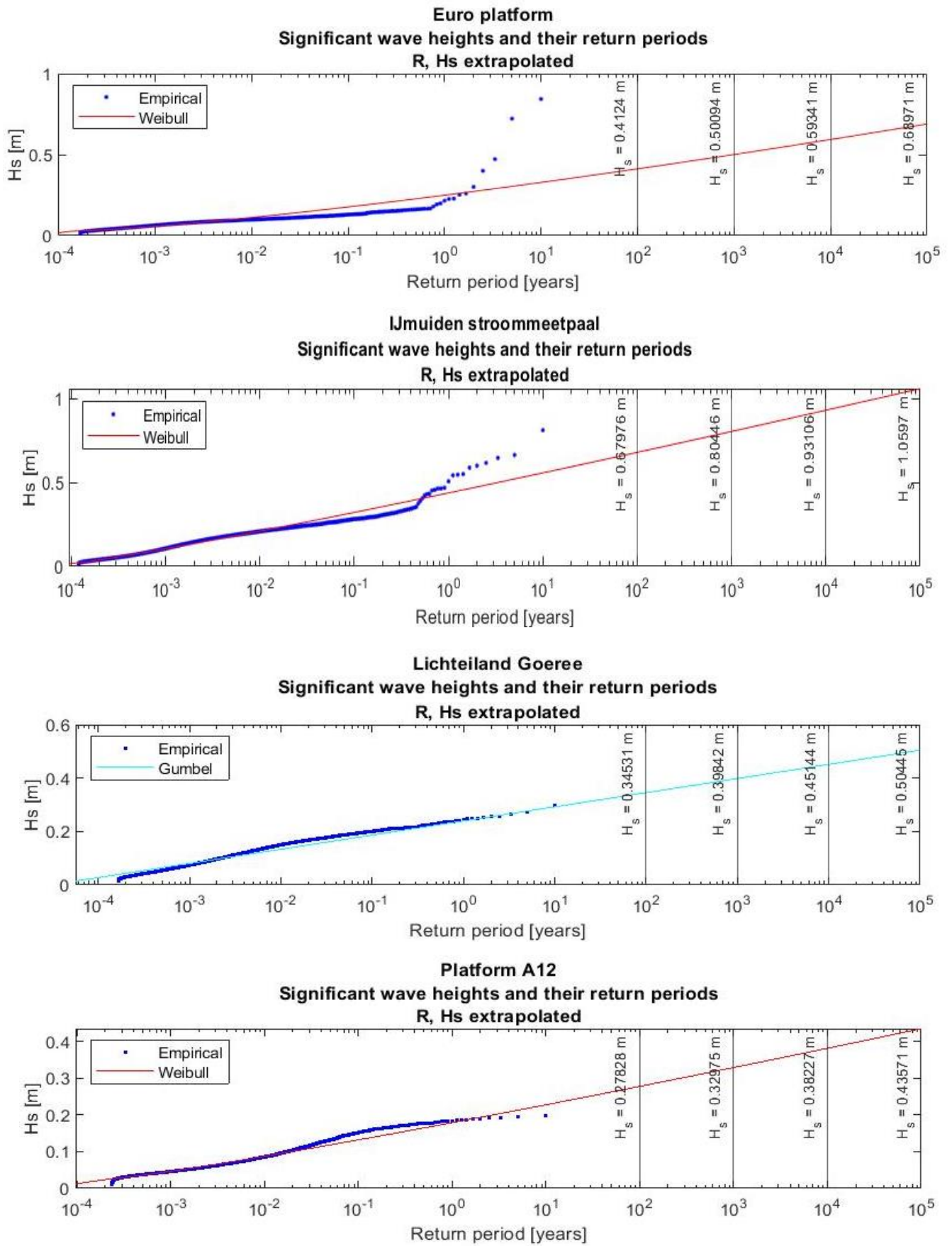
Figure 46 The results of the spectral analysis (blue dots) with their best fit probabilistic distribution type (solid line)

Rijkswaterstaat
Ministry of Infrastructure and the
Environment

TUDelft
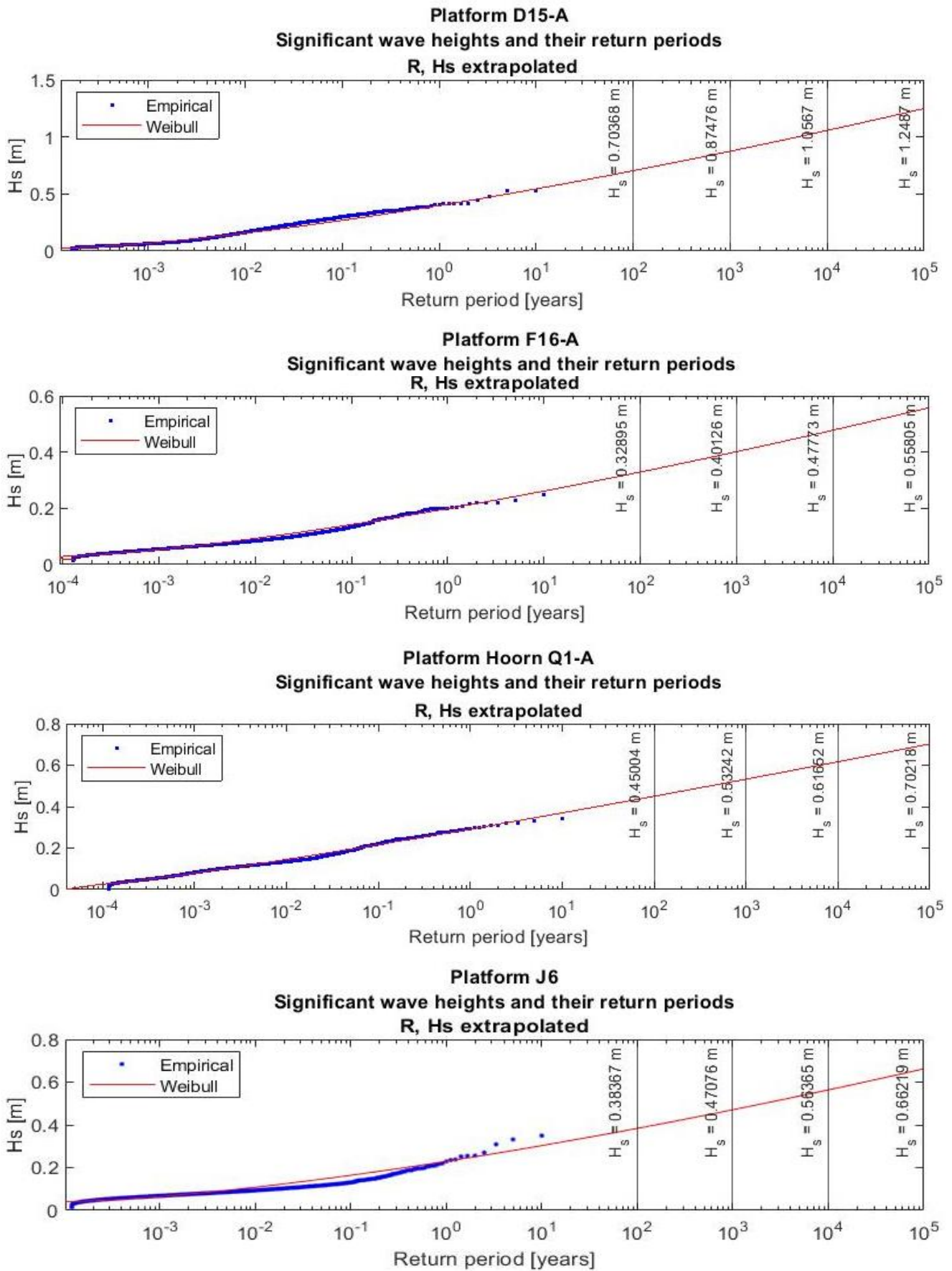
Figure 47 The results of the spectral analysis (blue dots) with their best fit probabilistic distribution type (solid line)

8.1   DISCUSSION

Data on long waves has been provided for a limited frequency range ($0 < f < 0,0125\ Hz$), which limits the research to these frequencies. Even though the provided frequency range is limited, results have shown that in this frequency range valuable information on long waves activity is captured. It remains unknown what is contained in the higher frequency band of long waves ($0,0125 < f < 0,05\ Hz$).

During high long wave activity, the data contained significantly more errors compared to mild conditions (Figure 23 and Figure 25). The filter that has been applied to process the provided water surface elevation data has removed the wave records containing a high concentration of errors. Missing out on data during the most interesting events has most likely influenced the results. By missing data during high long wave activity, the number of points containing high hourly significant long wave heights is reduced, causing probability functions and extreme long wave predictions to be less accurate.

With the current measuring method it is not possible to construct the phase lag between short waves and long waves, since short wave information has been filtered out of the water surface elevation time-series. The phase lag is needed to accurately determine the contribution of bound long waves by bispectral analysis. In this research the bound long wave contribution has been predicted using Hasselmann's second order non-linear theory. This theory has shown to be accurate for a wide range of conditions in (Herbers et al., 1994), but still remains a prediction.
Hasselmann's second order non-linear theory determines bound long wave activity based on theory. For varying input conditions (wind velocity, water depth, etc.) the output (bound long wave activity) responds immediately, while in reality some time is required for all parameters involved to adapt, which could lead to an overestimation of bound long wave activity at a certain point in time (Herbers, et al., 1997). This could provide an explanation for why the predicted bound long wave activity exceeded the observed total long wave activity.

Long wave directional information is not available, making it impossible to make a distinction between incident (locally generated) and reflected long waves. Not knowing the fraction of incident long waves makes deriving the relevant generation mechanisms harder. Additional directional information is required to be able to make the distinction between incident and reflected long waves.

The analysis of the relation between waves and wind at a location has been performed for all wind directions. For the given locations, the fetch varies considerably for various wind directions. This has resulted in a weak correlation between wind and significant long wave heights, while the correlation is most likely stronger for a fixed fetch.

In general, the coefficients of variation are not very high for any of the distributions or parameters. An explanation for the low coefficient of variation can be found by the way the most probable value has been determined. All values over the year/season have been processed in a probability function. While this is an appropriate way to determine the probabilities over the full year or season, it does not give a proper representation of the events during which the vast majority of long waves are mainly active, namely storms. Storms only cover a fraction of the total period ($0,6 - 2,5\%$ of the full year in 2013), while mild/medium weather conditions cover the largest part. Long waves have shown low activity during mild/medium weather conditions. Hence, the low long wave activity during mild/medium weather conditions even out the long wave activity during storms to very low values over the full year. This causes the most probable value for the parameters to be representative for the full period, but not for the conditions in which long waves are active for the vast majority.

The data that has been used to predict extreme wave conditions displayed on occasion remarkable extreme long wave heights at some locations (Europlatform and Stroommeetpaal IJmuiden, see Figure 66). These waves are most likely caused by external factors, like passing ships or maintenance works. Automatic filtering has not removed these waves from the data, since their properties are similar to long waves. Manual filtering has removed most of these waves, but some of them might still be contained in the analysis. An observation of a long term (several years) significant increase

Rijkswaterstaat
Ministry of Infrastructure and the Environment

in the amplitude of observed long wave water surface oscillations at another location (Platform D15, see Figure 65) is also remarkable. The extreme value predictions at these locations therefore have a high uncertainty. There's a number of possible explanations for the variations of the data at these locations. For example, mooring ships could cause high local variations of the water level, maintenance of the measurement device could result in some weird values, ships sailing under the radar cause a high local increase of the water level, and so on.

The prediction of extreme long wave conditions is based on 10 years of data. The usual measurement period for such predictions is about 30 years. The combination of the short measurement duration of the data and the remarkable observations result in an increase of the extreme long wave predictions.

8.2   CONCLUSIONS

The goal of this thesis was to explore the contents and possibilities of the data on long waves in the North Sea that has been provided by Rijkswaterstaat, together with obtaining an impression of the long wave spatial/temporal distribution and finding the relevant mechanisms responsible for the generation of long waves. Since long waves (mainly infragravity waves) have a significant influence on several coastal processes, such as coastal erosion or flood defense failure, it is of crucial importance for coastal safety to have a thorough understanding of their origin, magnitude and distribution. This is the first long wave dataset that covers such a wide area (57.000 km^2) and long period (approximately 10 years) in the North Sea.

The data provided by Rijkswaterstaat contains the water surface elevation time-series, with a sampling frequency of $0,08\ Hz$. Data has been recorded at 8 measurement stations spread out over the Dutch territorial waters in the North Sea, starting in February 2009. The content of the data is affected by a filter, which is designed to only retain low frequency oscillations in the water level. All frequencies higher than approximately $0,0125\ Hz$ are filtered out, leaving the data with a frequency range of $0 < f < 0,0125\ Hz$. In this frequency range only a small fraction of infragravity waves frequencies ($0,004 < f_{IGW} < 0,04\ Hz$) is captured.

Since the North Sea is a semi-enclosed basin, long waves are most likely mainly generated locally in the North Sea. The parameters that are expected to be most relevant for long wave generation are wind, atmospheric pressure, storm surge and short waves. These have been compared with long wave activity to find the most relevant long wave generation mechanisms.

Long wave activity is low during mild conditions and rapidly increases during storms, implying the long waves are indeed mainly locally generated. The parameters that have the strongest correlation with long wave activity are wind velocity and short waves. Atmospheric pressure and storm surge seem to have little to no correlation with long wave activity.

Non-linear interactions between short waves are a well-known generation mechanism for long waves. Hasselmann's second order non-linear theory has been used to predict the contribution of bound long waves at every possible location. Analysis of bound long wave activity shows that bound long wave activity is very low or absent during mild conditions, and rapidly increases during storms. The relative contribution of bound long waves to the total long wave activity (E_{BLW}/E_{LW}) is high. The percentage of E_{BLW}/E_{LW} reaches values of up to a maximum of 60% for the frequency band $0,005 < f < 0,015\ Hz$ and reaches up to 100% in the frequency band $0,015 < f < 0,035\ Hz$, whereas other studies have shown percentages of up to a maximum of 30%. The high ratio of the relative bound long wave contribution, in combination with very low bound long wave activity during mild conditions, shows that the generation mechanism involving non-linear interactions between short waves is indeed a major generation mechanism of long wave activity in the North Sea.

A high relative contribution of bound long waves also means a (relatively) low relative contribution of free long waves. The free long waves at a certain point concern the incoming and reflected free long waves. The high relative contribution of the bound long waves could also be a result of a low fraction of reflected free long waves. If that is the case, free long waves do not reflect at nearshore coastlines, but instead break and dissipate.

Though it is not evident that wind is directly responsible for the generation of long waves, it is responsible for the generation of short waves. Short waves are crucial in the process of long wave generation, since they are involved in several long wave generation mechanisms (i.e. wave group forcing, and varying breakpoint mechanism). This makes wind velocity in combination with wind direction a valuable indicator for long wave activity. The weak correlation

Rijkswaterstaat
Ministry of Infrastructure and the Environment

TUDelft

between wind velocity and significant long wave heights can be explained by the wind direction. With varying wind directions, the fetch changes considerably. Which means that for the same wind velocity, coming from another direction, the significant short wave height (and thus significant long wave height) varies.

Analysis of the spatial variation shows that the most likely values for the yearly averaged significant long wave height varies from 2,4 - 3,3 cm, with an outlier at 3,9 cm. Most likely values for the mean long wave period go from 125 to 140 s. The spatial variation of the significant long wave heights ($c_{v,Hs} = 0,159$) is considerably larger than the mean long wave period's variation ($c_{v,Tm} = 0,038$). This observation is not very surprising since the wave period is a parameter that, when looking at a single propagating wave with no external forcing, does not change in time (Holthuijsen, 2007). Meaning that when such a wave passes several locations, the wave period will be the same at all of those locations, while other parameters may vary. There is no clear trend in the spatial distribution of the decade averaged significant wave heights. Off-shore locations show slightly higher wave heights compared to nearshore stations, but the difference is negligible ($\Delta \overline{H}_{s,offshore\ vs.\ nearshore} = 0,38\ cm$).

The seasonal variation analysis shows that the spatially averaged mean significant wave height varies from 2,8 cm (summer) to 3,5 cm (fall), see Figure 38. Winter and fall are the seasons with highest long wave heights, followed up by spring and then summer. Mean wave periods vary from 127 s (spring) to 136 s (fall). Again the significant wave height is the stronger varying parameter, $c_{v,Hs} = 0,11$, whereas $c_{v,Tm} = 0,04$.

In general yearly averaged mean long wave periods are not affected much by seasonal or spatial variations. The spatial variation of the significant wave height is stronger than the temporal variation, which indicates that, in this case, the long wave height is more sensitive to spatially varying properties.

Extreme value predictions of significant long wave heights show that a return period of 100 years results in long waves with a height of 30 to 45 cm. A return period of 1.000 years results in waves with a height of 30 to 50cm, and a return period of 10.000 years (Dutch design conditions for, amongst others, coastal flood defenses) results in waves with a height of 40 to 60 cm.

Rijkswaterstaat
Ministry of Infrastructure and the Environment

TUDelft

Store raw data instead of filtering the data with the FIR filter

Currently, not all wave frequencies are included in the data. $f < 0,0125\ Hz$ (low frequency long waves) are included in the data, while $0,0125 < f < 0,04\ Hz$ (higher frequency long waves), and $f > 0,04\ Hz$ (short waves) are missing. This means a large fraction of the total long wave frequency band is not available for research. In addition, the ingredients needed for performing a bispectral analysis are not available. The bispectral analysis is capable of accurately determining the bound long wave contribution to the total long wave spectrum during all conditions. It is recommended to directly store the raw water surface elevation time-series, instead of filtering it with a FIR filter. The benefits are expanding the long wave frequencies available for research from $0 < f < 0,0125\ Hz$ to $0 < f < 0,04\ Hz$. Together with allowing a bispectral analysis to be performed, so the bound long wave contribution can be determined.

Add long wave directional information

Adding long wave directional information allows to make the distinction between incident and reflected waves, providing better insights into the fraction that has been locally generated and therefor into the relevant generation mechanisms of long waves. With backward ray tracing (Smit, et al., 2018) it is possible to determine the origin of the fraction of reflected waves. This provides a powerful tool to determine the origin and paths free long waves travel through the North Sea basin. Including directional information allows confirming if the high relative contribution of bound long waves is caused by a high local generation, or is the result of a large amount of long waves breaking nearshore.

Analyze the correlation between the significant long wave height and the variation in atmospheric pressure

In the current analysis method, the atmospheric pressure showed no correlation with long wave activity. However, analysis of their time-series does show they coincidentally increase and decrease, implying there is some sort of correlation. Whereas the atmospheric pressure itself shows no correlation with long wave activity, the variation in atmospheric pressure might. Studying the correlation between the significant long wave height and the variation in atmospheric pressure ($\frac{\delta P}{\delta t}$) might result in more interesting results.

Improve the database that stores the provided data

Rijkswaterstaat possesses an immense database with a lot of valuable information relevant for the research of long waves in the North Sea. However, retrieving data from that database has proven to be a difficult operation. For example, long wave data has been measured at 18 locations, of which only 8 have been retrieved. The other 10 locations cover a wider variety of areas (stations located further inland or in tidal basins and harbors) in which long waves have been measured. The problem of missing data per location did not only occur for long wave data, but also occurred for several other types of data. Other examples are the short wave energy density- and frequency direction spectra. These are available for all 8 locations, but have been provided for only 2 locations. The relatively short time span over which this thesis has been conducted, together with the duration required to retrieve required data, has unfortunately resulted in a delay of the research data not arriving in time. Improving the system for retrieving data from their database opens up a lot of research possibilities. Having all data available for all locations allows a more extensive research. Besides measurement stations located in open sea/nearshore, measurement stations inside of tidal basins, harbors and estuaries will also be available for analysis.

Visual inspection of the measurement device and its surroundings

The long wave data showed some remarkable extreme long wave observations, a number of explanations are possible, but exact explanation remains unknown. Filtering these errors is not possible as they often contain the same properties as actual waves. This means that if they are filtered out, actual data will be lost as well. It is recommended to find a method to identify these remarkable extreme long wave observations. Visual surveillance (i.e. photo graphs or video images) of the measurement device and its surrounding area offers a solution. When a remarkable extreme wave height has been observed, the visual surveillance is able to show whether it has a physical explanation (for example, a passing ship or a change of the environment of the measurement area) or not. If it has a physical explanation, the observation

Rijkswaterstaat
Ministry of Infrastructure and the Environment

can be filtered out accurately. This will remove the actual errors from the data, while maintaining the actual extreme wave heights. Thus improving the extreme wave height predictions.

Expand the area in which long wave are being measured by collaborating with other countries
Not just the Netherlands, but other countries surrounding the North Sea perform measurements in the sea as well. Rijkswaterstaat already collaborates with Great Britain to collect, for example, short wave data. A collaboration between the measurement networks of the countries could provide a network of measurement stations covering a large area of the North Sea. A wide variety of areas would be included in this network, opening up a lot of research possibilities. The spatial variation of long waves in the North Sea can be studied to a much larger extent. The current area in which the spatial variation is studied covers approximately 57.000 km^2 and is relatively shallow in the North Sea. The full size of the North Sea is 575.000 km^2 and covers more divers area types.

Perform the analysis between the wind velocity and long waves for certain wind direction intervals
With varying wind directions, the fetch changes considerably. Which means that for the same wind velocity, coming from another direction, the significant short wave height (and thus significant long wave height) varies. In this research the relation between wind velocity and long waves has been performed over all wind directions, resulting into a medium to weak correlation between long waves and wind. Performing the same analysis for certain fixed wind direction intervals (i.e. fixed fetch) gives a better representation of the relation between wind and long waves.

TUDelft

A.   METADATA

A.   LONG WAVES

In each file the metadata (data about the data) is given prior to the data. Figure 48 shows the general metadata for location Europlatform. After the general metadata a description of the frequency intervals follows (Figure 49 and Figure 50), these describe the frequency intervals used for the amplitude spectrum. Just before the actual data starts, the measurement duration and frequency is given, see Figure 51. An example of one row of data is shown in Figure 52.

```
 1   [W3H]
 2   MUX;SEICHS;Seiches, periodieke oscillaties van de waterhoogte
 3   IVS;NVT;Niet van toepassing
 4   BTX;NVT;NVT;Niet van toepassing
 5   BTN;Niet van toepassing
 6   ANI;NZXXMTZRWK;Dienst Noordzee - afdeling WSM te Rijswijk
 7   BHI;RIKZITSDHG;RIKZ - afdeling ZDI te Den Haag
 8   BMI;NZXXMTZRWK;Dienst Noordzee - afdeling WSM te Rijswijk
 9   OGI;RIKZ_GOLVEN;RIKZ - Landelijke golven gegevens
10   GBD;NOORDZE;Noordzee  (internationaal)
11   LOC;EURPFM;Euro platform;P;E50;3163500;51595500
12   ANA;F168;Herbemonsterd van 2,56 HZ naar 0,08 HZ (RMI Seiches-module)
13   BEM;VELDMTG;Veldmeting, directe bepaling in het veld
14   BEW;NVT;Niet van toepassing
15   VAT;SAAB;Radar - type Saab
16   TYP;TE
```

Figure 48: Long wave general metadata from location Europlatform

2: Type of observation

3, 4, 5: Non relevant fields

6, 7, 8, 9: Involved departments of Rijkswaterstaat

10: Area

11: Location name (Europlatform), type (P stands for point), coordinate system (E50 stands for ED 1950, type of coordinate system varies per location), coordinates indicative for measurement

12: Processing method applied to data (resampled from 2,56 Hz to 0,08 Hz (FIR-filter, see 4.2.2) to filter out short waves (Kamminga, 2001)). This operation has been applied to all long wave data

13: Type of measurement (field measurement, same for all locations)

14: Non relevant fields

15: Type of measuring device (Radar, type: Saab).

16: Type of series (TE means equidistant time series)

Rijkswaterstaat
Ministry of Infrastructure and the Environment

TU Delft

```
102    MXW;13;5973
103    MXP;13;LG;Golfhoogte uit spectrum van 0,083 mHz - 8,33 mHz;J
104    MXC;13;10;Oppervlaktewater
105    MXE;13;I;cm
106    MXH;13;NVT;Niet van toepassing
107    MXO;13;NVT;Niet van toepassing
108    MXS;13;TS13
```

Figure 49 Example of frequency interval description, this is interval 13

103: What exacly is measured (wave height in range 0,083 mHz – 8,33 mHz). This is the same for all measurement locations.

104: What is measured: water surface elevation. Same for all locations

105: Unit: cm. Same for all locations

108: To which frequency interval the above metadata applies (since this applies to every frequency interval this information is repeated for all 48 frequency intervals). Same for all locations

```
379    KLS;13;TSG100;> 100 sec
380    KLS;13;TSK112;< 112,5 sec
```

Figure 50 Example of one of the frequency classes in which the long

379: Describes the lower bound of frequency interval 13

380: Describes the upper bound of frequency interval 13

```
451    [RKS]
452    TYD;20050113;0800;20090102;1710;10;min
453    PLT;NVT;-999999999;3163500;51595500
454    SYS;CENT
455    [TPS]
456    STA;20050113;0800;20090102;1710;O
```

Figure 51 Measurement period and exact location

452: Start- (13-1-2005 08:00) and end time (2-1-2009 17:10) of the measurements in the file, followed by interval of each given value (10 min.)

453: Exact location (might deviate slightly from location mentioned line 11)

```
457    [WRD]
458    8/0;8;7;7;6;6;5;6;6;6;5;4;4;4;4;4;4;4;4;3;3;2;2;1;2;2;3;3;3;3;3;3;3;3;3;3;2;1;1;0;1;1;1;0;0;0;0;0:
```

Figure 52 Line denoting start of data and first row of data

457: Denotes start of data

458: First row of data. Each row represents a value for the water level elevation every 10 min. A row consists of 48 elements (so 480 min), each element describes the amplitude of that frequency interval. The first value in a row is

Rijkswaterstaat
Ministry of Infrastructure and the Environment

TUDelft

accompanied by a rating of the quality of the data, this is the '/0' following the first values. This rating is valid for the whole row. '/0' means the quality of the measurement is good.

B. SHORT WAVES

The short wave metadata is shown in Figure 53 together with the first line of data of that location. Some lines are similar to the ones from the long wave data and will therefore be left out of this analysis.

```
 1  {\rtf1\ansi\deff0\nouicompat{\fonttbl{\f0\fnil\fcharset0 Courier New;}{\f1\fnil\fcharset0 Calibri;}}
 2  {\*\generator Riched20 10.0.17134}\viewkind4\uc1
 3  \pard\f0\fs22\lang1033 [W3H]\par
 4  WNS;22\par
 5  PAR;Hm0;Significante golfhoogte uit energiespectrum van 30-500 mHz;J\par
 6  CPM;10;Oppervlaktewater\par
 7  EHD;I;cm\par
 8  HDH;NVT;Niet van toepassing\par
 9  ORG;NVT;Niet van toepassing\par
10  SGK;NVT\par
11  IVS;NVT;Niet van toepassing\par
12  BTX;NVT;NVT;Niet van toepassing\par
13  BTN;Niet van toepassing\par
14  ANI;NZXXMTZHVHLD;Dienst Noordzee – afdeling MTZ (vervalt, gebruik NZXXMTZRWK)\par
15  BHI;RIKZITSDHG;RIKZ – afdeling ZDI te Den Haag\par
16  BMI;NZXXMTZHVHLD;Dienst Noordzee – afdeling MTZ (vervalt, gebruik NZXXMTZRWK)\par
17  OGI;RIKZMON_GOLVEN;RIKZ – Landelijke monitoring golvenmeetnet gegevens\par
18  GBD;NOORDZE;Noordzee  (internationaal)\par
19  LOC;EURPFM;Euro platform;P;E50;3163500;51595500\par
20  ANA;F043;Tijdreeks en frequentie analyse, methode CIC/GLFPAR\par
21  BEM;VELDMTG;Veldmeting, directe bepaling in het veld\par
22  BEW;NVT;Niet van toepassing\par
23  VAT;MARN300;Stappenbaak – type Marine 300\par
24  TYP;TE\par
25  [RKS]\par
26  TYD;19871101;0100;19991123;0000;60;min\par
27  PLT;NVT;-999999999;3163500;51595500\par
28  SYS;CENT\par
29  [TPS]\par
30  STA;19871101;0100;19970901;0000;D\par
31  STA;19970901;0100;19991123;0000;O\par
32  [WRD]\par
33  54/0:62/0:71/0:75/0:84/0:86/0:87/0:93/0:89/0:98/0:109/0:103/0:100/0:88/0:82/0:83/0:77/0:77/0:97/0:114/0:113/0:109/0:\par
```

Figure 53: Short wave metadata

5: Type of observation; Significant wave height from energy spectrum frequency 0,03 – 0,5 Hz (period of 2 s to 33 s)

6: What has been measured; Water surface elevation

7: Unit; cm

8-13: Non-relevant fields

20: Processing method applied to data (CIC = controle- en informatiecentrum = Control and information centre);

33: First line of data; Significant wave height per interval of 60 min.

C. WATER LEVEL

```
 1 [IDT;*DIF*;A;CENT;20190510]
 2 [W3H]
 3 WNS;54
 4 PAR;WATHTE;Waterhoogte;J
 5 CPM;10;Oppervlaktewater
 6 EHD;I;cm
 7 HDH;MSL;T.o.v. Mean Sea Level
 8 ORG;NVT;Niet van toepassing
 9 SGK;NVT
10 IVS;NVT;Niet van toepassing
11 BTX;NVT;NVT;Niet van toepassing
12 BTN;Niet van toepassing
13 ANI;NZXXMTZRWK;Dienst Noordzee - afdeling WSM te Rijswijk
14 BHI;RIKZITSDHG;RIKZ - afdeling ZDI te Den Haag
15 BMI;NZXXMTZRWK;Dienst Noordzee - afdeling WSM te Rijswijk
16 OGI;RIKZMON_WAT;RIKZ - Landelijke monitoring waterhoogten gegevens
17 GBD;NOORDZE;Noordzee  (internationaal)
18 LOC;A12;Platform A12;P;W84;3480000;55230000
19 ANA;F007;Rek. gem. waterhoogte over vorige 5 en volgende 5 min(MSW90)
20 BEM;VELDMTG;Veldmeting, directe bepaling in het veld
21 BEW;NVT;Niet van toepassing
22 VAT;SAAB;Radar - type Saab
23 TYP;TE
24 [RKS]
25 TYD;20090201;1150;20190510;0050;10;min
26 PLT;NVT;-999999999;3480000;55230000
27 SYS;CENT
28 [TPS]
29 STA;20090201;1150;20190510;0050;0
30 [WRD]
```

Figure 54 Water level metadata

4: Type of data being measured; Water level

5: What has been measured; Water surface

6: Unit; Cm

7: Reference level; MSL

13-16: Departments involved

17: Area; North Sea

18: Location

19: Processing method; Time-series of the water level, average over every 5 minutes before and 5 minutes after

20: Type of measurement; Field observation

22: Measurement device

25: Measurement period

26: Location coordinates

TUDelft

D. WIND

```
 1  [W3H]
 2  WNS;38
 3  PAR;WINDSHD;Windsnelheid;J
 4  CPM;80;Lucht
 5  EHD;F;m/s
 6  HDH;NVT;Niet van toepassing
 7  ORG;NVT;Niet van toepassing
 8  SGK;NVT
 9  IVS;NVT;Niet van toepassing
10  BTX;NVT;NVT;Niet van toepassing
11  BTN;Niet van toepassing
12  ANI;EXT.KNMIDBT;KNMI te De Bilt
13  BHI;RIKZITSDHG;RIKZ - afdeling ZDI te Den Haag
14  BMI;EXT.KNMIDBT;KNMI te De Bilt
15  OGI;RIKZ_METEO;RIKZ - Landelijke meteorologische gegevens
16  GBD;NOORDZE;Noordzee  (internationaal)
17  LOC;EURPFM;Euro platform;P;E50;3163500;51595500
18  ANA;F018;10 minuut scalair gemiddelde van de windsnelheid
19  BEM;VELDMTG;Veldmeting, directe bepaling in het veld
20  BEW;NVT;Niet van toepassing
21  VAT;FASTRCDR;Windsnelheidsmeter - type Fast recorder
22  TYP;TE
23  [RKS]
24  TYD;20080604;1000;20090102;1710;10;min
25  PLT;MSL;1000;3163500;51595500
26  SYS;CENT
27  [TPS]
28  STA;20080604;1000;20090102;1710;O
29  [WRD]
30  2.38/0:2.57/0:2.61/0:3.18/0:2.96/0:3.21/0:3.24/0:3.2/0:2.98/0:3.02/0:3.71/0:3.46/0:2.74/0:2.63/0:2.1/0:1.74/0:1.45/0:
```

Figure 55: Metadata on wind velocity

```
 1  [W3H]
 2  WNS;41
 3  PAR;WINDRTG;Windrichting;J
 4  CPM;80;Lucht
 5  EHD;F;graad
 6  HDH;WARNDN;T.o.v. ware Noorden
 7  ORG;NVT;Niet van toepassing
 8  SGK;NVT
 9  IVS;NVT;Niet van toepassing
10  BTX;NVT;NVT;Niet van toepassing
11  BTN;Niet van toepassing
12  ANI;EXT.KNMIDBT;KNMI te De Bilt
13  BHI;RIKZITSDHG;RIKZ - afdeling ZDI te Den Haag
14  BMI;EXT.KNMIDBT;KNMI te De Bilt
15  OGI;RIKZ_METEO;RIKZ - Landelijke meteorologische gegevens
16  GBD;NOORDZE;Noordzee  (internationaal)
17  LOC;EURPFM;Euro platform;P;E50;3163500;51595500
18  ANA;F034;10 minuut gemiddelde van de windrichting
19  BEM;VELDMTG;Veldmeting, directe bepaling in het veld
20  BEW;NVT;Niet van toepassing
21  VAT;FASTRCDR;Windsnelheidsmeter - type Fast recorder
22  TYP;TE
23  [RKS]
24  TYD;19830103;2000;20041229;1600;60;min
25  PLT;MSL;1000;3163500;51595500
26  SYS;CENT
27  [TPS]
28  STA;19830103;2000;20040801;0100;G
29  STA;20040801;0200;20041229;1600;O
30  [WRD]
31  220/0:210/0:220/0:220/0:220/0:210/0:210/0:210/0:210/0:210/0:200/0:200/0:200/0:210/0:230/0:240/0:250/0:260/0:270/0:270/0:
```

Figure 56: Metadata on wind direction

E. LONG WAVES

No.	Naam	Start	End	Coordinate system	Coordinates
1	Europlatform	13-1-2005 08:00	29-4-2019 00:50	ED 1950 [lat/lon]	51° 59' 55"; 3° 16' 35"
2	Lichteiland Goeree	13-1-2005 08:00	29-4-2019 00:50	ED 1950 [lat/lon]	51° 55' 33"; 3° 40' 11"
3	Platform A12	1-2-2009 11:40	29-4-2019 00:40	WGS84 [lat/lon]	55° 23' 0.000"; 3° 48' 00.00"
4	Platform D15	1-2-2009 13:00	29-4-2019 00:50	WGS84 [lat/lon]	54° 19' 3.240"; 2° 56' 08.70"
5	Platform F16 A	1-2-2009 13:50	29-4-2019 00:50	WGS84 [lat/lon]	54° 07' 0.000"; 4° 00' 44.00"
6	Platform Hoorn Q 1A	1-2-2009 15:10	29-4-2019 00:50	RD new [X, Y]	71820.00, 549410.00
7	Platform J06	1-2-2009 14:30	29-4-2019 00:50	RD new [X, Y]	-55200.0, 650620.0
8	Stroommeetpaal IJmond	13-1-2005 08:00	29-4-2019 00:50	RD new [X, Y]	95902.21, 497709.72

Table 11: Long wave data collection locations and measurement periods

Missing long wave data

- Stroommeetpaal IJmond 2-1-2009 17:10 – 4-1-2009 16:40
- Lichteiland Goeree 2-1-2009 17:10 – 4-1-2009 9:30
- Europlatform 2-1-2009 17:10 – 4-1-2009 6:00
- Europlatform 28-9-2009 10:40 – 28-9-2009 18:50

F. SHORT WAVES

I. SIGNIFICANT WAVE HEIGHT

No.	Naam	Start (height)	End (height)
1	Europlatform	29-11-2006 10:00	26-4-2019 00:50
2	Lichteiland Goeree	2-2-1976 01:00	26-4-2019
3	Platform A12	1-2-2009 11:50	26-4-2019 00:40
4	Platform D15	1-2-2009 13:10	26-4-2019 00:50
5	Platform F16 A	1-2-2009 14:00	26-4-2019 00:50
6	Platform Hoorn Q 1A	1-2-2009 15:20	26-4-2019 00:50
7	Platform J06	1-2-2009 14:40	26-4-2019 00:50
8	Stroommeetpaal IJmond	30-10-2002 06:00	26-4-2019 00:50

Table 12: Significant short wave height data availability and measurement duration

II. ENERGY DENSITY SPECTRUM

No.	Naam	Start	End
1	Europlatform	N/A	N/A
2	Lichteiland Goeree	N/A	N/A
3	Platform A12	1-2-2009 11:20	7-6-2019 00:40
4	Platform D15	N/A	N/A
5	Platform F16 A	N/A	N/A
6	Platform Hoorn Q 1A	1-2-2009 14:50	7-6-2019 00:50
7	Platform J06	N/A	N/A
8	Stroommeetpaal IJmond	N/A	N/A

Table 13 Short wave energy density spectrum availability and measurement duration

III. FREQUENCY DIRECTION SPECTRUM

No.	Naam	Start	End
1	Europlatform	N/A	N/A
2	Lichteiland Goeree	N/A	N/A
3	Platform A12	1-2-2009 12:10	7-6-2019 00:40
4	Platform D15	N/A	N/A
5	Platform F16 A	N/A	N/A
6	Platform Hoorn Q 1A	1-2-2009 15:40	7-6-2019 00:50
7	Platform J06	N/A	N/A
8	Stroommeetpaal IJmond	N/A	N/A

Table 14 Short wave frequency direction spectrum availability and measurement duration

Rijkswaterstaat
Ministry of Infrastructure and the Environment

TUDelft

G. WATER LEVEL

No.	Naam	Start	End	Reference point
1	Europlatform	15-3-1987 00:00	30-6-2001 23:50	MSL &
		1-7-2001 00:00	10-5-2019 00:50	NAP
2	Lichteiland Goeree	31-12-1985 22:00	30-6-2001 23:50	MSL &
		1-7-2001 00:00	10-5-2019 00:50	NAP
3	Platform A12	1-2-2009 11:50	10-5-2019 00:50	MSL
4	Platform D15	1-2-2009 13:10	10-5-2019 00:50	MSL
5	Platform F16 A	1-2-2009 14:00	10-5-2019 00:50	MSL
6	Platform Hoorn Q 1A	13-5-2007 00:00	10-5-2019 00:50	MSL
7	Platform J06	1-2-2009 14:40	10-5-2019 00:50	MSL
8	Stroommeetpaal IJmond	30-10-2002 5:10	10-5-2019 00:50	NAP

Table 15 Measurement locations and the period in which the water level measurements have been performed

- Stroommeetpaal IJmond 2-1-2009 17:10 – 4-1-2009 17:00

Rijkswaterstaat
Ministry of Infrastructure and the Environment

TUDelft

H. METEOROLOGICAL DATA

IV. WIND

No.	Naam	Start (velocity)	End (velocity)	Start (direction)	End (direction)
1	Europlatform	1-1-1983 02:00	26-4-2019 00:50	3-1-1983 20:00	26-4-2019 00:50
2	Lichteiland Goeree	1-1-1981 02:00	26-4-2019 00:50	1-1-1981 02:00	26-4-2019 00:50
3	Platform A12	1-2-2009 12:00	26-4-2019 00:50	1-2-2009 12:00	26-4-2019 00:50
4	Platform D15	1-2-2009 13:20	26-4-2019 00:50	1-2-2009 13:20	26-4-2019 00:50
5	Platform F16 A	1-2-2009 14:00	26-4-2019 00:50	1-2-2009 14:00	26-4-2019 00:50
6	Platform Hoorn Q 1A	1-2-2009 15:30	26-4-2019 00:50	1-2-2009 15:30	26-4-2019 00:50
7	Platform J06	1-2-2009 14:40	26-4-2019 00:50	1-2-2009 14:40	26-4-2019 00:50
8	Stroommeetpaal IJmond	N/A	N/A	N/A	N/A

Table 16 Wind (speed and direction) data measurement locations and periods

V. ATMOSPHERIC PRESSURE

No.	Naam	Start	End
1	Europlatform	1-7-1996 00:00	28-6-2019 00:00
2	Lichteiland Goeree	1-1-1981 00:00	28-6-2019 00:00
3	Platform A12	16-3-2009 00:00	28-6-2019 00:00
4	Platform D15	16-3-2009 00:00	28-6-2019 00:00
5	Platform F16 A	7-12-2006 00:00	28-6-2019 00:00
6	Platform Hoorn Q 1A	16-3-2009 00:00	28-6-2019 00:00
7	Platform J06	16-3-2009 00:00	28-6-2019 00:00
8	Stroommeetpaal IJmond	N/A	N/A

Table 17 Atmospheric pressure measurement locations and duration

Missing:

Europlatform: 1-1-2001 00:00 - 10-9-2003 00:00

B. SPATIAL AND TEMPORAL DISTRIBUTION OF LONG WAVES IN THE NORTH SEA

A. SHORT TERM ANALYSIS

Rijkswaterstaat
Ministry of Infrastructure and the
Environment

TUDelft
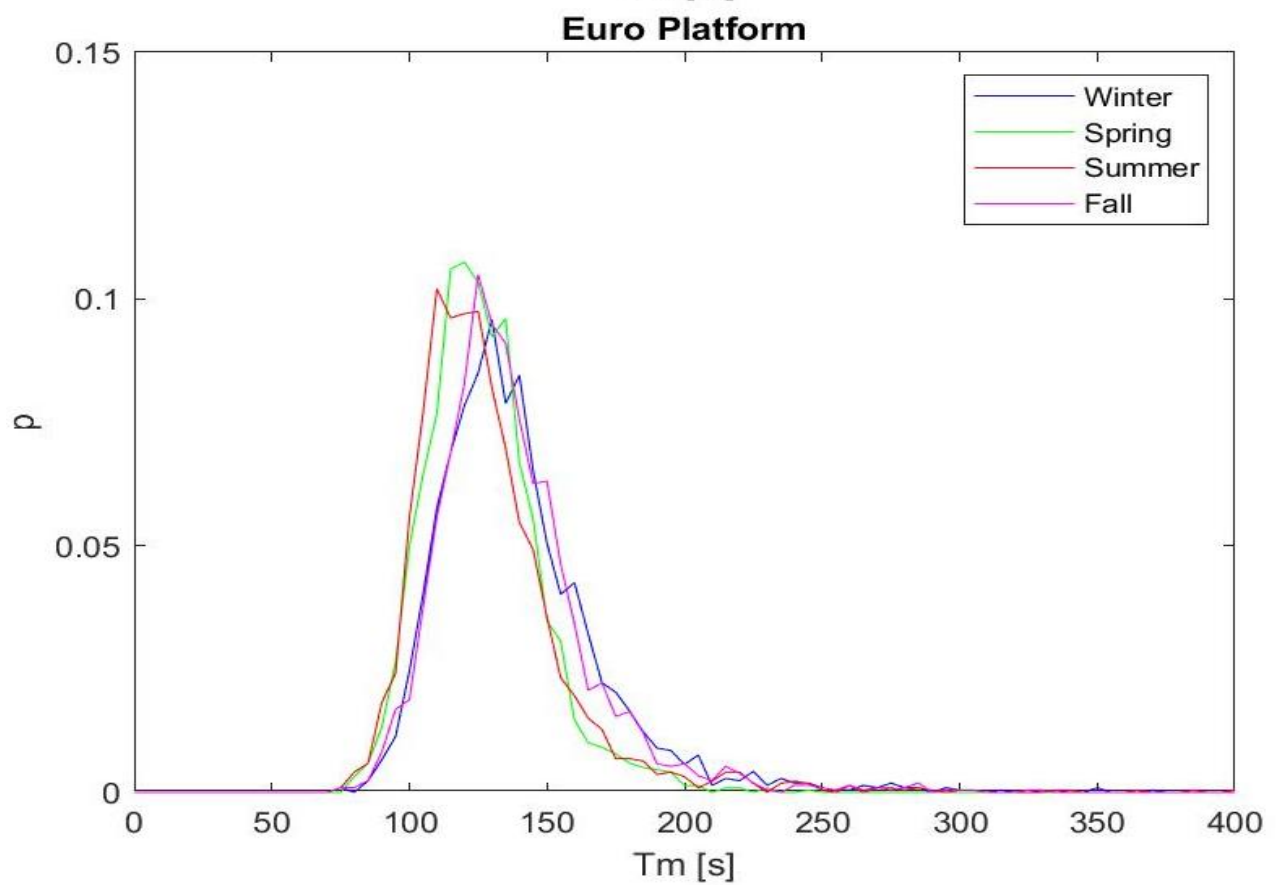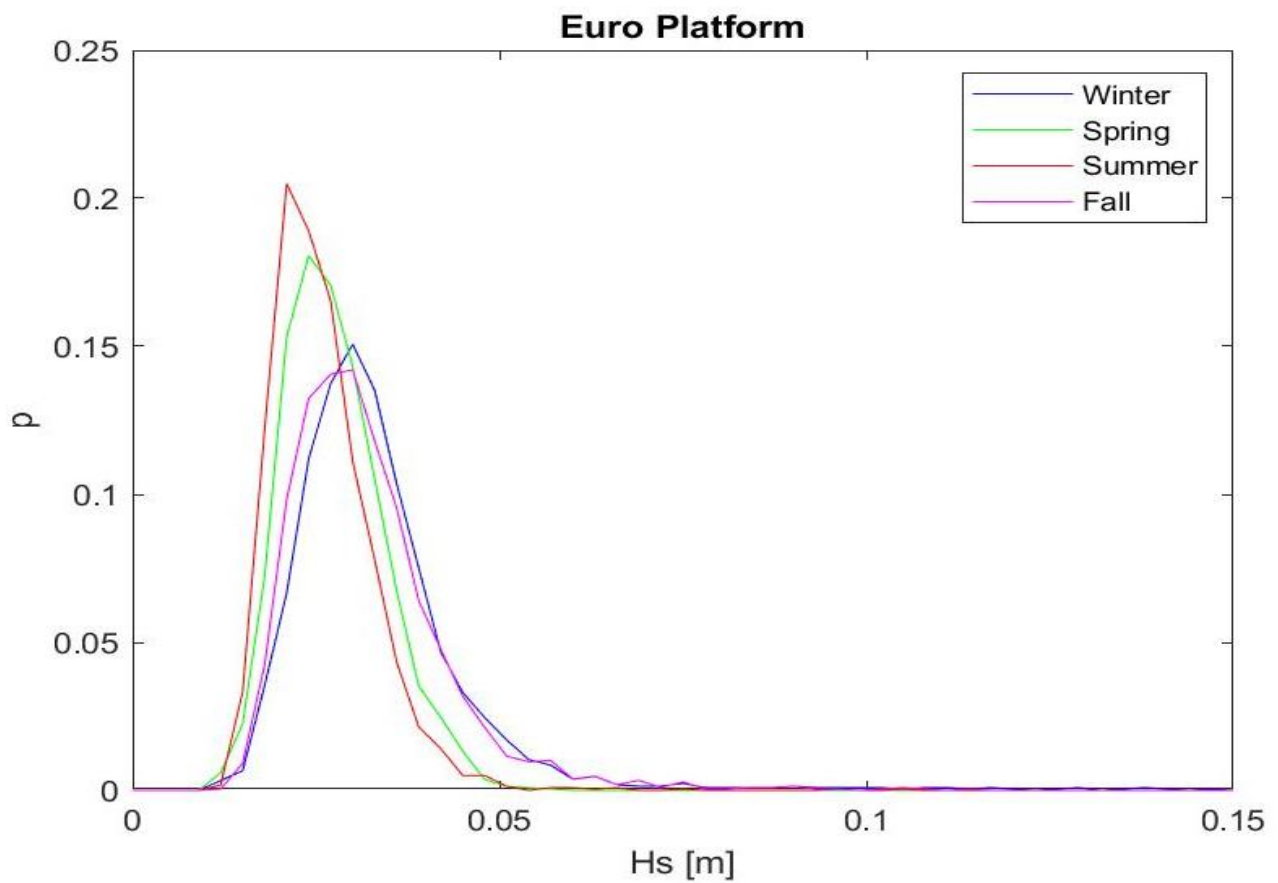
Figure 57 Upper graph: Distribution of the long wave significant wave height per season in the year 2013
Lower graph: Distribution of the long wave mean wave period per season in the year 2013
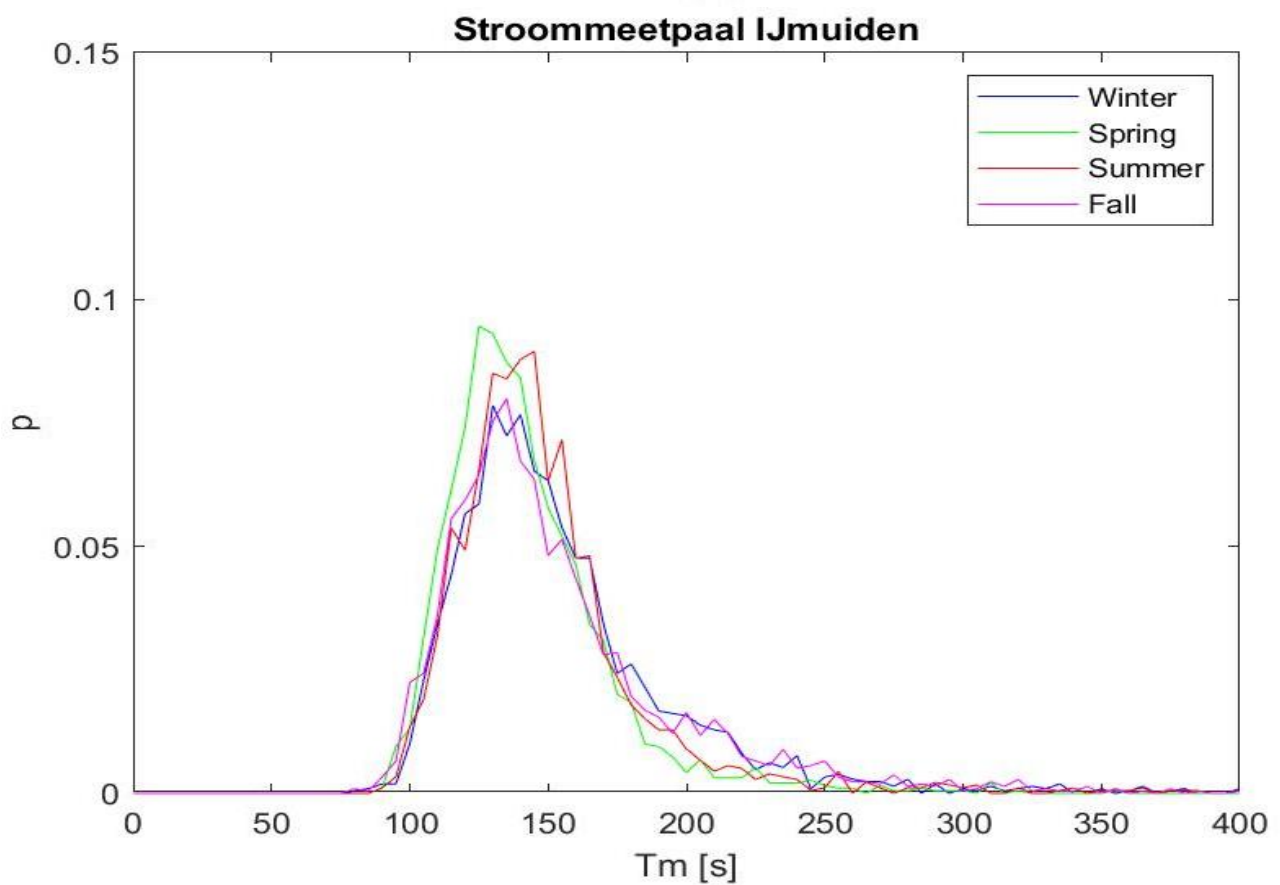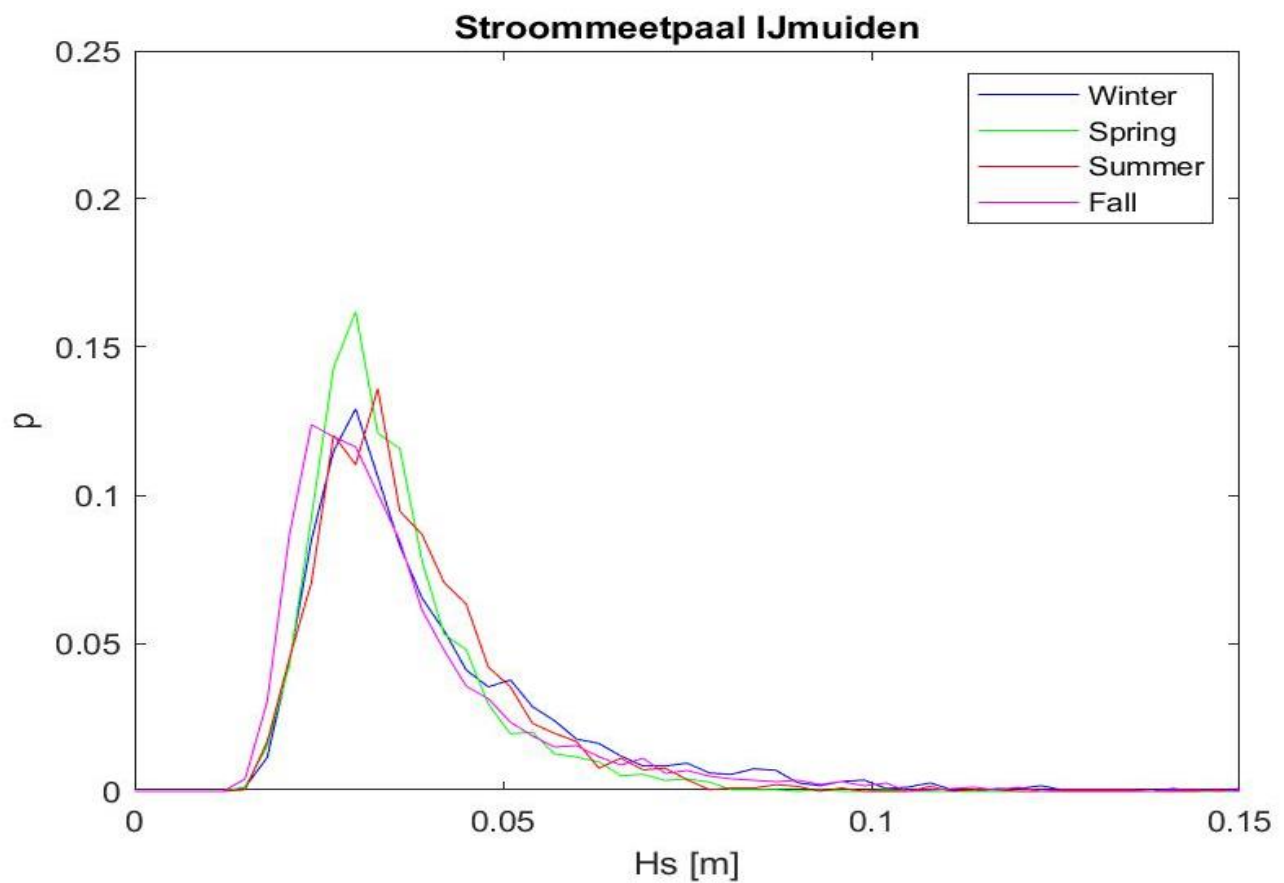
Figure 58 Upper graph: Distribution of the long wave significant wave height per season in the year 2013
Lower graph: Distribution of the long wave mean wave period per season in the year 2013

Rijkswaterstaat
Ministry of Infrastructure and the
Environment

TU Delft
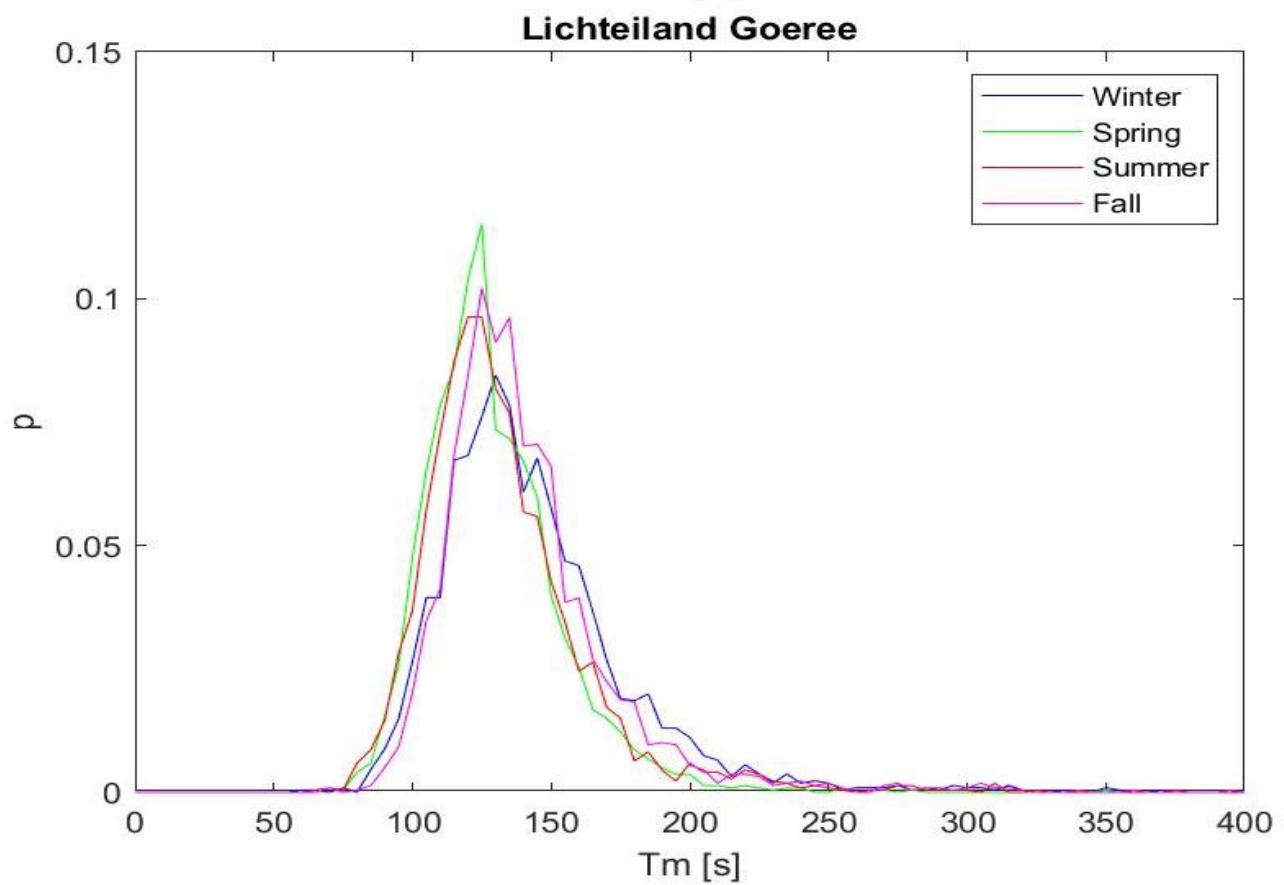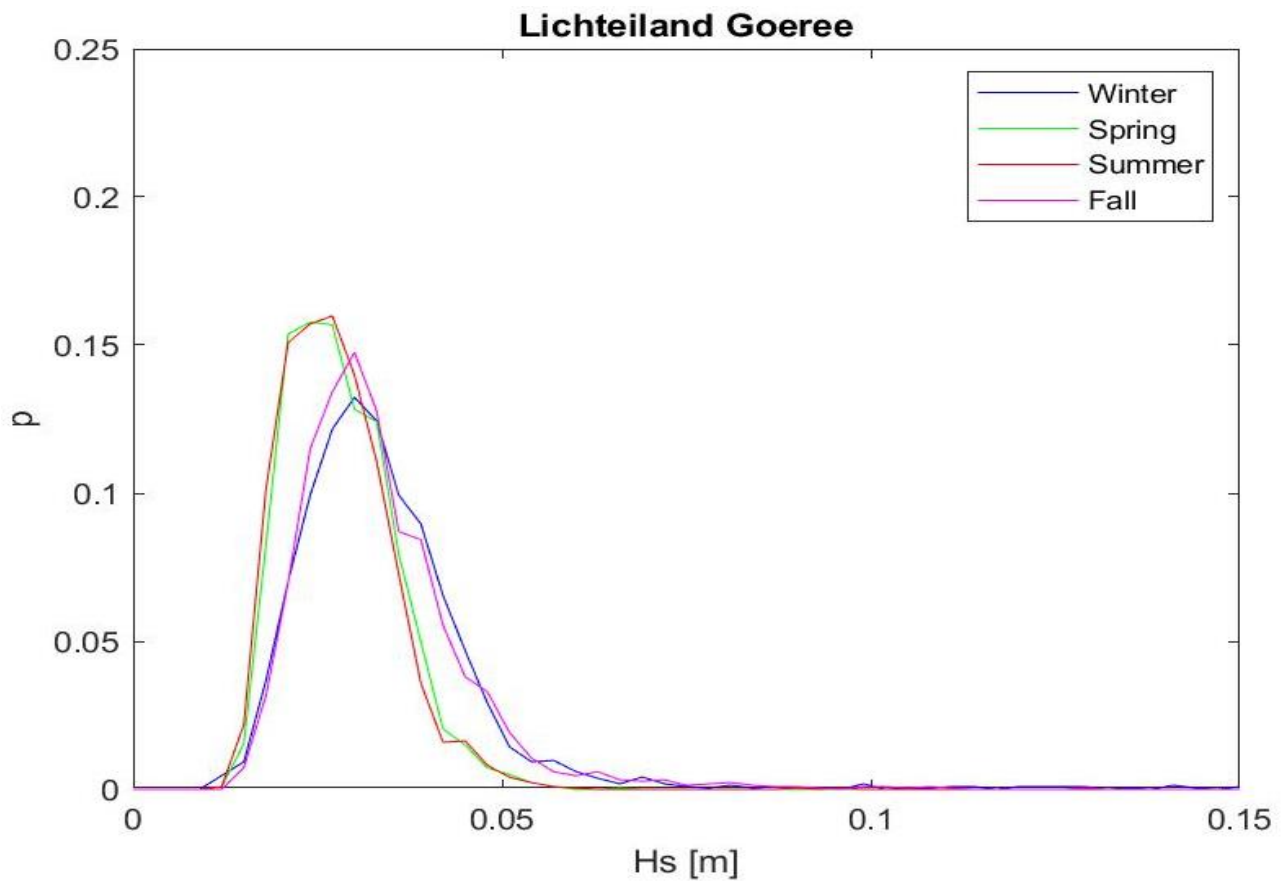
Figure 59 Upper graph: Distribution of the long wave significant wave height per season in the year 2013
Lower graph: Distribution of the long wave mean wave period per season in the year 2013
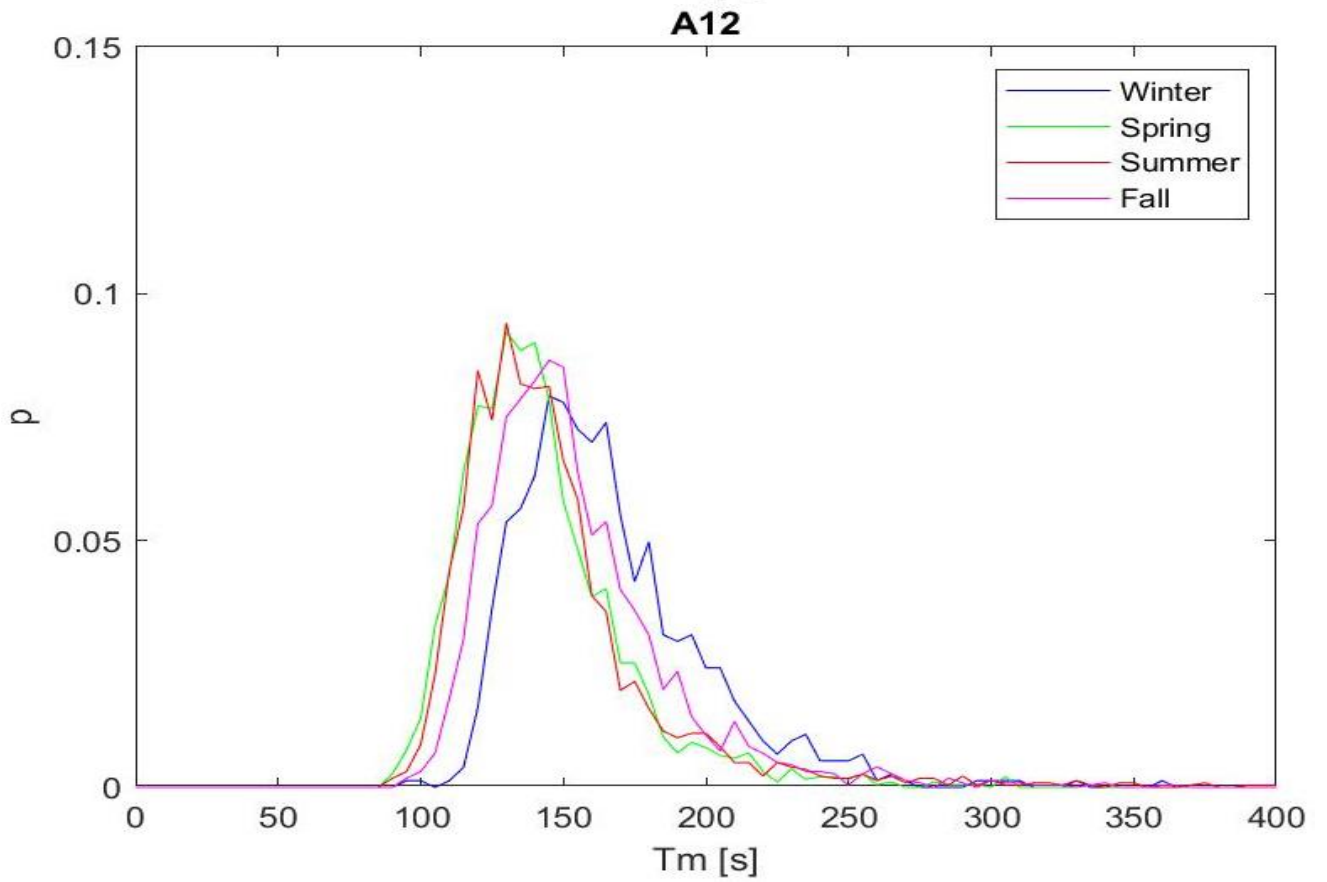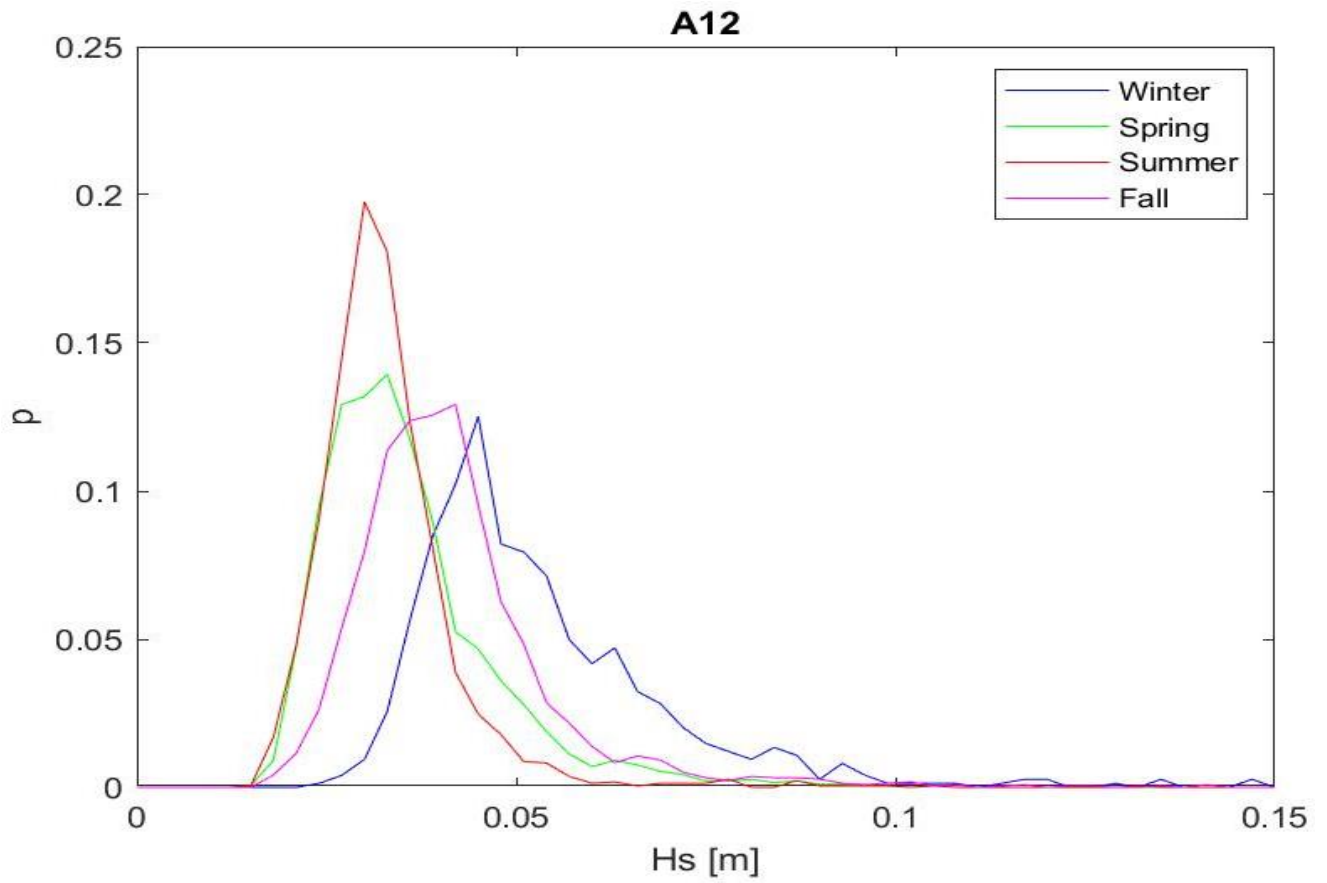
Figure 60 Upper graph: Distribution of the long wave significant wave height per season in the year 2013
Lower graph: Distribution of the long wave mean wave period per season in the year 2013
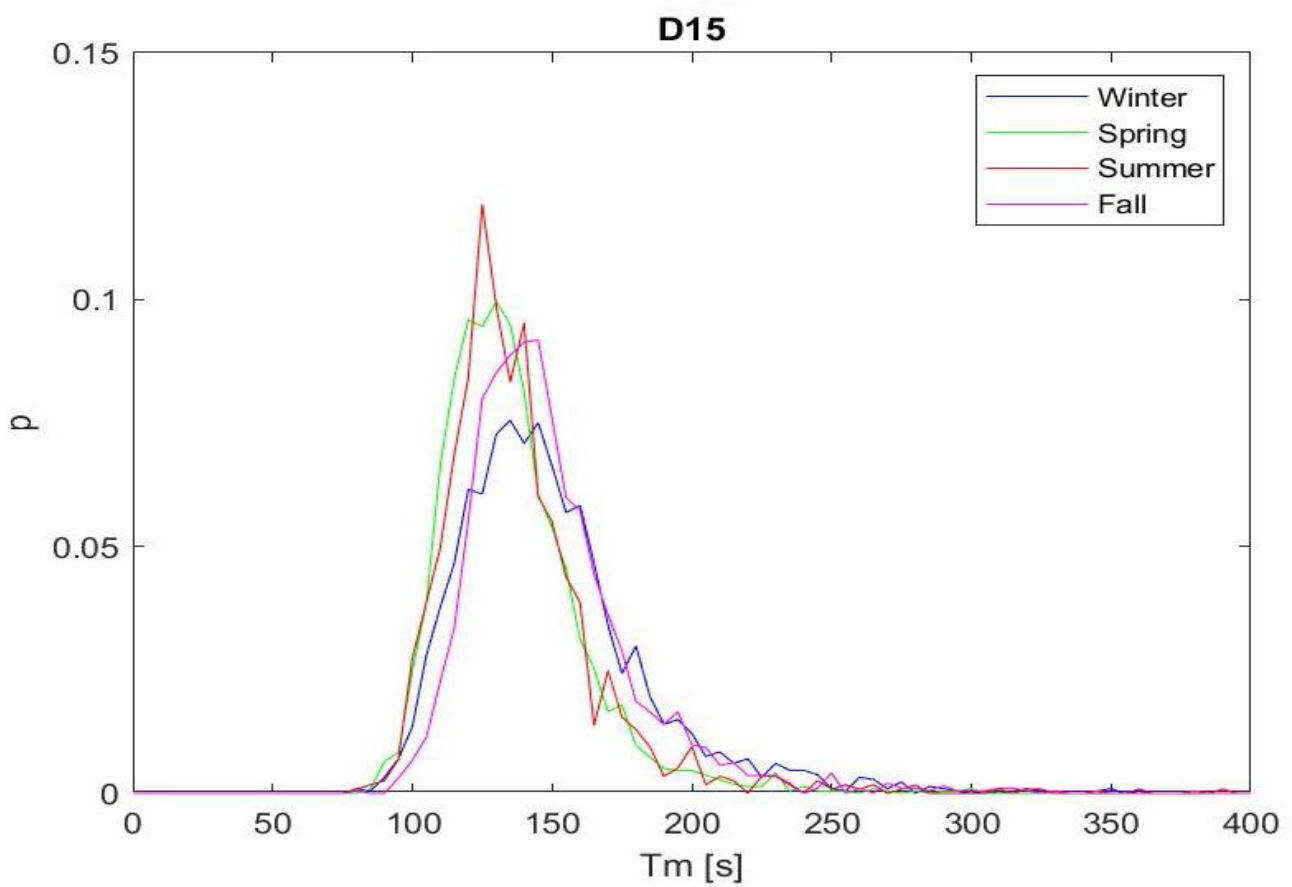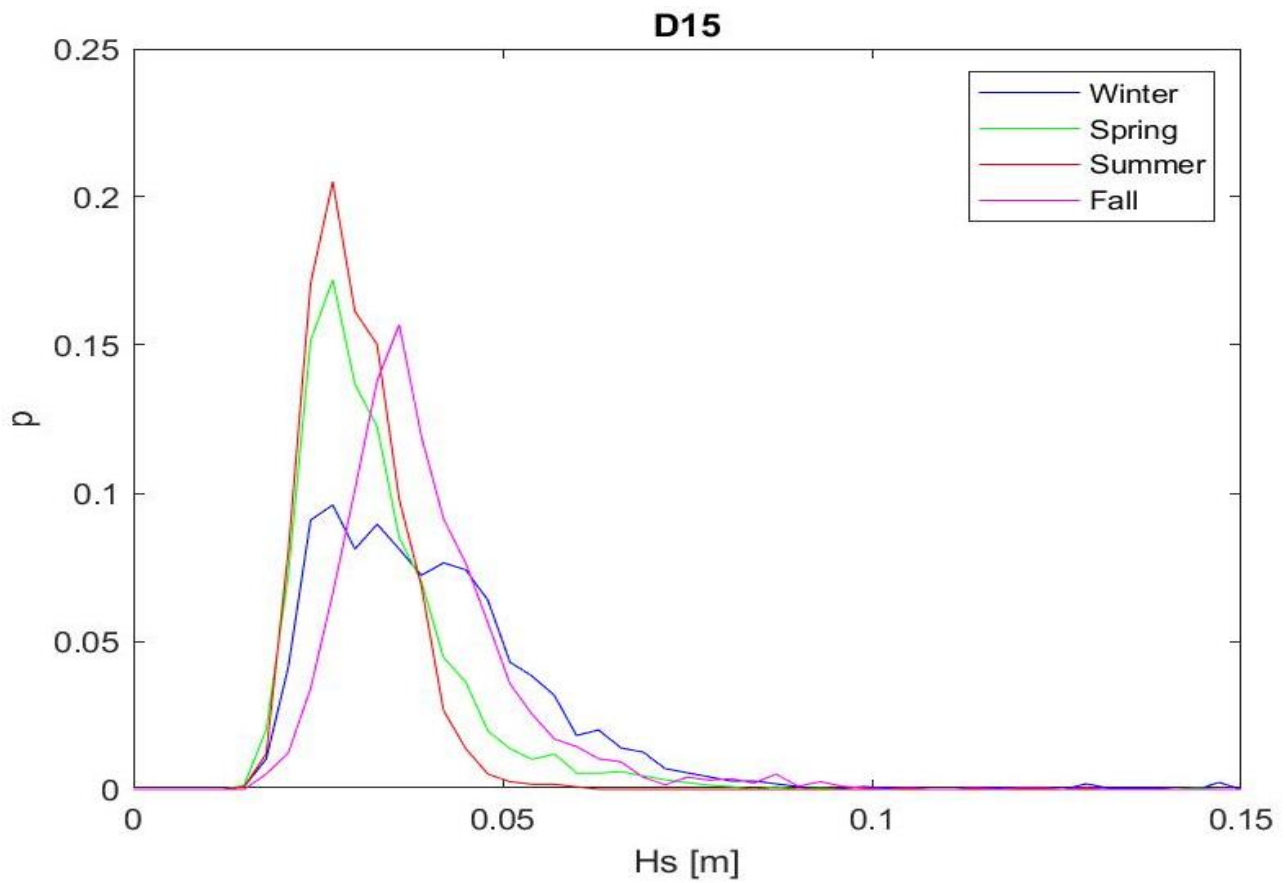
Figure 61 Upper graph: Distribution of the long wave significant wave height per season in the year 2013
Lower graph: Distribution of the long wave mean wave period per season in the year 2013
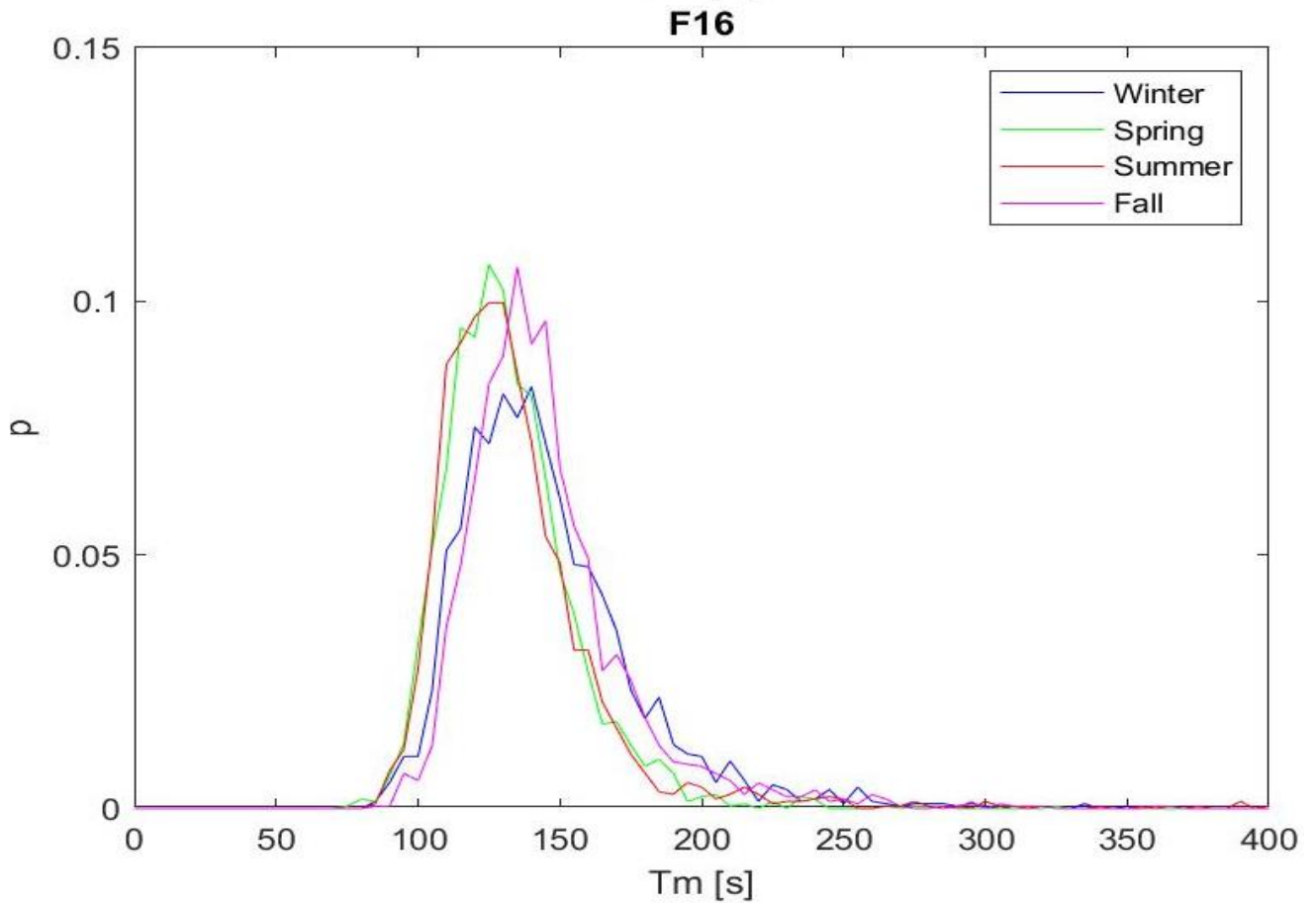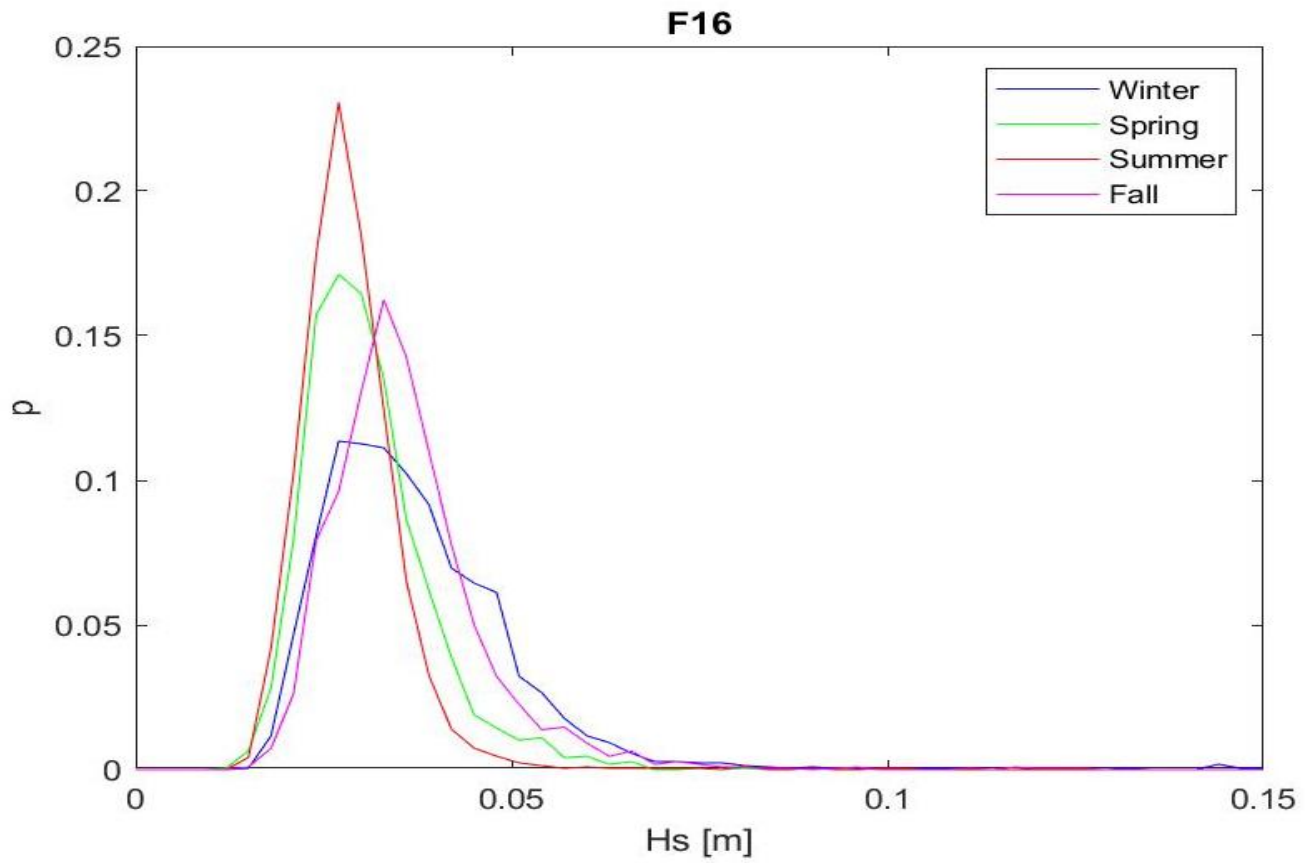
Figure 62 Upper graph: Distribution of the long wave significant wave height per season in the year 2013
Lower graph: Distribution of the long wave mean wave period per season in the year 2013

Rijkswaterstaat
Ministry of Infrastructure and the
Environment

TUDelft
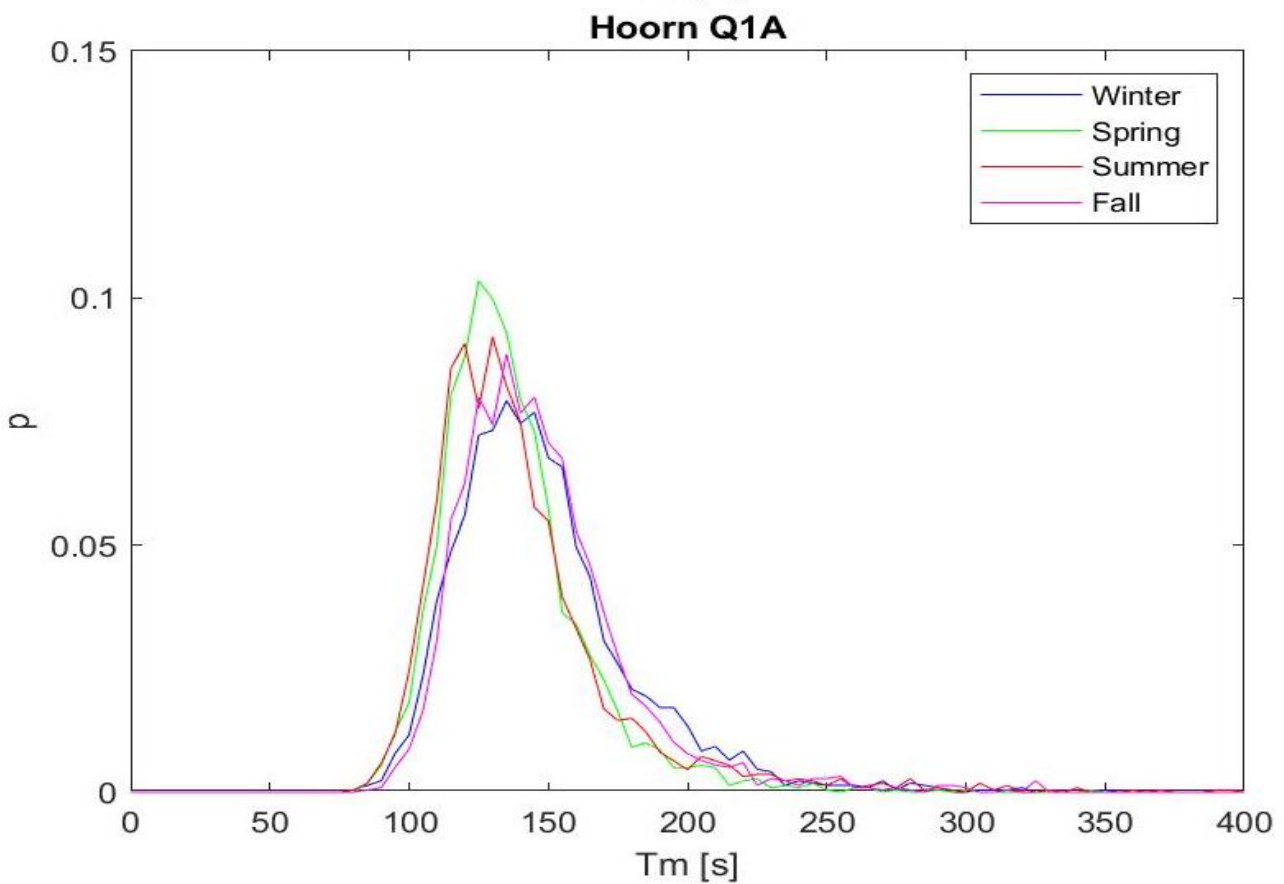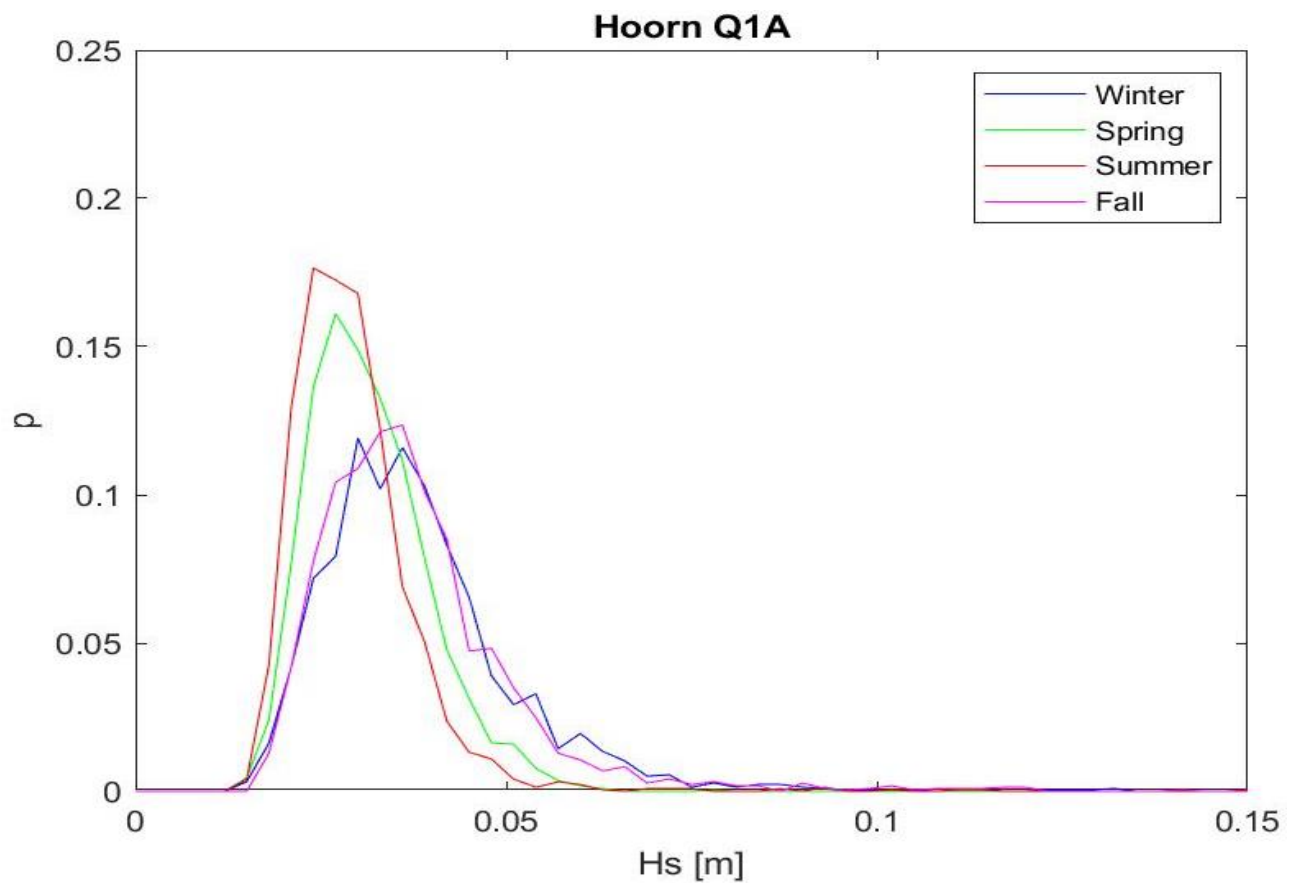
Figure 63 Upper graph: Distribution of the long wave significant wave height per season in the year 2013
Lower graph: Distribution of the long wave mean wave period per season in the year 2013
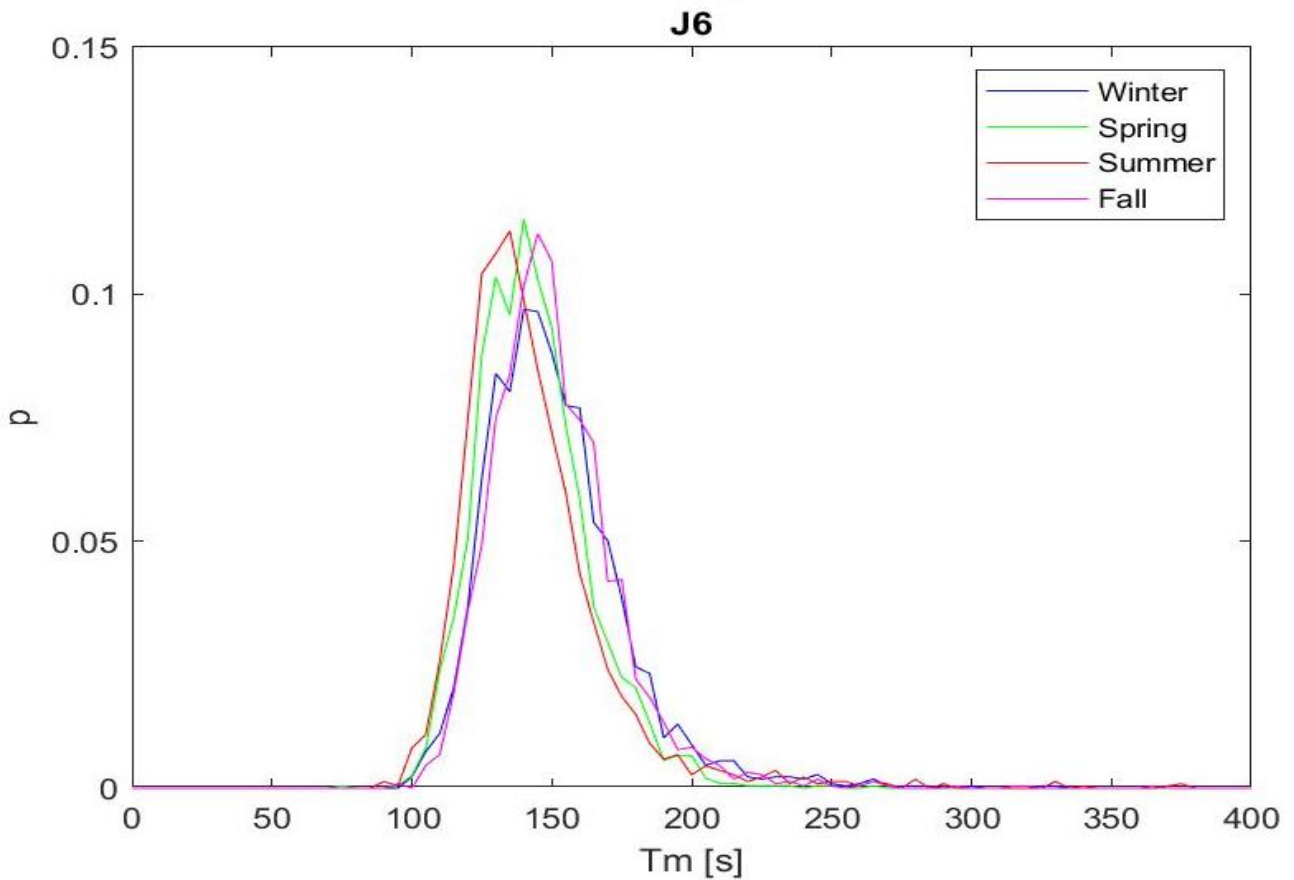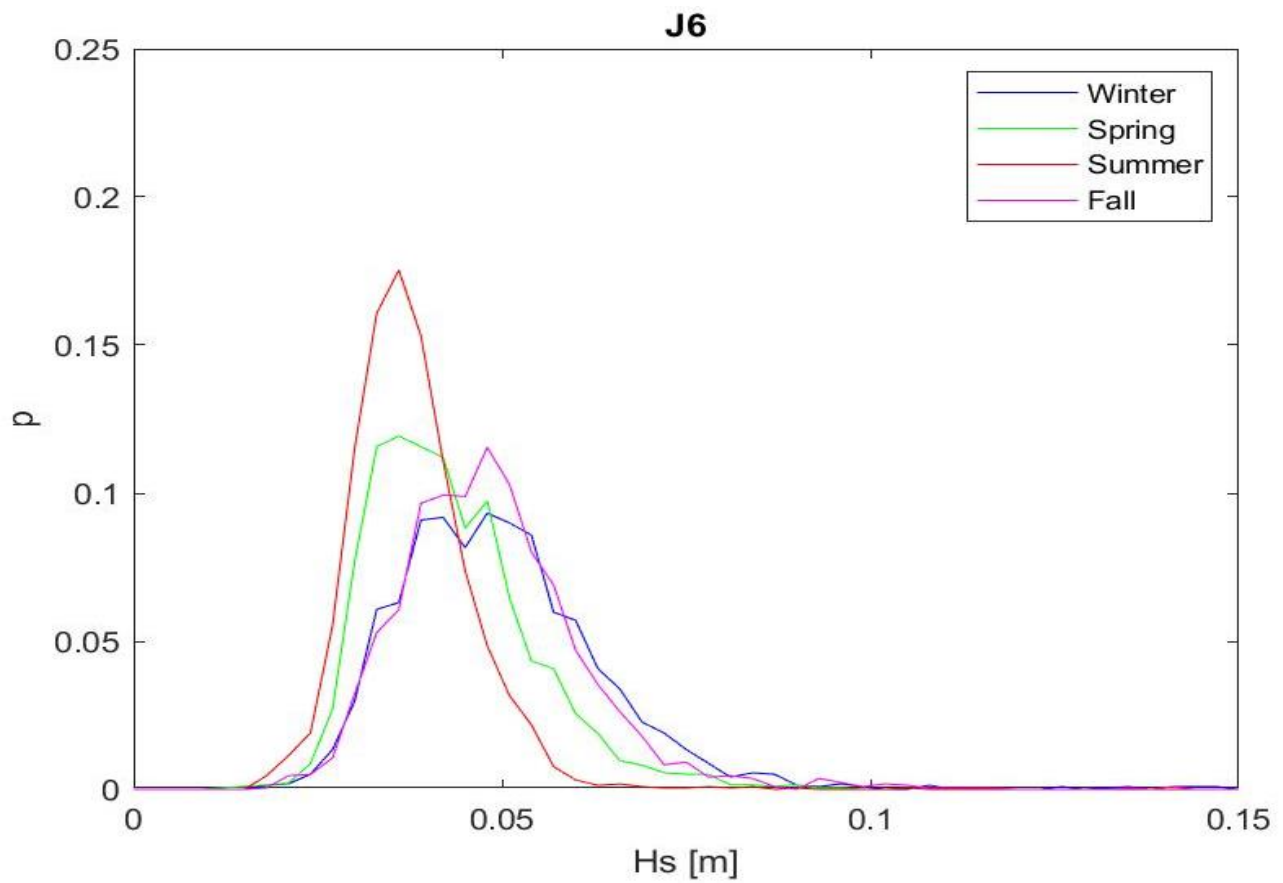
Figure 64 Upper graph: Distribution of the long wave significant wave height per season in the year 2013
Lower graph: Distribution of the long wave mean wave period per season in the year 2013

Euro platform
Significant wave heights and their return periods
R, Hs
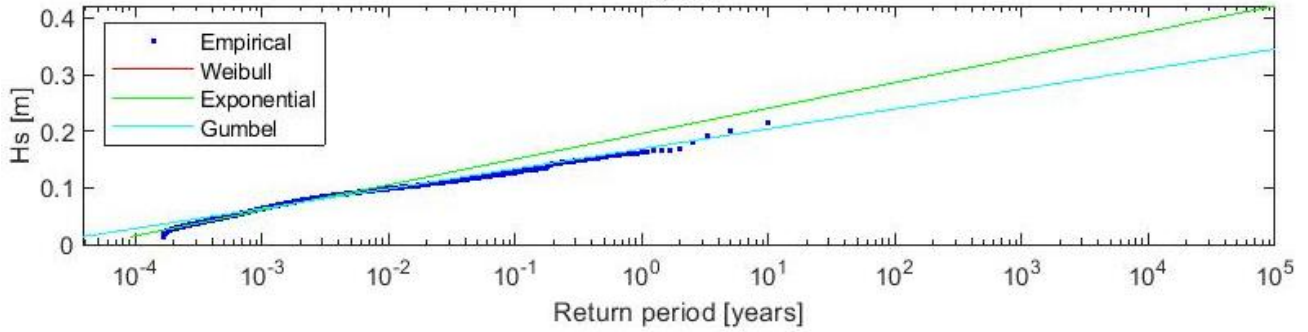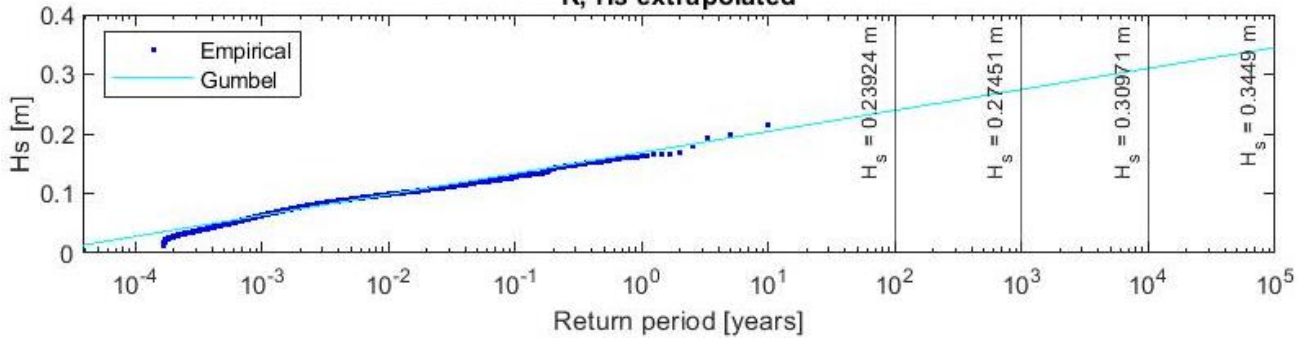
R, Hs extrapolated

IJmuiden stroommeetpaal
Significant wave heights and their return periods
R, Hs

R, Hs extrapolated

Rijkswaterstaat
Ministry of Infrastructure and the
Environment

TUDelft
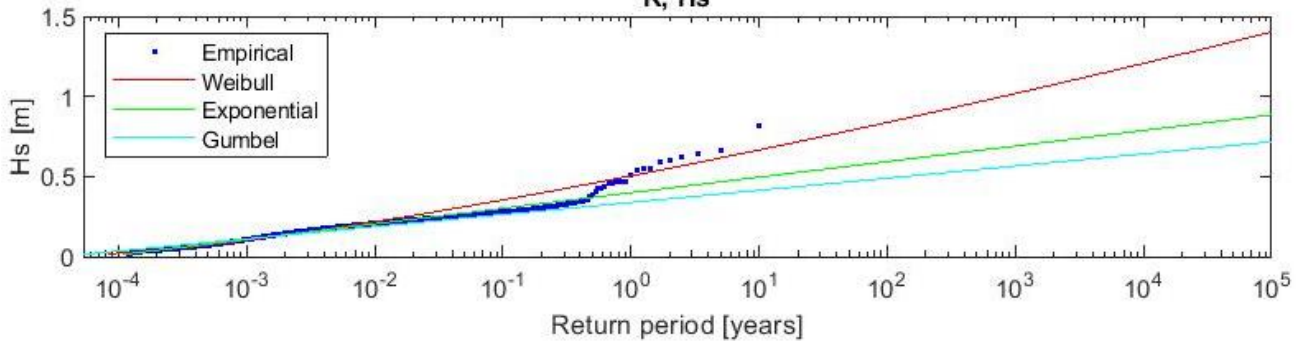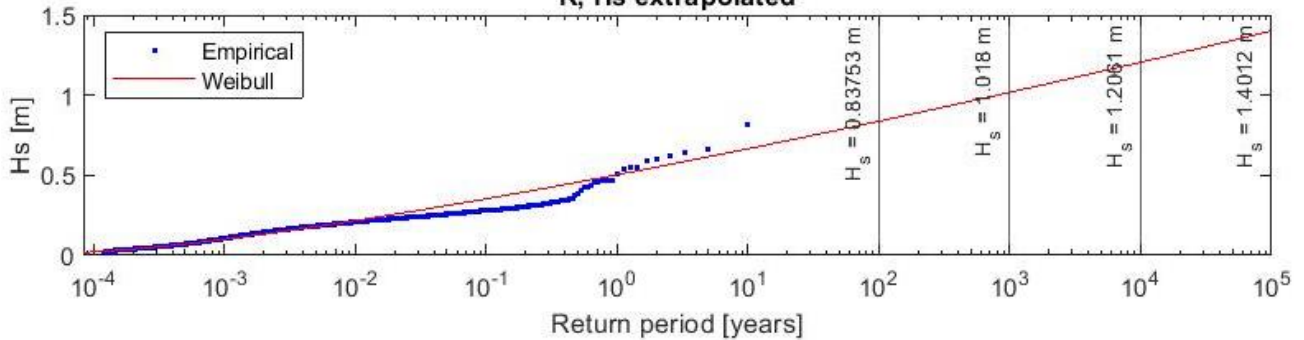
Lichteiland Goeree
Significant wave heights and their return periods
R, Hs

R, Hs extrapolated
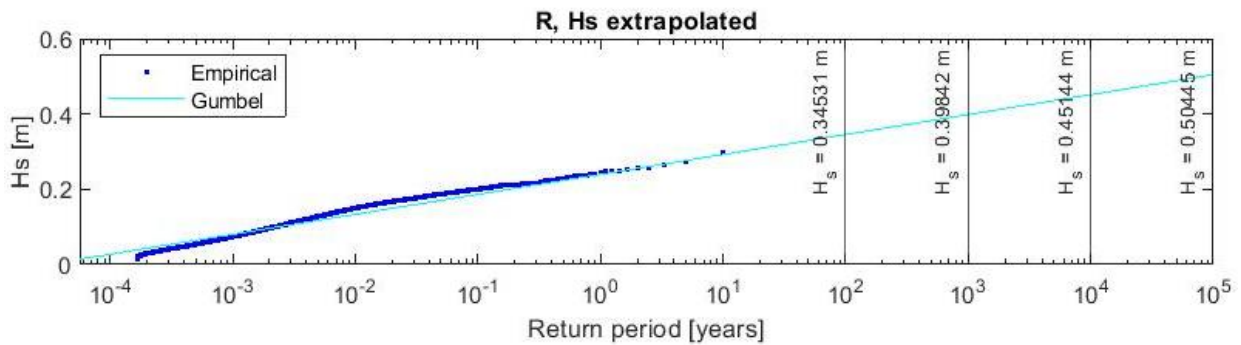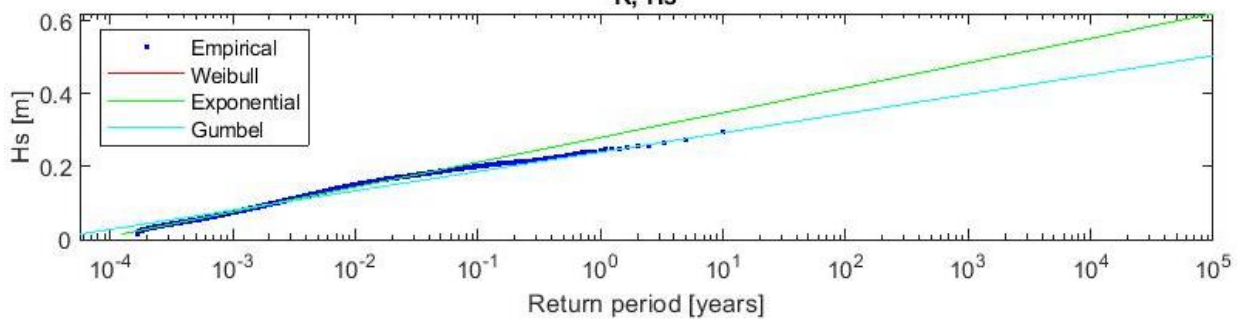
Platform A12
Significant wave heights and their return periods
R, Hs

R, Hs extrapolated

Rijkswaterstaat
Ministry of Infrastructure and the Environment

TUDelft
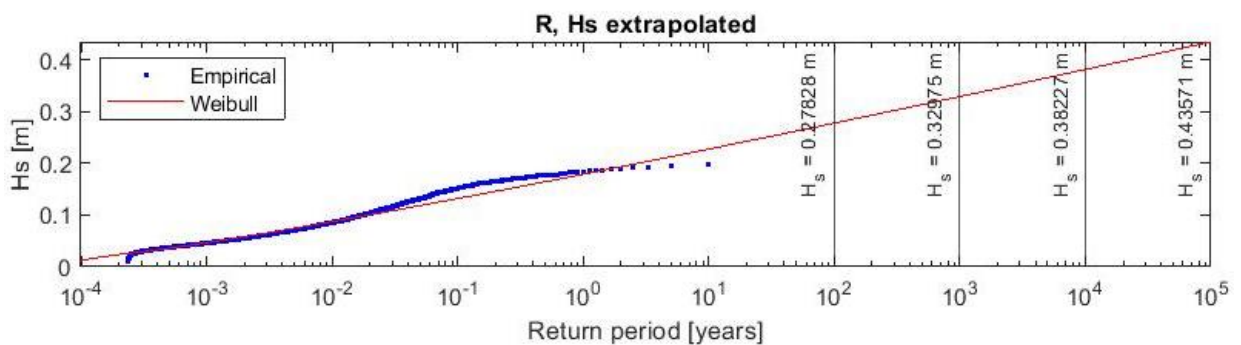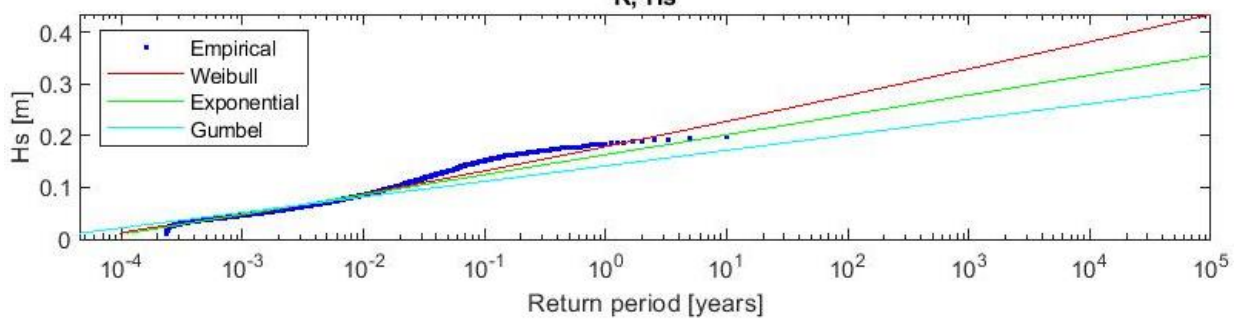
Platform D15-A
Significant wave heights and their return periods
R, Hs
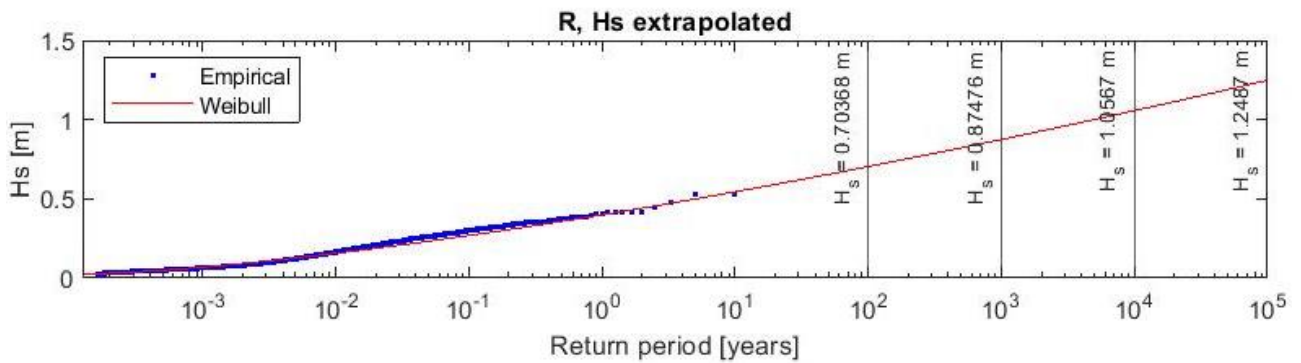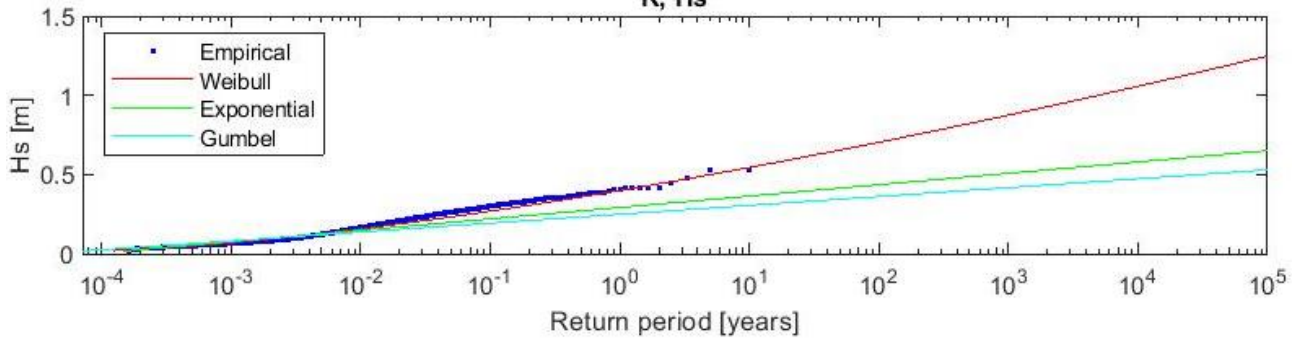
R, Hs extrapolated

Platform F16-A
Significant wave heights and their return periods
R, Hs

R, Hs extrapolated

Rijkswaterstaat
Ministry of Infrastructure and the Environment

TUDelft
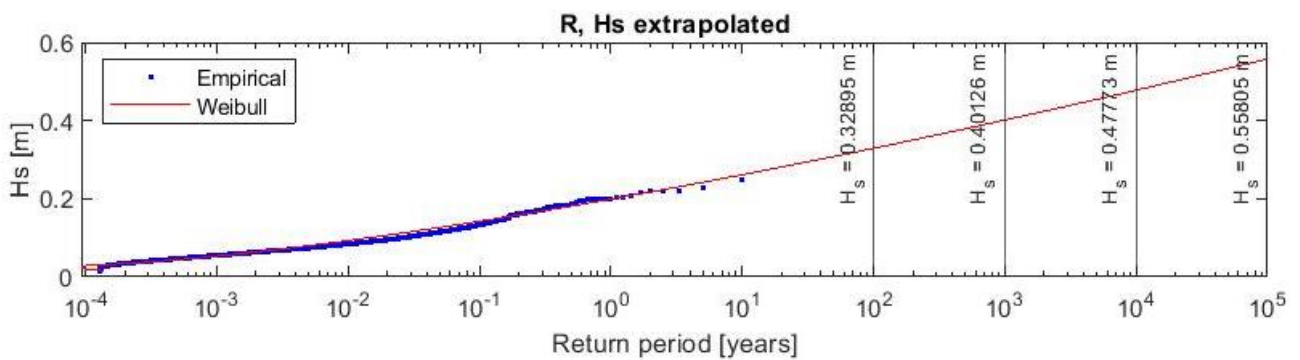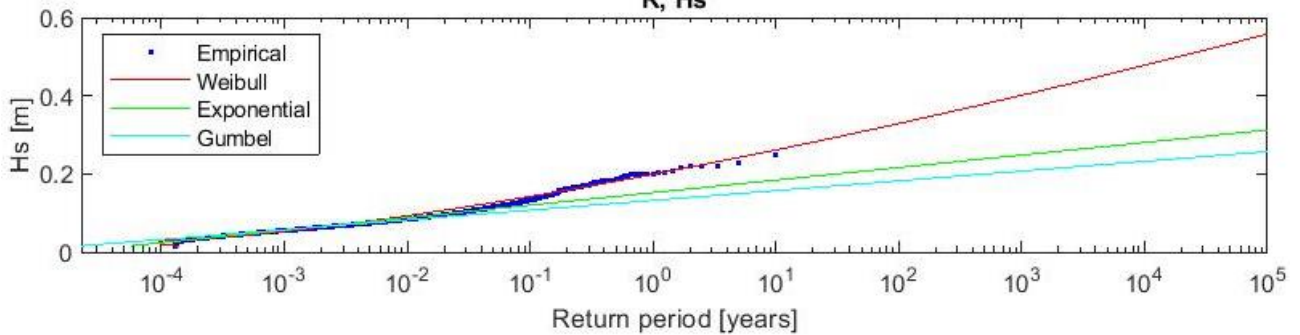
Platform Hoorn Q1-A
Significant wave heights and their return periods
R, Hs
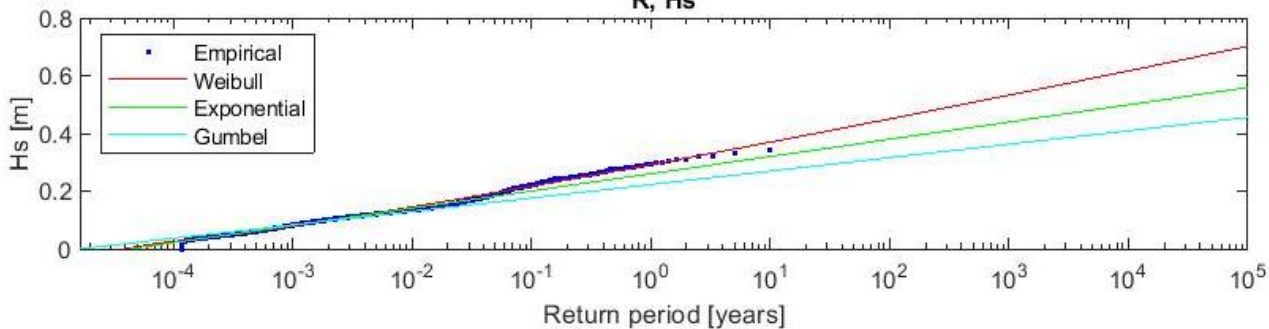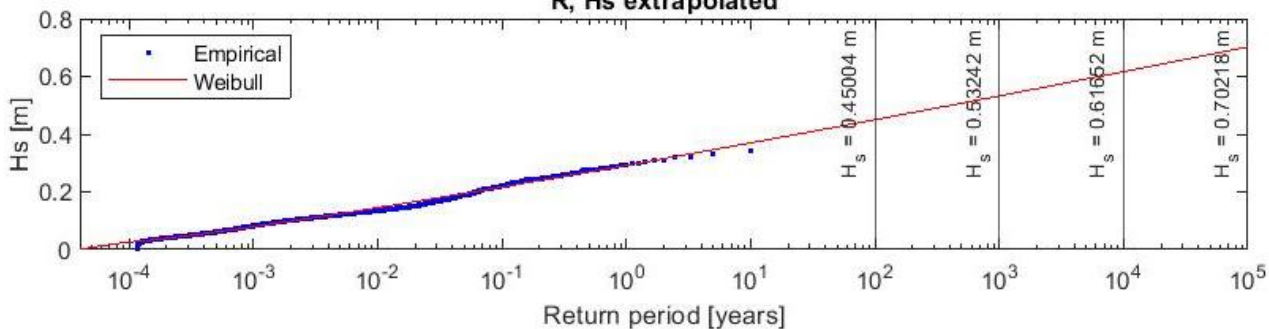
R, Hs extrapolated

Platform J6
Significant wave heights and their return periods
R, Hs

R, Hs extrapolated

Rijkswaterstaat
Ministry of Infrastructure and the Environment

TUDelft
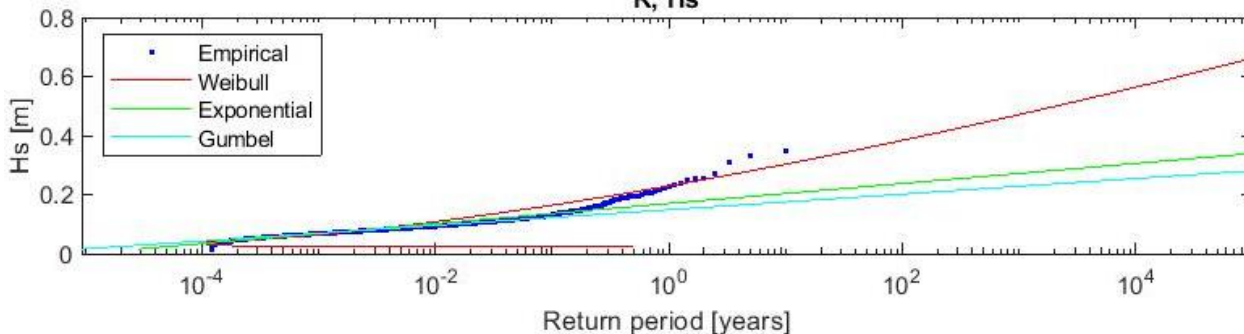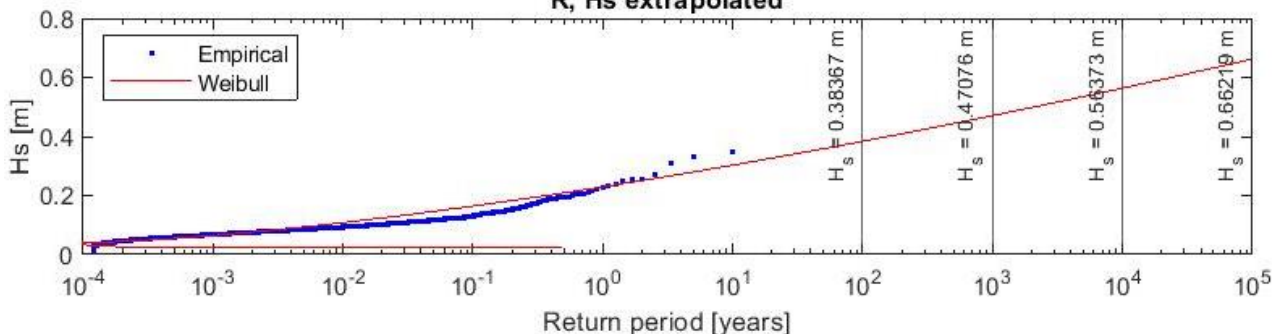
An explanation for the shift in locations which have the highest significant wave height can be found by looking at the results of the long term spectral analysis and the long wave water surface elevation time-series. Locations Euro platform and Stroommeetpaal IJmuiden show a large increase in significant wave height at the probabilities of $10^0 - 10^1$, see Figure 46 and Figure 47. Platform D15 also seems to have a lot of high extreme significant wave heights. Now looking at the water surface elevation time-series in Figure 65, the reason why becomes clear. Euro platform and Stroommeetpaal IJmuiden contain some incidental extreme values and Platform D15 shows a considerable increase in water surface elevation variation towards the end of the measurement period.

For an unknown reason, the water surface elevation time-series of Platform D15 starts oscillating with a rapidly increasing amplitude towards the end of the measurement period. Other nearby locations do not show a similar development. The amplitudes of the water surface oscillations are much higher than the amplitudes at the same location earlier in time. Since there is no explanation for why the amplitudes start increasing, and similar developments are not visible at other locations, these are most likely measurement errors.
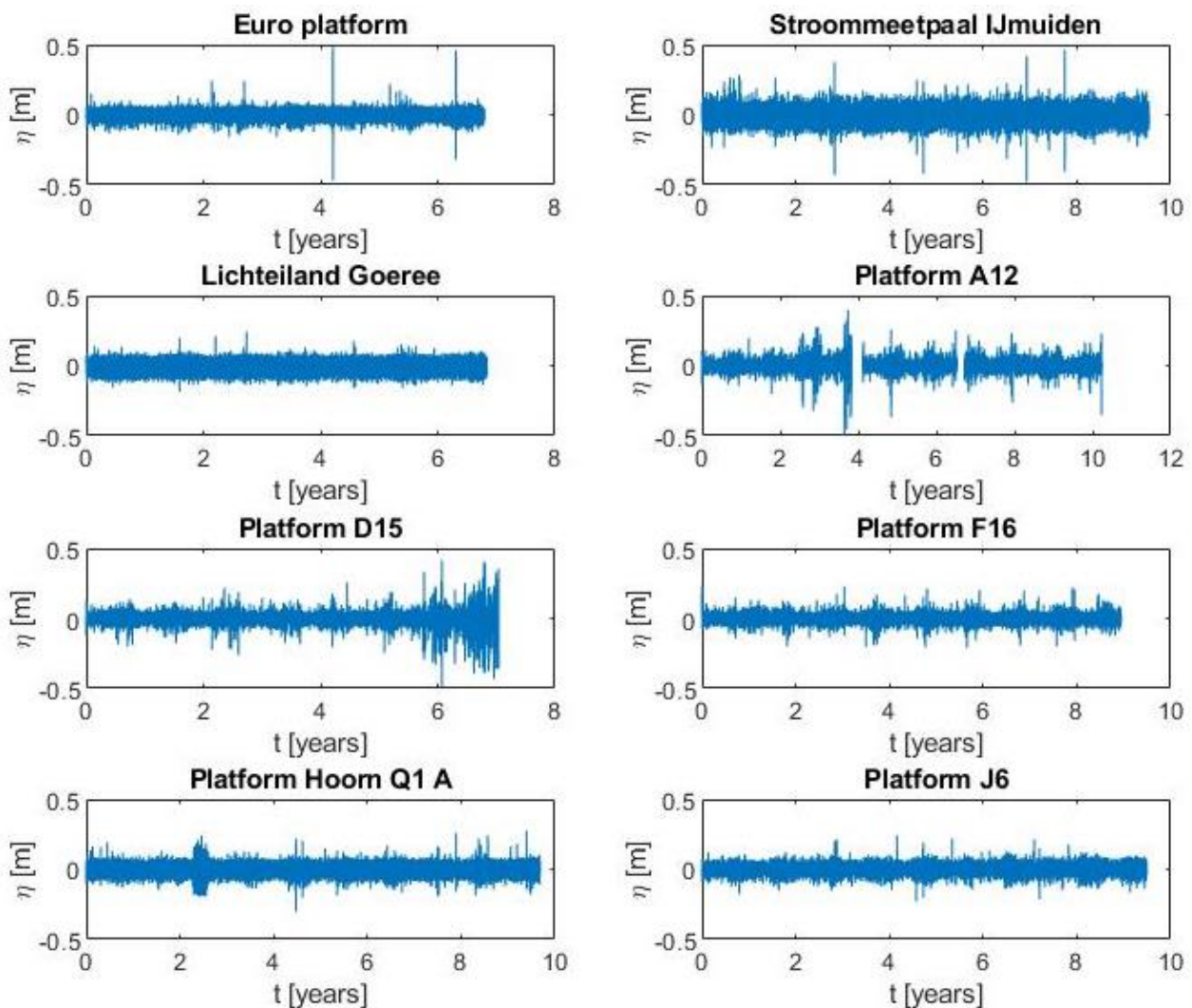
Figure 65 The long wave water surface elevation time series for all locations. Variations in length are caused by error filtering

Zooming in on some of the extreme waves from Euro platform and IJmuiden Stroommeetpaal shows how they look, see Figure 66. These extremely high waves appear to partially be an error, but also contain actual waves. The fact that this phenomenon is not a single occasion, but returns to a small extent, implies it is not always an error. Suggesting that some of those high wave heights have most likely actually occurred in the long wave frequency band.

Extreme wave predictions are calibrated on the highest significant wave heights in the data. Since the observations mentioned above are some of the highest waves in the record, and their existence is questionable, the uncertainty of the predictions at these locations increases by an unknown amount. The reliability of these predictions therefor greatly decreases.
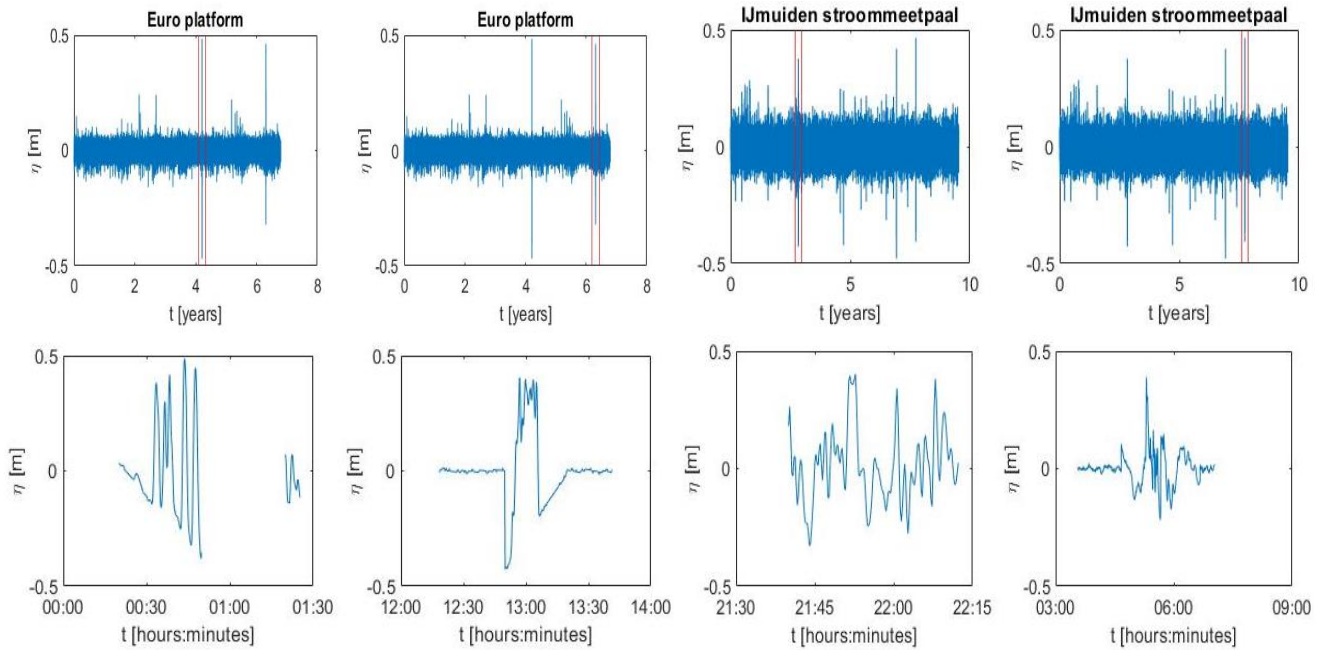
Figure 66 Zooming in on the extreme wave heights of location Euro platform (left) and IJmuiden stroommeetpaal (right)

Ardhuin, F, Rawat, A and Aucan, J. 2014. *A numerical model for free infragravity waves: Definition and validation at regional and global scales.* s.l. : OCEAN MODELLING, 2014.

Aucan, J and Ardhuin, F. 2013. *Infragravity waves in the deep ocean: An upward revision.* s.l. : GEOPHYSICAL RESEARCH LETTERS, 2013.

Battjes, JA, et al. 2004. *Shoaling of subharmonic gravity waves.* s.l. : JOURNAL OF GEOPHYSICAL RESEARCH-OCEANS, 2004.

Baumann, J, et al. 2017. *Importance of infragravity waves for the generation of washover deposits.* s.l. : Marine Geology, 2017.

Bertin, X, de Bakker, A and Ap van Dongeren, Giovanni Coco, Gael André, Fabrice Ardhuin, Philippe Bonneton, Frédéric Bouchette, Bruno Castelle, Wayne C. Crawford, Mark Davidson, Martha Deen, Guillaume Dodet, Thomas Guérin, Kris Inch, Fabien Leckler, R. 2018. *Infragravity waves: From driving mechanisms to impacts.* s.l. : Earth-Science Reviews, 2018.

Bowen, AJ and Inman, DL. 1969. *Rip currents: 2. Laboratory and field observations.* s.l. : Oceans and atmospheres, 1969.

CBS, PBL, RIVM, WUR. 2017. Beschrijving van de Noordzee. *Compendium voor de Leefomgeving.* [Online] Oktober 30, 2017.

Coastal Dynamics 1. **Bosboom, J and Stive, MJF. 2015.** Delft : Delft Academic Press, 2015.

de Bakker, ATM, Tissier, MFS and Ruessink, BG. 2014. *Shoreline dissipation of infragravity waves.* s.l. : CONTINENTAL SHELF RESEARCH, 2014.

de Vries, JSMV, et al. 2008. *Analysis of dune erosion processes in large-scale flume experiments.* s.l. : COASTAL ENGINEERING, 2008.

Godin. 1972. 1972.

Hasselmann. 1962. *On the non-linear energy transfer in a gravity wave spectrum. Part 1: General theory.* 1962.

Hasselmann, et al. 1963. *Bispectra of ocean waves.* 1963.

Henderson, SM, et al. 2006. *Nonlinear generation and loss of infragravity wave energy.* s.l. : JOURNAL OF GEOPHYSICAL RESEARCH-OCEANS, 2006.

Herbers et al., Elgar, S. and Guza, R. 1994. *Infragravity-frequency (0.005-0.05 hz) motions on the shelf, part i, forced waves.* s.l. : J. Phys. Oceanograph, 1994.

Herbers, T., Elgar, S. and Guza, R. 1995. *Generation and propagation of infragravity waves.* s.l. : J. Geophys. Res. , 1995.

Herbers, THC and Burton, MC. 1997. *Nonlinear shoaling of directionally spread waves on a beach.* 1997.

Holthuijsen, L.H. 2007. *Waves in oceanic and coastal waters.* s.l. : Cambridge university press, 2007.

Janssen, TT, Battjes, JA and van Dongeren, AR. 2003. *Long waves induced by short-wave groups over a sloping bottom.* s.l. : JOURNAL OF GEOPHYSICAL RESEARCH-OCEANS, 2003.

Kamminga, Koster. 2001. *Een algoritme voor de opslag van data van lange golven.* 2001.

Longuet-Higgins, MS and Stewart, RW. 1962. *Radiation stress and mass transport in gravity waves, with application to 'surf beats'.* s.l. : Cambridge university press, 1962.

Munk, W. 1950. *Proceedings of First Confeernce on Coastal Engineering; Origin and generation of waves.* California : s.n., 1950.

Munk, W. H. 1949. *Surf beats.* s.l. : Trans. Am. Geophys. Union 30, 1949.

Okihiro et al, Guza, RT, Seymour, RJ. 1993. *Excitation of Seiche Observed in Small Harbor.* La Jolla : Journal of geophysical research, 1993.

Rabinovich, A. 2009. *Seiches and harbor oscillations.* 2009.

Rawat, A, et al. 2014. *Infragravity waves across the oceans.* s.l. : GEOPHYSICAL RESEARCH LETTERS, 2014.

Reniers, A., Groenewegen, M., Ewans, K., Masterton, S., Stelling, G. and Meek, J. 2010. *Estimation of infragravity waves at intermediate water depth, .* s.l. : Coastal Eng, 2010.

Rijnsdorp, DP, Ruessink, G and Zijlema, M. 2015. *Infragravity-wave dynamics in a barred coastal region, a numerical study.* s.l. : JOURNAL OF GEOPHYSICAL RESEARCH-OCEANS, 2015.

Roelvink, D, et al. 2009. *Modelling storm impacts on beaches, dunes and barrier islands.* s.l. : COASTAL ENGINEERING, 2009.

Roelvink, D. and Reniers, A. 2011. *A guide to modeling coastal morphology.* s.l. : World Scientific press, 2011.

Roelvink, J. and Stive, M. 1989. *Bar generating cross-shore flow mechanisms on a beach.* s.l. : J. Geophys. Res., 1989.

Ruessink, BG. 1998. *Bound and free infragravity waves in the nearshore zone under breaking and nonbreaking conditions.* s.l. : JOURNAL OF GEOPHYSICAL RESEARCH-OCEANS, 1998.

—. 1998. *The temporal and spatial variability of infragravity energy in a barred nearshore zone.* s.l. : CONTINENTAL SHELF RESEARCH, 1998.

Senechal, N, Bonneton, P and Dupuis, H. 2001. *Field observations of irregular wave transformation in the surf zone.* s.l. : Fourth Conference on Coastal Dynamics , 2001.

Smit, PB, et al. 2018. *Infragravity Wave Radiation Across the Shelf Break.* s.l. : JOURNAL OF GEOPHYSICAL RESEARCH-OCEANS, 2018.

Symonds, G and Ranasinghe, R. 2000. *On the formation of rip currents on a plane beach.* s.l. : Coastal Engineering, 2000.

Symonds, G, Huntley, DA and Bowen, AJ. 1982. *Two-dimensional surf beat: Long wave generation by a time-varying breakpoint.* s.l. : JOURNAL OF GEOPHYSICAL RESEARCH, 1982.

Tissier, M, et al. 2015. *Infragravity-wave modulation of short-wave celerity in the surf zone.* s.l. : Journal of Geophysical Research: Oceans, 2015.

Tucker, M. 1952. *Surf beats: sea waves of 1 to 5 min period.* s.l. : Proc. R. Soc. London, 1952.

van Dongeren, A, et al. 2007. *Shoaling and shoreline dissipation of low-frequency waves.* s.l. : JOURNAL OF GEOPHYSICAL RESEARCH-OCEANS, 2007.